THE EFFECT OF IMPERFECTIONS ON THE BUCKLING OF CYLINDRICAL SHELLS

Thesis by

Jean-Francois Imbert

In Partial Fulfillment of the Requirements

For the Degree of

Aeronautical Engineer

California Institute of Technology

Pasadena, California

1971

(Submitted September 14, 1970)

ACKNOWLEDGMENT

The author is deeply indebted to Dr. C. D. Babcock, Jr. for guidance and encouragement during the course of this investigation, to Dr. J. Arbocz for many helpful discussions and suggestions, to Dr. E. E. Sechler for his support and encouragement. Many thanks are also due to Miss Helen Burrus for the typing and to Mrs. Betty Wood for the graphs.

Finally the financial support of a Graduate Teaching Assistantship and a GALCIT Fellowship is gratefully acknowledged.

ABSTRACT

A theoretical investigation of the effect of general imperfections on the buckling of a cylindrical shell under axial compression was carried out. A limit point analysis was performed to determine the buckling loads using a simplified imperfection and displacement model consisting of one axisymmetric and two asymmetric components with the same circumferential wave number.

The wave number dependence of imperfections for a class of shells obtained by the same manufacturing processes was characterized by using an imperfection model to fit the experimental imperfection coefficients available. Buckling load calculations were performed using both experimental and fitted data as imperfection coefficients.

For the experimental data available the three-mode solution was found to have only a small additional effect with respect to the two-mode solution. In addition, by extrapolating imperfection coefficients for high wave numbers by means of the imperfection model, it was found that a strong interaction effect would exist between a low wave number axisymmetric mode and two classical asymmetric modes.

LIST OF SYMBOLS

λ	Nondimensional loading parameter ($\lambda = \sqrt{3(1-\nu^2)}\,\frac{R}{t}\,\frac{\sigma}{E}$)
ν	Poisson's ratio
E	Young's modulus
R	Shell radius
t	Shell thickness
L	Length of the shell
σ	Axial stress
x, y	Axial and circumferential coordinates on middle surface of shell, respectively
$\bar{x}, \bar{y}$	Nondimensional coordinates
i, k_1, k_2	Axial wave numbers
j, m_1, m_2	Axial half wave numbers
ℓ	Circumferential wave number
λ_x, λ_y	Wave lengths in the axial and circumferential directions respectively
w, W	Radial displacement
$\overline{W}$	Radial imperfection from perfect circular cylinder
ξ_i	Nondimensional radial displacement amplitude
$\overline{\xi}_i$	Nondimensional radial imperfection amplitude
f, F	Airy stress function
α, α_i, β	Mode shape parameters defined on pages 5, 10 and in Appendix A
γ_i	Constants defined in Appendix A

LIST OF SYMBOLS (Cont'd)

A_{ij}	Coefficient of $\cos i\bar{x} \cos j\bar{y}$
B_{ij}	Coefficient of $\cos i\bar{x} \sin j\bar{y}$
C_{ij}	Coefficient of $\sin i\bar{x} \cos j\bar{y}$
D_{ij}	Coefficient of $\sin i\bar{x} \sin j\bar{y}$
K_i	Coefficients of the stress function listed in Appendix A
E_i	Coefficients of the error function listed in Appendix A
C_i	Coefficients of the buckling equations for the three-mode case listed in Appendixes A and B
D_i	Coefficients of the buckling equations for the two-mode case listed in Appendixes A and B
$\hat{\xi}_A$	Imperfection model for axisymmetric imperfections
$\hat{\xi}$	Imperfection model for asymmetric imperfections
S, T, S_i, T_i	Expressions defined in Appendix C
P_i	Coefficients of polynomials in λ, defined in Appendix C
∇^4	Biharmonic operator $\left(\frac{\partial^4}{\partial x^4} + 2\frac{\partial^4}{\partial x^2 \partial y^2} + \frac{\partial^4}{\partial y^4}\right)$

LIST OF TABLES

LIST OF FIGURES

LIST OF FIGURES (Cont'd)

TABLE OF CONTENTS

TABLE OF CONTENTS (Cont'd)

I. GENERAL INTRODUCTION

It is well known (Refs. 1 and 2) that it is impossible to predict buckling loads of isotropic cylindrical shells in axial compression by using linearized small deflection theories. In fact all experimental values of buckling loads are much lower than the so-called classical value and furthermore present a large scatter band. The main reason for this discrepancy between theory and experimental data advanced by most of the previous investigators is the effect of initial geometrical imperfections.

Donnell and Wan (Ref. 3) were among the first to investigate the effect of initial imperfections using the nonlinear Donnell's equations. In order to simplify calculations, they assumed proportionality of the imperfection and deformed shape. It should be underlined that they tried to characterize the dependence of imperfection coefficients on wave numbers of mode shapes by assuming a semi-empirical relationship.

In the past few years, investigations have been made by studying the effects of nonlinear coupling between several modes. Koiter (Refs. 4 and 5), investigated the interaction between the classical axisymmetric mode and two classical asymmetric modes with the same circumferential wave number. Assuming a very special initial imperfection in the form of the classical axisymmetric mode, he obtained an upper bound for the buckling load corresponding to such an imperfection.

Hutchinson (Ref. 6) derived a solution for pressurized cylinders using two modes, the classical axisymmetric one and one classical asymmetric mode with the same wave length in the axial and circumferential directions. He also included two parameters in the imperfection shape corresponding to these modes.

Arbocz and Babcock (Ref. 7) investigated the effect of general imperfections. They obtained a solution of Donnell's equations by using for initial imperfections and radial displacements three terms of the general double Fourier series: one cosine term for the axisymmetric mode and both sine and cosine terms for the asymmetric mode. Only two of these three modes acting at once were considered in this analysis. In addition, it should be noticed that these Fourier coefficients were experimentally obtained from measurements on shells.

On the other hand, Thurston and Freeland (Ref. 8) used a quasi-linearization method to obtain a numerical solution of Donnell's equations. In this method as many modes as necessary for convergence can be used which is an important advantage for the accuracy of numerical results.

The two-mode solution is important, since it shows analytically the influence of imperfections of some critically coupled modes but it may lead to some inaccuracy in the numerical results. On the other hand, some measurements of individual modal components made by Arbocz and Babcock (Ref. 7) show that more than two modal components may show a significant prebuckling growth. Therefore, it is logical to investigate the effects of nonlinear coupling between

several modes in order to test the accuracy of the two-mode solution. In addition, other critical coupling may be found that did not occur in the two-mode case.

In the present analysis, an approximate solution of Donnell's equations for isotropic imperfect cylindrical shells under axial compression is carried out by using one general axisymmetric mode and two general asymmetric modes for both sine and cosine axial representation. Moreover the dependence of imperfection coefficients on wave numbers is studied from experimental data obtained from surface measurements (Ref. 9) of several copper shells. Some attempt is made to determine the most probable dependence for a class of shells, by fitting experimental data by a power law, more general than the Donnell and Wan relationship (Ref. 3). Finally, critical loads are determined from a limit point analysis using both experimental and fitted data as imperfection coefficients.

II. THEORETICAL ANALYSIS

In order to investigate the nonlinear interaction between one general axisymmetric mode and two general associated asymmetric modes the following method was used.

1. An exact particular solution of the compatibility equation is found in terms of the assumed radial displacement w and initial imperfection $\overline{w}$.

2. The equilibrium equation is solved approximately by a Galerkin procedure.

The same method was used by Hutchinson (Ref. 6) and Arbocz and Babcock (Ref. 7) in their two-mode analysis. It should be noticed that no attempt is made to satisfy the shell boundary conditions. Hence the important effect of interaction between imperfections and prebuckling deformations caused by edge restraints is neglected in this analysis.

1. Mode Selection

In order to compare the mode selection used in this analysis to those of previous investigators it seemed worthwhile to recall some fundamental results of the linearized theory.

If f^* and w^* represent the perturbation quantities added to the membrane prebuckling solution to describe any equilibrium state of a perfect axially loaded shell, then f^* and w^* satisfy the following linearized quations:

$$\frac{1}{Et} \nabla^4 f^* - \frac{1}{R} w^*_{xx} = o \qquad (2.1)$$

$$\frac{Et^3}{4c^2}\nabla^4 w^* + \frac{1}{R} f^*_{,xx} + \sigma t w^*_{,xx} = o \tag{2.2}$$

where

$$c = \sqrt{3(1-\nu^2)}$$

and x, y are the axial and circumferential coordinates respectively. This is a well-known linear eigenvalue problem. A nontrivial solution in the form of an asymmetric mode

$$w^* = a \sin k \frac{2\pi x}{L} \sin \ell \frac{y}{R} \tag{2.3}$$

$$f^* = b \sin k \frac{2\pi x}{L} \sin \ell \frac{y}{R} \tag{2.4}$$

can be found if and only if

$$\lambda = c \frac{R}{t} \frac{\sigma}{E} = \frac{1}{2}\left[\frac{\alpha^2}{(\alpha^2+\beta^2)^2} + \frac{(\alpha^2+\beta^2)^2}{\alpha^2}\right] \tag{2.5}$$

where:

$$\alpha^2 = k^2 \frac{Rt}{2c} \left(\frac{2\pi}{L}\right)^2 \tag{2.6}$$

$$\beta^2 = \ell^2 \frac{Rt}{2c} \left(\frac{1}{R}\right)^2 \tag{2.7}$$

The classical value of the buckling parameter is obtained by minimizing the eigenvalue λ with respect to α and β. The minimum:

$$\lambda_c = c \frac{R}{t} \frac{\sigma_c}{E} = 1$$

is reached for the set of so-called classical buckling modes which satisfy the condition:

$$\alpha^2 + \beta^2 - \alpha = o \tag{2.8}$$

This condition is represented in α, β coordinates by the so-called Koiter circle. Among these classical modes is one axisymmetric mode:

$$w_o^* = a_o \sin i_o \frac{2\pi x}{L} \tag{2.9}$$

where

$$i_o^2 = \frac{c}{2\pi^2} \frac{L^2}{Rt} \tag{2.10}$$

By using the Koiter circle representation, the modes selection of the present analysis is compared with those of Hutchinson, Koiter, Arbocz and Babcock in figure 1. Hutchinson uses the classical axisymmetric mode ($\alpha_A = 1$) and the classical asymmetric mode with $k = i/2$ ($\alpha = \beta = 1/2$) which is a particular case of Koiter's selection of modes: Koiter uses the classical axisymmetric mode and two classical asymmetric modes with the same circumferential wave number. The analysis of Arbocz and Babcock is a generalization of Hutchinson's work. They use one general axisymmetric mode ($\alpha_A \neq 1$) and one general asymmetric mode ($\alpha \neq \beta \neq 1/2$) with $k = i/2$. Similarly, one general axisymmetric mode ($\alpha_A \neq 1$) and two general asymmetric modes with the same circumferential wave number are used in this analysis, which constitutes a generalization of Koiter's selection of modes. It was found that Koiter's choice is a particular

case of one coupling $(k_1 + k_2 - i = o)$ in the present analysis but that other couplings can generate other combinations of modes.

2. Donnell's Shell Equations

Assuming that the radial displacement W is positive outward, the nonlinear Donnell equations for an imperfect cylindrical shell can be written:

$$\frac{1}{Et} \nabla^4 F - \frac{1}{R} W_{,xx} + \frac{1}{2} L(W, W + 2\overline{W}) = o \tag{2.11}$$

$$\frac{Et^3}{12(1-\nu^2)} \nabla^4 W + \frac{1}{R} F_{,xx} - L(F, W + \overline{W}) = o \tag{2.12}$$

where L is a nonlinear operator defined by

$$L(S, T) = S_{,xx} T_{,yy} - 2S_{,xy} T_{,xy} + S_{,yy} T_{,xx} \tag{2.13}$$

Equation (2.11) is the compatibility equation. Equation (2.12) is the third equilibrium equation, the first two being identically satisfied by using the Airy stress function:

$$\left.\begin{aligned} N_{,xx} &= F_{,yy} \\ N_{,yy} &= F_{,xx} \\ N_{,xy} &= F_{,xy} \end{aligned}\right\} \tag{2.14}$$

It is convenient in the analysis to solve with respect to w and f which represent an additional state to a uniform membrane state so that:

$$W = \frac{\nu}{E}\sigma R + w \tag{2.15}$$

$$F = -\frac{1}{2}\sigma t y^2 + f \tag{2.16}$$

After using (2.15) and (2.16) the Donnell equations can be written:

$$\frac{1}{Et}\nabla^4 f - \frac{1}{R}w_{xx} + w_{,xx}w_{yy} + w_{xx}\overline{W}_{yy} + w_{yy}\overline{W}_{xx} - w_{xy}^2 - 2w_{,xy}\overline{W}_{xy} = o \tag{2.17}$$

$$\frac{Et^3}{4c^2}\nabla^4 w + \frac{1}{R}f_{,xx} - f_{xx}(w+\overline{W})_{,yy} + 2f_{,xy}(w+\overline{W})_{,xy} - f_{,yy}(w+\overline{W})_{,xx} + \sigma t(w+\overline{W})_{,xx} = o \tag{2.18}$$

3. Derivation of Nonlinear Buckling Equations for Cosine Axial Representation

Initial imperfections are represented by:

$$\frac{\overline{W}}{t} = \xi_A \cos i\bar{x} + \xi_1 \cos k_1\bar{x} \cos \ell\bar{y} + \xi_2 \cos k_2\bar{x} \cos \ell\bar{y} \tag{2.19}$$

where $\bar{x} = 2\pi\frac{x}{L}$ and $\bar{y} = \frac{y}{R}$ are nondimensional coordinates.

Moreover w is approximated as:

$$\frac{w}{t} = \xi_A \cos i\bar{x} + \xi_1 \cos k_1\bar{x} \cos \ell\bar{y} + \xi_2 \cos k_2\bar{x} \cos \ell\bar{y} \tag{2.20}$$

Using (2.19) and (2.20) an exact particular solution of the compatibility equation (2.17) is found to be

$$f = K_1 \cos i\bar{x} + K_2 \cos k_1\bar{x} \cos \ell\bar{y} + K_3 \cos k_2\bar{x} \cos \ell\bar{y} + K_4 \cos(k_1+i)\bar{x} \cos \ell\bar{y}$$

$$+ K_5 \cos(k_1-i)\bar{x} \cos \ell\bar{y} + K_6 \cos(k_2+i)\bar{x} \cos \ell\bar{y} + K_7 \cos(k_2-i)\bar{x} \cos \ell\bar{y}$$

$$+ K_8 \cos 2k_1\bar{x} + K_9 \cos 2k_2\bar{x} + K_{10} \cos 2\ell\bar{y} + K_{11} \cos(k_1+k_2)\bar{x}$$

$$+ K_{12} \cos (k_1-k_2)\bar{x} + K_{13} \cos (k_1+k_2)\bar{x} \cos 2\ell\bar{y}$$

$$+ K_{14} \cos (k_1 - k_2)\bar{x} \cos 2\ell\bar{y} \qquad (2.21)$$

Coefficients K_i are listed in Appendix A.

The equilibrium equation (2.18) is then solved approximately by using a Galerkin procedure. After substituting W, w, f of (2.19) (2.20), (2.21) in (2.18) the following error function is obtained where third order terms as $\xi_i\xi_j^2$, $\xi_i^2\xi_j$ and ξ_i^3 are neglected:

$$\epsilon(\bar{x}, \bar{y}) = 2\frac{Et^2}{R^2} \Big\{ E_1 \cos i\bar{x} + E_2 \cos k_1\bar{x} \cos \ell\bar{y} + E_3 \cos k_2\bar{x} \cos \ell\bar{y}$$

$$+ E_4 \cos 2k_1\bar{x} + E_5 \cos 2k_2\bar{x} + E_6 \cos(k_1+k_2)\bar{x} + E_7 \cos (k_1-k_2)\bar{x}$$

$$+ E_8 \cos(k_1+i)\bar{x} \cos \ell\bar{y} + E_9 \cos(k_1-i)\bar{x} \cos \ell\bar{y} + E_{10} \cos(k_2+i)\bar{x} \cos \ell\bar{y}$$

$$+ E_{11} \cos(k_2-i)\bar{x} \cos \ell\bar{y} + E_{12} \cos 2\ell\bar{y} + E_{13} \cos 2k_1\bar{x} \cos 2\ell\bar{y}$$

$$+ E_{14} \cos 2k_2\bar{x} \cos 2\ell\bar{y} + E_{15} \cos(k_1+k_2)\bar{x} \cos 2\ell\bar{y}$$

$$+ E_{16} \cos (k_1 - k_2)\bar{x} \cos 2\ell\bar{y} + 0(\xi^3) \Big\} \qquad (2.22)$$

Coefficients E_i of the error function are listed in Appendix A. The three nonlinear buckling equations are obtained by the following orthogonality conditions:

$$\iint_0^{2\pi} \epsilon(x, y) \cos i\bar{x}\, d\bar{x}\, d\bar{y} = o \tag{2.23}$$

$$\iint_0^{2\pi} \epsilon(x, y) \cos k_1\bar{x} \cos \ell\bar{y}\, d\bar{x}\, d\bar{y} = o \tag{2.24}$$

$$\iint_0^{2\pi} \epsilon(x, y) \cos k_2\bar{x} \cos \ell\bar{y}\, d\bar{x}\, d\bar{y} = o \tag{2.25}$$

The coupling relationships between modes are obtained by prescribing that all the quadratic terms do not vanish identically. Without that restriction the equations will describe an imperfection insensitive structure with stable postbuckled states. The relationships that guarantee second order terms in the buckling equations are found to be any combination of the following:

$$\begin{aligned} 2k_1 &= i \\ 2k_2 &= i \\ k_1 + k_2 - i &= o \\ k_1 - k_2 - i &= o \\ k_1 - k_2 + i &= o \end{aligned} \tag{2.26}$$

It should be mentioned that the condition $k_1 = k_2$ leads to additional first order terms in the second and third buckling equations. After having examined all combinations of coupling relationships, it

appears that the four following basic cases are to be considered where each of these corresponds to a particular set of buckling equations:

Case A $\quad k_1 = k_2 - i = o \qquad (k_1 \neq k_2 \neq i/2$

Case B $\quad$ 1) $k_1 - k_2 - i = o$
$\quad\quad\quad$ 2) $k_1 - k_2 + i = o$ $\Big\}$ $(k_1 \neq k_2 \neq i/2)$

(2.27)

Case C $\quad$ 1) $k_1 = 3k_2 \qquad k_2 = i/2$

$\quad\quad\quad$ 2) $k_2 = 3k_1 \qquad k_1 = i/2$

Case D $\quad k_1 = k_2 = i/2$

Some other degenerate cases can be found which are neglected in the present analysis. It is sufficient to interchange k_1 and k_2 to see that cases B_1 and B_2 (and similarly C_1 and C_2) are equivalent.

The following nondimensional wave parameters can be introduced.

$$\alpha_A^2 = i^2 \frac{Rt}{2c} \left(\frac{2\pi}{L}\right)^2 \tag{2.28}$$

$$\alpha_1^2 = k_1^2 \frac{Rt}{2c} \left(\frac{2\pi}{L}\right)^2 \tag{2.29}$$

$$\alpha_2^2 = k_2^2 \frac{Rt}{2c} \left(\frac{2\pi}{L}\right)^2 \tag{2.30}$$

$$\beta^2 = \ell^2 \frac{Rt}{2c} \left(\frac{1}{R}\right)^2 \tag{2.31}$$

λ_A, λ_1, λ_2 are respectively the eigenvalues associated with the axisymmetric and the first and second asymmetric modes:

$$\lambda_A = \frac{1}{2}\left(\alpha_A^2 + \frac{1}{\alpha_A^2}\right) \tag{2.32}$$

$$\lambda_1 = \frac{1}{2}\left[\frac{\alpha_1^2}{(\alpha_1^2+\beta^2)^2} + \frac{(\alpha_1^2+\beta^2)^2}{\alpha_1^2}\right] \tag{2.33}$$

$$\lambda_2 = \frac{1}{2}\left[\frac{\alpha_2^2}{(\alpha_2^2+\beta)^2} + \frac{(\alpha_2^2+\beta^2)^2}{\alpha_2^2}\right] \tag{2.34}$$

For cases A, B and C($k_1 \neq k_2$) the buckling equations can be written in the following general form:

$$\begin{aligned}&\xi_A(\lambda_A-\lambda) + C_1(\xi_1\xi_2+\xi_1\bar{\xi}_2+\xi_2\bar{\xi}_1) + C_2\xi_1(\xi_2+\bar{\xi}_2) + C_3\xi_2(\xi_1+\bar{\xi}_1)\\ &\quad + C_4\left(\frac{\xi_1^2}{2}+\xi_1\bar{\xi}_1\right) + C_5\xi_1(\xi_1+\bar{\xi}_1) + C_6\left(\frac{\xi_2^2}{2}+\xi_2\bar{\xi}_2\right)\\ &\quad + C_7\xi_2(\xi_2+\bar{\xi}_2) = \lambda\bar{\xi}_A\end{aligned} \tag{2.35}$$

$$\begin{aligned}&\xi_1(\lambda_1-\lambda) + C_8\left[\xi_1(\xi_A+\bar{\xi}_A)+\xi_A\bar{\xi}_1\right] + C_9\xi_A(\xi_1+\bar{\xi}_1) + C_{10}\xi_1(\xi_A+\bar{\xi}_A)\\ &\quad + C_{11}\left[\xi_2(\xi_A+\bar{\xi}_A)+\xi_A\bar{\xi}_2\right] + C_{12}\xi_A(\xi_2+\bar{\xi}_2) + C_{13}\xi_2(\xi_A+\bar{\xi}_A) = \lambda\bar{\xi}_1\end{aligned} \tag{2.36}$$

$$\xi_2(\lambda_2-\lambda) + C_{14}\left[\xi_1(\xi_A+\bar{\xi}_A) + \xi_A\bar{\xi}_1\right] + C_{15}\xi_A(\xi_1+\bar{\xi}_1) + C_{16}\xi_1(\xi_A+\bar{\xi}_A)$$

$$+ C_{17}\left[\xi_2(\xi_A+\bar{\xi}_A) + \xi_A\bar{\xi}_2\right] + C_{18}\xi_A(\xi_2+\bar{\xi}_2) + C_{19}\xi_2(\xi_A+\bar{\xi}_A) = \lambda\bar{\xi}_2 \tag{2.37}$$

Coefficients C_i are listed in Appendix A for cases A, B, and C. Case D leads to the two-mode solution. Letting

$$\left.\begin{aligned} k_1 &= k_2 = k \\ \bar{\xi}_1 &= \bar{\xi}_2 = \frac{\bar{\xi}}{2} \\ \xi_1 &= \xi_2 = \frac{\xi}{2} \end{aligned}\right\} \tag{2.38}$$

the following can be written:

$$\frac{\bar{W}}{t} = \bar{\xi}_A \cos i\bar{x} + \bar{\xi} \cos k\bar{x} \cos \ell\bar{y} \tag{2.39}$$

$$\frac{w}{t} = \xi_A \cos i\bar{x} + \xi \cos k\bar{x} \cos \ell\bar{y} \tag{2.40}$$

Then the buckling equations can be written as follows

$$\xi_A(\lambda_A-\lambda) + D_1\left(\frac{\xi^2}{2} + \xi\bar{\xi}\right) + D_2\xi(\xi+\bar{\xi}) = \lambda\bar{\xi}_A \tag{2.41}$$

$$\xi(\lambda_1-\lambda) + D_3\left[\xi(\xi_A+\bar{\xi}_A) + \xi_A\bar{\xi}\right] + D_4\xi_A(\xi+\bar{\xi}) + D_5\xi(\xi_A+\bar{\xi}_A) = \lambda\bar{\xi} \tag{2.42}$$

Coefficients D_i are listed in Appendix A.

4. Derivation of Nonlinear Buckling Equations for Sine Axial Representation

Initial imperfections are represented by

$$\frac{\overline{W}}{t} = \bar{\xi}_A \sin i\bar{x} + \bar{\xi}_1 \sin k_1\bar{x} \sin \ell\bar{y} + \bar{\xi}_2 \sin k_2\bar{x} \sin \ell\bar{y} \qquad (2.43)$$

Moreover w is approximated as:

$$\frac{w}{t} = \xi_A \sin i\bar{x} + \xi_1 \sin k_1\bar{x} \sin \ell\bar{y} + \xi_2 \sin k_2\bar{x} \sin \ell\bar{y} \qquad (2.44)$$

As previously, using (2.43) and (2.44), a particular solution of the compatibility equation (2.17) is found which can be written:

$$\begin{aligned} f = {} & K_1 \sin i\bar{x} + K_2 \sin k_1\bar{x} \sin \ell\bar{y} + K_3 \sin k_2\bar{x} \sin \ell\bar{y} \\ & - K_4 \cos(k_1 + i)\bar{x} \sin \ell\bar{y} + K_5 \cos(k_1 - i)\bar{x} \sin \ell\bar{y} - K_6 \cos(k_2 + i)\bar{x} \sin \ell\bar{y} \\ & + K_7 \cos(k_2 - i)\bar{x} \sin \ell\bar{y} - K_8 \cos 2k_1\bar{x} - K_9 \cos 2k_2\bar{x} - K_{10} \cos 2\ell\bar{y} \\ & - K_{11} \cos(k_1 + k_2)\bar{x} + K_{12} \cos(k_1 - k_2)\bar{x} + K_{13} \cos(k_1 + k_2)\bar{x} \cos 2\ell\bar{y} \\ & - K_{14} \cos(k_1 - k_2)\bar{x} \cos 2\ell\bar{y} \end{aligned} \qquad (2.45)$$

Coefficients K_i are the same as those listed in Appendix A for cosine axial representation.

After substituting W, w, f of (2.43), (2.44), and (2.45) in the equilibrium equation (2.18) the following error function is obtained where third order terms are neglected as previously:

$$\epsilon(\bar{x},\bar{y}) = \frac{2Et^2}{R^2}\Big\{ E_1 \sin i\bar{x} + E_2 \sin k_1\bar{x} \sin \ell\bar{y} + E_3 \sin k_2\bar{x} \sin \ell\bar{y}$$

$$- E_4 \cos 2k_1\bar{x} - E_5 \cos 2k_2\bar{x} - E_6 \cos(k_1 + k_2)\bar{x} + E_7 \cos(k_1 - k_2)\bar{x}$$

$$- E_8 \cos(k_1 + i)\bar{x} \sin \ell\bar{y} + E_9 \cos(k_1 - i)\bar{x} \sin \ell\bar{y} - E_{10} \cos(k_2 + i)\bar{x} \sin \ell\bar{y}$$

$$+ E_{11} \cos(k_2 - i)\bar{x} \sin \ell\bar{y} + E_{12} \cos 2\ell\bar{y} + E_{13} \cos 2k_1\bar{x} \cos 2\ell\bar{y}$$

$$+ E_{14} \cos 2k_2\bar{x} \cos 2\ell\bar{y} + E_{15} \cos(k_1 + k_2)\bar{x} \cos 2\ell\bar{y}$$

$$+ E_{16} \cos(k_1 - k_2)\bar{x} \cos 2\ell\bar{y} + 0(\xi^3)\Big\} \qquad (2.46)$$

Coefficients E_i are found to be the same as those listed in Appendix A for cosine axial representation.

The buckling equations are then obtained by the three following orthogonality conditions:

$$\iint_0^{2\pi} \epsilon(\bar{x},\bar{y}) \sin i\bar{x}\, d\bar{x}\, d\bar{y} = 0 \qquad (2.47)$$

$$\iint_0^{2\pi} \epsilon(\bar{x},\bar{y}) \sin k_1\bar{x} \sin \ell\bar{y}\, d\bar{x}\, d\bar{y} = 0 \qquad (2.48)$$

$$\iint_0^{2\pi} \epsilon(\bar{x},\bar{y}) \sin k_2\bar{x} \sin \ell\bar{y}\, d\bar{x}\, d\bar{y} = 0 \qquad (2.49)$$

For convenience the following half wave numbers which must be integers are introduced.

$$
\begin{aligned}
j &= 2i \\
m_1 &= 2k_1 \\
m_2 &= 2k_2
\end{aligned}
\tag{2.50}
$$

Then the condition that quadratic terms do not vanish identically in the buckling equations is found to be satisfied by any combination of the following conditions:

$$
\begin{aligned}
&2m_1 + j \quad \text{odd} \\
&2m_1 - j \quad \text{odd} \\
&2m_2 + j \quad \text{odd} \\
&2m_2 - j \quad \text{odd} \\
&j \quad \text{odd} \\
&m_1 + m_2 + j \quad \text{odd} \\
&m_1 + m_2 - j \quad \text{odd} \\
&m_1 + m_2 + j \quad \text{odd} \\
&m_1 - m_2 - j \quad \text{odd}
\end{aligned}
\tag{2.51}
$$

As previously, the condition $k_1 = k_2$ leads to additional first order terms in the second and third buckling equations. After having examined all combinations of the coupling conditions (2.51), it appears that four basic cases are to be considered. Each of these corresponds to a particular set of buckling equations:

$$\left.\begin{array}{lllll} \underline{\text{Case A}} & \text{j even}, & (m_1 + m_2) & \text{odd} & \\ \underline{\text{Case B}} & \text{j odd}, & (m_1 + m_2) & \text{odd} & \\ \underline{\text{Case C}} & \text{j odd}, & (m_1 + m_2 & \text{even} & \\ \underline{\text{Case D}} & \text{j odd}, & k_1 = k_2 & & \end{array}\right\} \quad k_1 \neq k_2 \qquad (2.52)$$

For cases A, B and C ($k_1 \neq k_2$) the buckling equations can be written in the same general form as for the cosine axial representation (2.35), (2.36), and (2.37). Coefficients C_i for cases A, B and C for the sine axial representation are listed in Appendix B.

As previously, case D leads to the two-mode solution. Letting

$$\begin{aligned} k_1 &= k_2 = k \\ \bar{\xi}_1 &= \bar{\xi}_2 = \frac{\bar{\xi}}{2} \\ \xi_1 &= \xi_2 = \frac{\xi}{2} \end{aligned} \qquad (2.53)$$

the following can be written:

$$\frac{\overline{W}}{t} = \bar{\xi}_A \sin i\bar{x} + \bar{\xi} \sin k\bar{x} \sin \ell\bar{y} \qquad (2.54)$$

$$\frac{W}{t} = \xi_A \sin i\bar{x} + \xi \sin k\bar{x} \sin \ell\bar{y} \qquad (2.55)$$

Then the buckling equations can be written in the same form (2.41) and (2.42) as for the cosine axial representation. Coefficients D_i of the buckling equations for the sine axial representation are listed in Appendix B.

III. BUCKLING BEHAVIOR OF A PERFECT SHELL

In order to compare the strength of the various couplings found in the present analysis it is important to compare the buckling behavior of perfect shells for those couplings. In this discussion it will always be assumed that $\lambda_A > \lambda_1$ and $\lambda_A > \lambda_2$. This is justified by some previous work. Arbocz and Babcock (Ref. 7) showed that axisymmetric imperfection coefficients with low wave numbers, corresponding to high eigenvalues had the largest magnitudes in practice and hence give the lowest buckling loads. Moreover the case where $\lambda_1 < \lambda_2 < \lambda_A$ only needs to be studied since the order of the two asymmetric modes has no importance and they can be interchanged if $\lambda_2 < \lambda_1 < \lambda_A$.

1. Two-mode Case (Case D for Both Sine and Cosine Axial Representations)

The buckling of perfect shells is discussed in some previous two-mode analyses (Refs. 6, 7 and 9) where both cosine and sine terms in the axial direction are used for the asymmetric mode. The two-mode solution of the present analysis is a special case of this one.

The governing equations in this two-mode solution are for the perfect shell ($\bar{\xi}_A = \bar{\xi} = o$) the following:

$$\xi_A(\lambda_A - \lambda) + \eta_1 \xi^2 = o \tag{3.1}$$

$$\xi\left\{(\lambda_1 - \lambda) + \eta_2 \xi_A\right\} = o \tag{3.2}$$

where

$$\eta_1 = \frac{D_1}{2} + D_2$$

$$\eta_2 = D_3 + D_4 + D_5$$

If the load is monotonically increased the trivial solution ($\xi = \xi_A$, o) can only exist for $\lambda < \lambda_1$. When λ reaches the value λ_1, then the bracket in (3.2) vanishes identically and a nontrivial solution is possible which satisfies both (3.1) and (3.2). This solution, defined as:

$$\xi_A = (\lambda - \lambda_1)/\eta_2 \tag{3.3}$$

$$\xi^2 = (\lambda - \lambda_1)(\lambda - \lambda_A)/\eta_1\eta_2 \tag{3.4}$$

is represented in Fig. 2. It should be noted that the trace of the solution in the (λ, ξ_A) plane is a straight line.

In addition, recall for this simple case, the buckling behavior of a shell with an axisymmetric imperfection ($\bar{\xi}_A \neq o$, $\bar{\xi} = o$). For this case the governing equations can be written:

$$\xi_A(\lambda_A - \lambda) + \eta_1\xi^2 = \lambda\bar{\xi}_A \tag{3.5}$$

$$\xi\left\{(\lambda_1 - \lambda) + \eta_2\xi_A + \eta_3\bar{\xi}_A\right\} = o \tag{3.6}$$

where $\eta_3 = D_3 + D_5$.

Since the imperfection is purely axisymmetric, the prebuckling solution is also purely axisymmetric. Equations (3.5) and (3.6) are identically satisfied by the following solution:

$$\left.\begin{aligned} \xi_A &= \bar{\xi}_A \frac{\lambda}{\lambda_A - \lambda} \\ \xi &= o \end{aligned}\right\} \tag{3.7}$$

This solution is no longer valid when there is a bifurcation in the axisymmetric mode. This occurs when the bracket in (3.4) vanishes identically, which condition is represented by the straight line Δ in (λ, ξ_A) coordinates.

$$\xi_A = \left\{ \lambda - (\lambda_1 + \eta_3 \bar{\xi}_A) \right\} / \eta_2 \tag{3.8}$$

Then the following solution in ξ is found:

$$\xi^2 = (\lambda - \lambda_A) \left\{ \lambda - (\lambda_1 + \eta_3 \bar{\xi}_A) \right\} / \eta_1 \eta_2 \tag{3.9}$$

It should be noted that the buckling equations describe an imperfection sensitive structure only if the signs of $\bar{\xi}_A$ and η_2 are different.

2. Three-mode Case

a. Cases A and B for the cosine axial representation and Case A for the sine axial representation

The governing equations for a perfect shell are in these cases:

$$(\lambda_A - \lambda)\xi_A + \eta_1 \xi_1 \xi_2 = o \tag{3.10}$$

$$(\lambda_1 - \lambda)\xi_1 + \eta_2 \xi_A \xi_2 = o \tag{3.11}$$

$$(\lambda_2 - \lambda)\xi_2 + \eta_3 \xi_A \xi_1 = o \tag{3.12}$$

where

$$\eta_1 = C_1 + C_2 + C_3$$
$$\eta_2 = C_{11} + C_{12} + C_{13}$$
$$\eta_3 = C_{14} + C_{15} + C_{16}$$

If the load is monotonically increased, the trivial solution can only exist for $\lambda < \lambda_1$. When λ reaches the value λ_1, there is a bifurcation of the solution in ξ_1. Equations (3.10), (3.11) and (3.12) are identically satisfied by:

$$\lambda = \lambda_1 \qquad \xi_1 \neq o \qquad \xi_A = \xi_2 = o$$

until there is a bifurcation in ξ_A and ξ_2.

Writing (3.10) and (3.12) as follows

$$\begin{bmatrix} \lambda_A - \lambda & \eta_1 \xi_1 \\ \eta_3 \xi_1 & \lambda_2 - \lambda \end{bmatrix} \begin{bmatrix} \xi_A \\ \xi_2 \end{bmatrix} = o$$

a nontrivial solution in ξ_A, ξ_2 can be found if:

$$\xi_1^2 = (\lambda_A - \lambda)(\lambda_2 - \lambda)/\eta_1\eta_3 \tag{3.13}$$

Then, after bifurcation in ξ_A and ξ_2 there exists a nontrivial solution in ξ_A, ξ_1, ξ_2 and hence the same arguments as previously can be used for (ξ_1, ξ_2) and (ξ_A, ξ_1) respectively to obtain the following solution:

$$\xi_A^2 = (\lambda_1 - \lambda)(\lambda_2 - \lambda)/\eta_2\eta_3 \tag{3.14}$$

$$\xi_2^2 = (\lambda_1 - \lambda)(\lambda_A - \lambda)/\eta_1\eta_2 \tag{3.15}$$

This solution is represented in Fig. 3 where the branches in dotted lines are of no interest for the present discussion.

In the case where $\lambda_1 = \lambda_2$, the trace of the solution in the (λ, ξ_A) plane then becomes two straight lines:

$$\xi_A = \pm (\lambda_1 - \lambda)/\sqrt{\eta_2 \eta_3} \tag{3.16}$$

This behavior is shown in Fig. 4.

For this special case, the buckling behavior of a perfect shell is found to be the same as for the two-mode cases. In addition it should be noted that, if all three-modes are located on the circle corresponding to the same eigenvalue, then the traces in the planes $(\lambda_1 \xi_A)$, (λ, ξ_1) and (λ, ξ_2) are straight lines which characterize the most imperfection sensitive behavior.

b. Case B for the sine axial representation

In this case the governing equation for a perfect shell can be written as:

$$(\lambda_A - \lambda)\xi_A + \eta_1 \xi_1^2 + \eta_2 \xi_2^2 = o \tag{3.17}$$

$$\xi_1 \left\{ (\lambda_1 - \lambda) + \eta_3 \xi_A \right\} = o \tag{3.18}$$

$$\xi_2 \left\{ (\lambda_2 - \lambda) + \eta_4 \xi_A \right\} = o \tag{3.19}$$

where:

$$\eta_1 = \frac{C_4}{2} + C_5$$

$$\eta_2 = \frac{C_6}{2} + C_7$$

$$\eta_3 = C_8 + C_9 + C_{10}$$

$$\eta_4 = C_{17} + C_{18} + C_{19}$$

If the load is monotonically increased, the trivial solution can only exist for $\lambda < \lambda_1$. Then when $\lambda = \lambda_1$, there is a bifurcation of the solution in the ξ_1 mode. Equations (3.17), (3.18) and (3.19) are identically satisfied by the following:

$$\begin{aligned} \xi_A &= (\lambda - \lambda_1)/\eta_3 \\ \xi_1^2 &= (\lambda - \lambda_A)(\lambda - \lambda_1)/\eta_1\eta_3 \\ \xi_2 &= o \end{aligned} \tag{3.20}$$

Afterwards a bifurcation may occur in the ξ_2 mode. This is only possible if $\left|\frac{\eta_3}{\eta_4}\right| < \frac{\lambda_1}{\lambda_2}$. Then the following solution satisfies the governing equations:

$$\begin{aligned} \xi_A &= (\lambda - \lambda_2)/\eta_4 \\ \xi_1 &= o \\ \xi_2^2 &= (\lambda - \lambda_A)(\lambda - \lambda_2)/\eta_2\eta_4 \end{aligned} \tag{3.21}$$

The buckling behavior for a perfect shell in this case is represented in Fig. 5a. If $\lambda_1 = \lambda_2$ a bifurcation occurs either in ξ_1 if $\left|\frac{\eta_3}{\eta_4}\right| < 1$, or in ξ_2 if $\left|\frac{\eta_3}{\eta_4}\right| > 1$. The solution is represented in Fig. 5b in the case of a bifurcation in ξ_1.

c. Case C for both sine and cosine representations

This is the most general case. For the sine axial representation, governing equations can be written as follows:

$$\xi_A(\lambda_A - \lambda) + \eta_1\xi_1\xi_2 + \eta_2\xi_1^2 + \eta_2\xi_1^2 + \eta_3\xi_2^2 = o \tag{3.22}$$

$$\xi_1(\lambda_1 - \lambda) + \eta_4\xi_1\xi_A + \eta_5\xi_2\xi_A = o \tag{3.23}$$

$$\xi_2(\lambda_2 - \lambda) + \eta_6\xi_1\xi_A + \eta_7\xi_2\xi_A = o \tag{3.24}$$

where

$$\eta_1 = C_1 + C_2 + C_3$$

$$\eta_2 = \frac{C_4}{2} + C_5$$

$$\eta_3 = \frac{C_6}{2} + C_7$$

$$\eta_4 = C_8 + C_9 + C_{10}$$

$$\eta_5 = C_{11} + C_{12} + C_{13}$$

$$\eta_6 = C_{14} + C_{15} + C_{16}$$

$$\eta_7 = C_{17} + C_{18} + C_{19}$$

For the cosine axial representation the governing equations are the same with $\eta_2 = \eta_4 = o$ for subcase C_1 and $\eta_3 = \eta_7 = o$ for subcase C_2.

If the load is monotonically increased, the trivial solution can only exist for $\lambda < \lambda_1$. When $\lambda = \lambda_1$ there is a bifurcation into the ξ_A, ξ_1, ξ_2 modes. There is a nontrivial solution in ξ, ξ_2 for every ξ_A, if the following condition is satisfied

$$\begin{vmatrix} (\lambda_1 - \lambda) + \eta_4\xi_A & \eta_5\xi_A \\ \eta_6\xi_A & (\lambda_2 - \lambda) + \eta_7\xi_A \end{vmatrix} = o \tag{3.25}$$

which leads to the following quadratic equation

$$\xi_A^2(\eta_4\eta_7 - \eta_5\eta_6) + \xi_A\left[\eta_4(\lambda_2 - \lambda) + \eta_7(\lambda_1 - \lambda)\right] + (\lambda_1 - \lambda)(\lambda_2 - \lambda) = o$$

The solution of interest (i.e., for which $\xi_A = o$ for $\lambda = \lambda_1$) is the following:

$$\xi_A = \frac{-\left[\eta_4(\lambda_2-\lambda)+\eta_7(\lambda_1-\lambda)\right]+\sqrt{\left[\eta_4(\lambda_2-\lambda)+\eta_7(\lambda_1-\lambda)\right]^2 - 4(\eta_4\eta_7-\eta_5\eta_6)(\lambda_1-\lambda)(\lambda_2-\lambda)}}{2(\eta_4\eta_7 - \eta_5\eta_6)} \tag{3.26}$$

From (3.22) and (3.23) the solution in ξ_1 and ξ_2 can be obtained:

$$\xi_2 = \xi_1 \frac{\lambda_1 - \lambda + \eta_4\xi_A}{\eta_5\xi_A} \tag{3.27}$$

$$\xi_1^2 = \xi_A \frac{\lambda - \lambda_A}{\eta_2 + \eta_1\dfrac{\lambda_1 - \lambda + \eta_4\xi_A}{\eta_5\xi_A} + \eta_3\left(\dfrac{\lambda_1 - \lambda + \eta_4\xi_A}{\eta_5\xi_A}\right)^2} \tag{3.28}$$

The buckling behavior of a perfect shell in this case is represented in Fig. 6. It should be noted that, if $\lambda_1 = \lambda_2$, the trace of the of the solution in the (ξ_A, λ) plane is a straight line given by the following equation:

$$\left.\begin{aligned} \xi_A &= (\lambda - \lambda_1)\bar{\eta} \\ \text{where} \qquad \bar{\eta} &= \frac{\eta_4 + \eta_7 - \sqrt{(\eta_4 + \eta_7)^2 - 4(\eta_4\eta_7 - \eta_5\eta_6)}}{2(\eta_4\eta_7 - \eta_5\eta_6)} \end{aligned}\right\} \tag{3.29}$$

IV. GEOMETRICAL IMPERFECTIONS

In most theoretical studies on the stability of cylindrical shells, the dependence of geometrical imperfections on wave numbers is not considered. As an exception, Donnell and Wan (Ref. 3) tried to characterize the imperfection distribution by a semi empirical law. In order to use reasonable data as imperfection coefficients in the present analysis, an attempt is made to characterize this dependence for several shells obtained by the same manufacturing processes by fitting the experimental data obtained by Arbocz and Babcock (Refs. 7 and 9).

1. Experimental Imperfection Coefficients

Arbocz and Babcock used a noncontacting probe to make surface measurements on electroformed copper shells. The geometrical properties of the shells considered in this thesis are listed in Table I. A complete surface map of these shells was recorded by a scanning device travelling in both the axial and circumferential directions. The data recording process was fully automated and the data reduction was done on a digital computer. All details on the experimental device and data reduction programs can be found in reference 9.

To obtain the shell imperfections, first a perfect reference cylinder was found by fitting the surface measurements. The measured displacements were then recomputed with respect to this "best fit" cylinder. Then a double harmonic analysis was performed. Three sets of Fourier coefficients were obtained by using the different Fourier representations.

For the full wave representation in the axial direction, imperfections can be written as:

$$\frac{\overline{w}}{t} = \sum_{k=o}^{M}\sum_{\ell=o}^{M} A_{k\ell}\cos\frac{2k\pi x}{L}\cos\frac{\ell y}{R} + \sum_{k=1}^{M}\sum_{\ell=o}^{M} B_{k\ell}\cos\frac{2k\pi x}{L}\sin\frac{\ell y}{R}$$
$$+\sum_{k=o}^{M}\sum_{\ell=1}^{M} C_{k\ell}\sin\frac{2k\pi x}{L}\cos\frac{\ell y}{R} + \sum_{k=1}^{M}\sum_{\ell=1}^{M} D_{k\ell}\sin\frac{2k\pi x}{L}\sin\frac{\ell y}{R} \tag{4.1}$$

For the half wave cosine representation in the axial direction, imperfections can be written as:

$$\frac{\overline{w}}{t} = \sum_{k=o}^{M}\sum_{\ell=o}^{M} A_{k\ell}\cos\frac{k\pi x}{L}\cos\frac{\ell y}{R} + \sum_{k=1}^{M}\sum_{\ell=o}^{M} B_{k\ell}\cos\frac{k\pi x}{L}\sin\frac{\ell y}{R} \tag{4.2}$$

For the half wave sine representation in the axial direction, imperfections can be written as:

$$\frac{\overline{w}}{t} = \sum_{k=o}^{M}\sum_{\ell=1}^{M} C_{k\ell}\sin\frac{k\pi x}{L}\cos\frac{\ell y}{R} + \sum_{k=1}^{M}\sum_{\ell=1}^{M} D_{k\ell}\sin\frac{k\pi x}{L}\sin\frac{\ell y}{R} \tag{4.3}$$

In this analysis only the half wave representation in the axial direction is used.

In addition Fourier modulus coefficients can be computed which are defined as follows:

$$\rho_{k\ell} = \sqrt{A_{k\ell}^2 + B_{k\ell}^2} \qquad \text{for the cosine axial representation}$$

$$\rho_{k\ell} = \sqrt{C_{k\ell}^2 + D_{k\ell}^2} \qquad \text{for the sine axial representation}$$

The modulus coefficients are represented in Figs. 7 and 11 for shell A8. They are also represented in Figs. 8 and 12 using log-log coordinates. The averages of these coefficients for seven electroformed copper shells tested are represented in Figs. 9 and 13. They are also represented using log-log coordinates in Figs. 10 and 14.

2. Dependence on Wave Numbers

Donnell and Wan (Ref. 3) assume that the imperfection coefficients are related to the wave lengths by the following relationship:

$$\bar{\xi} = \frac{U}{\pi^2 t^2} \lambda_x^{1.5} \lambda_y^{0.5} \tag{4.4}$$

where U is the so-called unevenness factor.

λ_x and λ_y are respectively the wave lengths in the axial and circumferential directions.

$$\left.\begin{aligned} \lambda_x &= \frac{L}{2k} \\ \lambda_y &= \frac{\pi R}{\ell} \end{aligned}\right\} \tag{4.5}$$

Nondimensional wave parameters are used as variables instead of wave lengths in the mathematical model to fit experimental data.

The Donnell and Wan representation rewritten in terms of α and β is the following:

$$\xi = \frac{1}{2c}\left(\frac{UR}{t}\right) \alpha^{-1.5} \beta^{-0.5} \tag{4.6}$$

In addition it can be observed in Figs. 9 and 13 that a power law is a good model for the asymmetric imperfections for $\ell \geq 2$. It can also be noticed for all of the seven shells tested that the asymmetric imperfections for $\ell = 1$ present a very small value for any axial wave number. Moreover it appeared very difficult with the data available to find a correlation between axisymmetric and asymmetric imperfections. It then seemed reasonable to fit separately the axisymmetric and the asymmetric imperfections by the following model:

$$\begin{aligned} \hat{\xi}_A &= X_A \alpha^{-q} \\ \hat{\xi} &= X \alpha^{-r} \beta^{-s} \quad \text{or} \quad \ell \geq 2 \end{aligned} \tag{4.7}$$

Modulus coefficients were used to fit the asymmetric imperfections. For both sine and cosine axial representations the parameters X_A and q for axisymmetric imperfections and X, r, s for asymmetric imperfections were determined by using a least squares method, i.e., for the data available, by minimizing:

$$\Phi = \sum_{7 \text{ shells}} \sum_{k=1}^{7} \sum_{\ell=2}^{21} (\xi_k - \xi)^2 \quad \text{for asymmetric imperfections}$$

$$\Phi = \sum_{7 \text{ shells}} \sum_{k=1}^{7} (\xi_k - \xi_A)^2 \quad \text{for axisymmetric imperfections}$$

The total numbers of observations were:

N = 49 for axisymmetric imperfections

N = 980 for asymmetric imperfections

The minimization was performed using an iterative process which is explained in reference 11. Finally, the following results were found:

Sine axial representation

- axisymmetric imperfections

$X_A = 0.0168$

$q = 0.383$

$\sqrt{\frac{\phi}{N}} = 0.10$ (average error)

- asymmetric imperfections

$X = 0.000275$

$r = 1.007$

$s = 1.329$

$\sqrt{\frac{\phi}{N}} = 0.051$

Cosine axial representation

- axisymmetric imperfections

$X_A = 0.00238$

$q = 1.174$

$\sqrt{\frac{\phi}{N}} = 0.09$

- asymmetric imperfections

$$X = 0.00475 \quad 10^{-3}$$

$$r = 1.974$$

$$s = 1.457$$

$$\sqrt{\frac{\phi}{N}} = 0.026$$

It should be noted that the model used for asymmetric imperfections is better than that for axisymmetric imperfections. Using these values, the model (4.7) is represented in Figs. 15 and 16. For the imperfections corresponding to $\ell = 1$, which are very small and of no importance for buckling load determination, the average of modulus coefficients ρ_{kl} ($\rho_{kl} = 0.12$) was used in these figures.

V. NUMERICAL RESULTS

1. Numerical Procedure

In the three-mode case the second and third buckling equations (2.36) and (2.37) can be solved with respect to ξ_1 and ξ_2 for a given ξ_A to obtain:

$$\xi_1 = \frac{-\xi_1 \lambda^2 + S_1(\xi_A)\lambda + T_1(\xi_A)}{\lambda^2 + S(\xi_A)\lambda + T(\xi_A)} \tag{5.1}$$

$$\xi_2 = \frac{-\xi_2 \lambda^2 + S_2(\xi_A)\lambda + T_2(\xi_A)}{\lambda^2 + S(\xi_A)\lambda + T(\xi_A)} \tag{5.2}$$

Coefficients S, T, S_1, T_1, S_2, T_2 are listed in Appendix C.

Then, after substituting ξ_1 and ξ_2 in the first buckling equation (2.35) the following fifth order polynomial equation in λ is obtained, which can be solved numerically:

$$P_1(\xi_A)\lambda^5 + P_2(\xi_A)\lambda^4 + P_3(\xi_A)\lambda^3 + P_4(\xi_A)\lambda^2 + P_5(\xi_A)\lambda + P_6(\xi_A) = o \tag{5.3}$$

Coefficients P_i are expressed in function of ξ_A in Appendix C.

Similarly, in the two-mode case, the second buckling equation (2.42) can be written as:

$$\xi = -\bar{\xi}\,\frac{\lambda - (D_4 + D_3)\xi_A}{\lambda - \lambda_1 - (D_3 + D_5)(\xi_A + \xi_A) - D_4\xi_A} \tag{5.4}$$

Then after substituting ξ from (5.4) in (2.41), the following third order polynomial equation in λ is obtained:

$$P_1(\xi_A)\,\lambda^3 + P_2(\xi_A)\,\lambda^2 + P_3(\xi_A)\,\lambda + P_4(\xi_A) = o \qquad (5.5)$$

Coefficients P_i are expressed in function of ξ_A in Appendix C.

Then the following procedure is used to compute the limit loads:

— A combination of modes $(i, k_1, k_2\, \ell)$ is selected.

— For a given ξ_A, coefficients P_i are evaluated and equation (5.3) (or equation (5.5) in the two-mode case) is solved.

— A "good" root of (5.3) or (5.5) is selected by continuity from the initial value $\lambda^* = o$ for $\xi_A = o$.

— ξ_A is incremented until the first local maximum in λ is reached which is defined as the buckling load (λ_B) corresponding to the given mode combination.

— The same calculations are performed for different ℓ to determine the minimum buckling load λ_B with respect to the circumferential wave numbers.

2. Calculations for the Two-mode Case

Buckling loads were determined for shell A8 using the experimental modulus coefficients available as imperfections coefficients. Numerical results are listed in Table II for both the cosine and sine axial representation. The same calculations were also performed using the imperfection model (4.7). The corresponding results are listed in Tables III and IV.

3. Calculations for the Three-mode Case

Buckling loads were determined for shell A8 using the following procedure. The critical mode combinations were found by using successively as imperfection coefficients A and B Fourier coefficients for the cosine axial representation and C and D Fourier coefficients for the sine axial representation. Results are listed in Tables V, VI, VIII and IX. The critical combinations are found to be:

$(i = 2,\ k_1 = 3,\ k_2 = 1,\ \ell = 13)$ for the cosine axial representation

and

$(i = 1,\ k_1 = 0.5,\ k_2 = 1,\ \ell = 10)$
$(i = 1.5,\ k_1 = 0.5,\ k_2 = 1,\ \ell = 10)$ for the sine axial
$(i = 1.5,\ k_1 = 0.5,\ k_2 = 2.5,\ \ell = 10)$ representation

Then a phase shifting (i.e., a change of reference of the y co-ordinate) was performed to determine the lowest buckling load for these critical combinations.

For the cosine axial representation $\rho_{k_1\ell}$, $\rho_{k_2\ell}$, $\varphi_{k_1\ell}$, $\varphi_{k_2\ell}$ are respectively the modulus Fourier coefficients and the phase angles of the asymmetric modes,

$$\begin{aligned} \rho_{k_1\ell} &= (A_{k_1\ell})^2 + (B_{k_1\ell})^2 \\ \rho_{k_2\ell} &= (A_{k_2\ell})^2 + (B_{k_2\ell})^2 \\ \varphi_{k_1\ell} &= (tg)^{-1}\,(B_{k_1\ell}/A_{k_1\ell}) \\ \varphi_{k_2\ell} &= (tg)^{-1}\,(B_{k_2\ell}/A_{k_2\ell}) \end{aligned} \qquad (5.6)$$

Then the imperfection coefficients corresponding to the shifting angle φ can be defined as

$$\xi_{k_1 \ell}(\varphi) = \rho_{k_1 \ell} \cos(\varphi_{k_1 \ell} - \varphi)$$
$$\xi_{k_2 \ell}(\varphi) = \rho_{k_2 \ell} \cos(\varphi_{k_2 \ell} - \varphi) \qquad (5.7)$$

For the sine axial representation, the A and B Fourier coefficients are to be replaced by the C and D coefficients in (5.6).

For the critical mode combinations, the buckling load is represented as a function of the phase angle φ in Figs. 21 and 22. Finally the following buckling loads were found for shell A8:

$\lambda_B = 0.737$ for the cosine axial representation

$\lambda_B = 0.768$ for the sine axial representation

The same calculations were also performed using the imperfection model (4.7) in the same range of wave numbers values as for experimental Fourier coefficients. These results are listed in Tables VII and X.

Finally, the buckling loads were also determined in the case of two classical asymmetric modes using fitted data as imperfection coefficients since no experimental data were available for these high wave number modes. These results are listed in Tables XI and XII.

VI. DISCUSSION AND CONCLUSIONS

1. Properties of the Two-mode and Three-mode Solution

It was found, as previously in reference 7 that, for a given combination of axial wave numbers, minimum buckling loads occur when one of the asymmetric modes is nearly classical.

In addition the two-mode solution for the sine axial representation presents an interesting property. In this case, the coupling condition (2i odd) implies that the number of possible mode combinations is greater than for the cosine axial representation (i = 2k). However, it can be seen in Fig. 20 that, for the smooth distribution of the fitted imperfection coefficients, the minimum buckling loads occur when approximately $k \simeq i/2$. As for the three modes solution, it can be seen in Tables V, VI and VII that the critical loads corresponding to the various coupling cases are the following for the cosine axial representation.

Case A	λ_B	= 0.851	(experimental Fourier coefficients A)
	λ_B	= 0.850	(experimental Fourier coefficients B)
	λ_B	= 0.981	(fitted coefficients)
Case B_1	λ_B	= 0.936	(experimental Fourier coefficients A)
	λ_B	= 0.966	(experimental Fourier coefficients B)
	λ_B	= 0.976	(fitted coefficients)
Case C_1	λ_B	= 0.750	(experimental Fourier coefficients A)
	λ_B	= 0.770	(experimental Fourier coefficients B)
	λ_B	= 0.813	(fitted coefficients)

Then it can be concluded that the cases A and B which have

the same behavior in the buckling of a perfect shell, correspond to a weak coupling and that the case C corresponds to a strong coupling. This result could have been predicted in Part III.

Similarly, for the sine axial representation, it can be seen in Tables VIII, IX and X that the minimum buckling loads are the following for the various coupling cases:

Case A	λ_B = 0.851	(experimental Fourier coefficients C)
	λ_B = 0.776	(experimental Fourier coefficients D)
	λ_B = 0.894	(fitted coefficients)
Case B	λ_B = 0.862	(experimental Fourier coefficients C)
	λ_B = 0.777	(experimental Fourier coefficients D)
	λ_B = 0.780	(fitted coefficients)
Case C	λ_B = 0.852	(experimental Fourier coefficients C)
	λ_B = 0.771	(experimental Fourier coefficients D)
	λ_B = 0.780	(fitted coefficients)

It can also be concluded that the case A corresponds to a weak coupling and the cases B and C correspond to a strong coupling. The most important results to justify this statement are those obtained by the smooth imperfection distribution of the fitted data. In fact the low buckling loads obtained for experimental Fourier coefficients in the case A correspond to i = 1 and hence are caused by a very high axisymmetric imperfection (see Fig. 11). A comparison of the three-mode solution for various coupling strengths is shown in Fig. 23.

Moreover, another property of the three-mode solution should also be noted. For the cosine axial representation there exists one

k_2 for a given i and k_1 and for a given coupling case. For the sine axial representation there is no unique value of k_2 corresponding to a given i and k_1 and a coupling case, but, as can be seen in Table X, the solution is poorly sensitive to k_2.

2. Comparison between the Results for the Two-and Three-mode Solutions

As far as the experimental imperfection data are concerned for shell A8 (i.e., for $k \leq 3.5$ and $\ell \leq 24$) the lowest buckling loads are the following:

- for the cosine axial representation

$\lambda_B = 0.748$ in the two-mode case
for $i = 2$ $k = 1$ $\ell = 13$ (see Table II)

$\lambda_B = 0.739$ in the three-mode case
for $i = 2$ $k_2 = 1$ $k_1 = 3$ $\ell = 13$ (see Tables V and VI and Fig. 21)

- for the sine axial representation

$\lambda_B = 0.775$ in the two-mode case
for $i = 1.5$ $k = 0.5$ $\ell = 10$ (see Table II)

$\lambda_B = 0.768$ in the three-mode case
for $i = 1$, $k_1 = 0.5$ $k_2 = 1$, $\ell = 10$
and $i = 1.5$ $k_1 = 0.5$, $k_2 = 2.5$ $\ell = 10$
(see Tables VIII, IX and Fig. 22)

Then it can be concluded that, adding one nonclassical asymmetric mode to the two-mode solution produces only a small effect. The results for the two- and three-mode solutions for shell A8 are approximately ten per cent above the experimental buckling load (see Table I). Moreover for the minimum buckling load found in the three-mode case the axisymmetric and first asymmetric modes are found to be the same as the critical modes in the two-mode solution.

No experimental data were available for the high wave number modes involved in the Hutchinson and Koiter theories. However the results obtained by using the fitted data lead to interesting possibilities since the critical combinations of modes could be determined without any restriction on wave numbers in that case. In the two-mode solution, it can be seen in Table III that the critical modes correspond to the lowest axial wave numbers:

- for the cosine axial representation

$$\lambda_B = 0.819 \quad i = 1 \quad k = 0.5$$

- for the sine axial representation

$$\lambda_B = 0.780 \quad i = 0.5 \quad k = 0.5$$

The buckling loads corresponding to the closest mode combination from the Hutchinson's case were found to be (see Table IV):

- for the cosine axial representation

$$\lambda_B = 0.923 \quad (i = 15 \quad k = 7.5)$$

- for the sine axial representation

$$\lambda_B = 0.827 \quad (i = 14.5 \quad k = 7)$$

These combinations are less critical than the previous low wave number combinations. This can be explained as follows: despite the fact that the Hutchinson combination of modes presents the strongest imperfection sensitivity (see Figs. 20 to 30), the critical combinations of modes occur for low axial wave numbers which correspond to the most severe imperfections.

Similarly, by using fitted data as imperfection coefficients in the three-mode solution for the cosine axial representation it is found (see Tables VII and XI) that the critical combination of modes corresponds to the lowest axial wave numbers:

$$\lambda_B = 0.813 \quad \text{for} \quad i = 1 \qquad k_1 = 1.5 \qquad k_2 = 0.5$$

For high axial wave numbers, the most critical combination was found to correspond to Koiter's theory:

$$\lambda_B = 0.901 \quad \text{for} \quad i = 15 \qquad k_1 = 0.5 \qquad k_2 = 14.5$$

For the sine axial representation, the most critical low wave number combination was found to be:

$$i = 0.5 \qquad k_1 = 0.5 \qquad k_2 = 1 \qquad (\lambda_B = 0.780)$$

But a high wave number combination with two classical asymmetric modes was found to be more critical (see Tables X and XII).

$$i = 1.5 \qquad k_1 = 0.5 \qquad k_2 = 14.5 \qquad (\lambda_B = 0.613)$$

It is interesting to note that this critical case does not occur for the classical axisymmetric mode but for a low wave number axisymmetric mode. Then a strong effect can exist if one imperfection,

even if small, corresponding to another classical asymmetric mode is added to the two imperfections corresponding to a low axial wave number combination in the two-mode case. For example, the buckling load $\lambda_B = 0.835$ which was found in the two-mode case for:

$$i = 1.5 \quad k_1 = 0.5 \quad \ell = 10$$

$$\xi_A = 0.040 \quad \xi_1 = 0.077$$

is decreased to the value 0.613 if the following classical asymmetric mode with the same circumferential wave number is added:

$$k_2 = 14.5 \quad \ell = 10 \quad \xi_2 = 0.003 \qquad \text{(see Fig. 24)}$$

This strong effect was not observed for the cosine axial representation. This was due to the fact that the high wave number imperfections extrapolated by using the model (4.7) are much smaller for the cosine axial representation than for the other representation.

3. Comparison between the Cosine and Sine Axial Representations

As far as the experimental imperfection coefficients are concerned, the lower buckling loads are obtained for the cosine axial representation. However, for the fitted imperfection coefficients, the lower buckling loads are obtained for the sine axial representation. The following explanation of these results can be given: the sine axial representation solution is less imperfection sensitive than the cosine axial representation solution (see Figs. 25 to 30), but, on the other hand, the fitted imperfection distribution is much more concentrated

in low wave numbers for the cosine than for the sine axial representation (see Figs. 17 and 18).

4. Conclusions

The limitations of this analysis are the same as those of references 6 and 7.

The boundary conditions of the finite shell are not considered. However the displacements assumed in the case of the sine axial representation are more satisfactory, since they satisfy the simple support boundary conditions.

The analysis is only valid for small imperfections and deflections (of the order of some fraction of the wall thickness), since third order terms were neglected in the buckling equations.

In addition the results obtained by using high wave numbers fitted imperfection coefficients are only qualitative since the imperfection model (4.7) was obtained by fitting only experimental low wave number data ($k \leq 3.5$ and $\ell \leq 24$ for shell A8).

Having these limitations in mind, the following conclusions of the present analysis can be drawn.

i. As far as experimental data are concerned, the three-mode solution has only a small additional effect (less than five per cent) with respect to the two-mode solution.

ii. A possible important effect of interaction between a low wave number axisymmetric mode with two classical asymmetric modes can be predicted from the present analysis. However this last conclusion is only qualitative since no experimental data were

available for the high wave number modes involved in this coupling.

iii. Using fitted experimental data, the high wave number axisymmetric imperfections were not found to be important for either the two-mode or three-mode analysis.

iv. For the class of electroformed shells studied, the exponents of the power law used as an imperfection model were found to differ very much from those assumed by Donnell and Wan.

REFERENCES

1. Fung, Y. C. and Sechler, E. E.: Instability of Thin Elastic Shells, Structural Mechanics, Pergamon Press, 1960.

2. Weingarten, V. I., Morgan, E. T. and Seide, P.: Final Report on Development of Design Criteria for Elastic Stability of Thin Shell Structures. STL/TR 60-000-19425. Space Technology Laboratories, 1960.

3. Donnell, L. M. and Wan, C. C.: Effect of Imperfections on Buckling of Thin Cylinders and Columns under Axial Compression. J. Appl. Mech., Vol. 17, p. 73, 1950.

4. Koiter, W. T.: The Effect of Axisymmetric Imperfections on the Buckling of Cylindrical Shells under Axial Compression. Koninkl. Nederl. Akademie Van Wetenschappen-Amsterdam. Reprinted from Proceedings, Series B, 66, No. 5, 1963.

5. Koiter, W. T.: Elastic Stability and Postbuckling Behavior Proceedings Symposium Non Linear Problems, edited by R. E. Langer, University of Wisconsin Press, Madison, Wisconsin, 1963.

6. Hutchinson, T.: Axial Buckling of Pressurized Imperfect Cylindrical Shells, AIAA J., Vol. 3, pp. 1461-1466, Aug. 1965.

7. Arbocz, J. and Babcock, C. D.: The Effect of General Imperfections on the Buckling of Cylindrical Shells, J. of Appl. Mech., March 1969.

8. Thurston, E. A. and Freeland, M. A.: Buckling of Imperfect Cylinders under Axial Compression, NASA CR-541, July 1966.

9. Arbocz, J.: The Effect of General Imperfections on the Buckling of Cylindrical Shells. Ph. D. Thesis, California Institute of Technology, 1968.

10. Babcock, C. D.: The Buckling of Cylindrical Shells with an Initial Imperfection under Axial Compression Loading. Ph. D. Thesis, California Institute of Technology, 1962.

11. Marquardt, D. C.: An Algorithm for Least-Squares Estimation of Nonlinear Parameters, J. Soc. Industrial and Applied Math., Vol. 11, No. 2, June 1963.

APPENDIX A

Coefficients for the Cosine Axial Representation

In the following, the non-dimensional parameters listed below will be used:

$$\alpha_A^2 = i^2 \frac{RT}{2c} \left(\frac{2\pi}{L}\right)^2$$

$$\alpha_1^2 = k_1^2 \frac{RT}{2c} \left(\frac{2\pi}{L}\right)^2$$

$$\alpha_2^2 = k_2^2 \frac{RT}{2c} \left(\frac{2\pi}{L}\right)^2$$

$$\beta^2 = \ell^2 \frac{RT}{2c} \left(\frac{1}{R}\right)^2$$

$$\alpha_3^2 = (k_1+k_2)^2 \frac{RT}{2c} \left(\frac{2\pi}{L}\right)^2$$

$$\alpha_4^2 = (k_1-k_2)^2 \frac{RT}{2c} \left(\frac{2\pi}{L}\right)^2$$

$$\alpha_5^2 = (k_1+i)^2 \frac{RT}{2c} \left(\frac{2\pi}{L}\right)^2$$

$$\alpha_6^2 = (k_1-i)^2 \frac{RT}{2c} \left(\frac{2\pi}{L}\right)^2$$

$$\alpha_7^2 = (k_2+i)^2 \frac{RT}{2c} \left(\frac{2\pi}{L}\right)^2$$

$$\alpha_8^2 = (k_2-i)^2 \frac{RT}{2c} \left(\frac{2\pi}{L}\right)^2$$

$$\gamma_j^2 = \frac{\alpha_j^2}{(\alpha_j^2+\beta^2)^2} \qquad (j = 1, 2, \ldots, 8)$$

A-1. Stress Function Coefficients in (2.21)

$$K_1 = -\frac{Et^3}{2c} \frac{\xi_A}{\alpha_A^2}$$

$$K_2 = -\frac{Et^3}{2c} \gamma_1^2 \xi_1$$

$$K_3 = -\frac{Et^3}{2c}\gamma_2^2\xi_2$$

$$K_4 = -\frac{Et^3}{2}\frac{\alpha_A^2}{\alpha_5^2}\beta^2\gamma_5^2(\xi_A\xi_1+\xi_A\bar{\xi}_1+\bar{\xi}_A\xi_1)$$

$$K_5 = -\frac{Et^3}{2}\frac{\alpha_A^2}{\alpha_6^2}\beta^2\gamma_6^2(\xi_A\xi_1+\xi_A\bar{\xi}_1+\bar{\xi}_A\xi_1)$$

$$K_6 = -\frac{Et^3}{2}\frac{\alpha_A^2}{\alpha_7^2}\beta^2\gamma_7^2(\xi_A\xi_2+\xi_A\bar{\xi}_2+\bar{\xi}_A\xi_2)$$

$$K_7 = -\frac{Et^3}{2}\frac{\alpha_A^2}{\alpha_8^2}\beta^2\gamma_8^2(\xi_A\xi_2+\xi_A\bar{\xi}_2+\bar{\xi}_A\xi_2)$$

$$K_8 = -\frac{Et^3}{32}\frac{\beta^2}{\alpha_1^2}(\xi_1^2+2\xi_1\bar{\xi}_1)$$

$$K_9 = -\frac{Et^3}{32}\frac{\beta^2}{\alpha_2^2}(\xi_2^2+2\xi_2\bar{\xi}_2)$$

$$K_{10} = -\frac{Et^3}{32}\left\{\frac{\alpha_1^2}{\beta^2}(\xi_1^2+2\xi_1\bar{\xi}_1)+\frac{\alpha_2^2}{\beta^2}(\xi_2^2+2\xi_2\bar{\xi}_2)\right\}$$

$$K_{11} = -\frac{Et^3}{4}\frac{\beta^2}{\alpha_3^2}(\xi_1\xi_2+\xi_1\bar{\xi}_2+\bar{\xi}_1\xi_2)$$

$$K_{12} = -\frac{Et^3}{4}\frac{\beta^2}{\alpha_4^2}(\xi_1\xi_2+\xi_1\bar{\xi}_2+\bar{\xi}_1\xi_2)$$

$$K_{13} = -\frac{Et^3}{4}\frac{\alpha_4^2}{\alpha_3^2}\beta^2\gamma_3^2(\xi_1\xi_2+\xi_1\bar{\xi}_2+\bar{\xi}_1\xi_2)$$

$$K_{14} = -\frac{Et^3}{4}\frac{\alpha_3^2}{\alpha_4^2}\beta^2\gamma_4^2(\xi_1\xi_2+\xi_1\bar{\xi}_2+\bar{\xi}_1\xi_2)$$

A-2. Error Function Coefficients in (2.22)

$$E_1 = \alpha_A^2\{\lambda_A\xi_A - \lambda(\xi_A+\bar{\xi}_A)\}$$

$$E_2 = \alpha_1^2\{\lambda_1\xi_1 - \lambda(\xi_1+\bar{\xi}_1)\}$$

$$E_3 = \alpha_2^2\{\lambda_2\xi_2 - \lambda(\xi_2+\bar{\xi}_2)\}$$

$$E_4 = \frac{c\beta^2}{8}(\xi_1^2+2\xi_1\bar{\xi}_1) + c\alpha_1^2\beta^2\gamma_1^2\xi_1(\xi_1+\bar{\xi}_1)$$

$$E_5 = \frac{c\beta^2}{8}(\xi_2^2+2\xi_2\bar{\xi}_2) + c\alpha_2^2\beta^2\gamma_2^2\xi_2(\xi_2+\bar{\xi}_2)$$

$$E_6 = \frac{c\beta^2}{4}\{(\xi_1\xi_2+\bar{\xi}_1\xi_2+\xi_1\bar{\xi}_2)+\alpha_3^2\gamma_1^2\xi_1(\xi_2+\bar{\xi}_2)+\alpha_3^2\gamma_2^2\xi_2(\xi_1+\bar{\xi}_1)\}$$

$$E_7 = \frac{c\beta^2}{4}\{(\xi_1\xi_2+\bar{\xi}_1\xi_2+\xi_1\bar{\xi}_2)+\alpha_4^2\gamma_1^2\xi_1(\xi_2+\bar{\xi}_2)+\alpha_4^2\gamma_2^2\xi_2(\xi_1+\bar{\xi}_1)\}$$

$$E_8 = \frac{c\beta^2}{2}\{\xi_A(\xi_1+\bar{\xi}_1)+\alpha_A^2\gamma_1^2\xi_1(\xi_A+\bar{\xi}_A)+\alpha_A^2\gamma_5^2(\xi_A\xi_1+\xi_A\bar{\xi}_1+\bar{\xi}_A\xi_1)\}$$

$$E_9 = \frac{c\beta^2}{2}\{\xi_A(\xi_1+\bar{\xi}_1)+\alpha_A^2\gamma_1^2\xi_1(\xi_A+\bar{\xi}_A)+\alpha_A^2\gamma_6^2(\xi_A\xi_1+\xi_A\bar{\xi}_1+\bar{\xi}_A\xi_1)\}$$

$$E_{10} = \frac{c\beta^2}{2}\{\xi_A(\xi_2+\bar{\xi}_2)+\alpha_A^2\gamma_2^2\xi_2(\xi_A+\bar{\xi}_A)+\alpha_A^2\gamma_7^2(\xi_A\xi_2+\xi_A\bar{\xi}_2+\bar{\xi}_A\xi_2)\}$$

$$E_{11} = \frac{c\beta^2}{2}\{\xi_A(\xi_2+\bar{\xi}_2)+\alpha_A^2\gamma_2^2\xi_2(\xi_A+\bar{\xi}_A)+\alpha_A^2\gamma_8^2(\xi_A\xi_2+\xi_A\bar{\xi}_2+\bar{\xi}_A\xi_2)\}$$

A-3. Coefficients of the Buckling Equations (2.35), (2.36), (2.37)

Cases A and B $\qquad k_1 \pm k_2 - i = 0 \quad (k_1 \neq k_2 \neq i/2)$

$$C_1 = \frac{c\beta^2}{4\alpha_A^2}$$

$$C_2 = \frac{c\beta^2}{4}\gamma_1^2$$

$$C_3 = \frac{c\beta^2}{4}\gamma_2^2$$

$$C_4 = C_5 = C_6 = C_7 = C_8 = C_9 = C_{10} = 0$$

$$C_{11} = \frac{c\beta^2}{2}\frac{\alpha_A^2}{\alpha_1^2}\gamma_1^2$$

$$C_{12} = \frac{c\beta^2}{2\alpha_1^2}$$

$$C_{13} = \frac{c\beta^2}{2}\frac{\alpha_A^2}{\alpha_1^2}\gamma_2^2$$

$$C_{14} = \frac{c\beta^2}{2}\frac{\alpha_A^2}{\alpha_2^2}\gamma_2^2$$

$$C_{15} = \frac{c\beta^2}{2\alpha_2^2}$$

$$C_{16} = \frac{c\beta^2}{2}\frac{\alpha_A^2}{\alpha_2^2}\gamma_1^2$$

$$C_{17} = C_{18} = C_{19} = 0$$

Case C. $k_1 = 3k_2$ $k_2 = i/2$

In this case, the coefficients C_i are the same as in Cases A and B, except the following:

$$C_6 = \frac{c\beta^2}{4\alpha_A^2}$$

$$C_7 = c\beta^2\frac{\alpha_2^2}{\alpha_A^2}\gamma_2^2$$

$$C_{17} = \frac{c\beta^2}{2}\frac{\alpha_A^2}{\alpha_2^2}\gamma_2^2$$

$$C_{18} = \frac{c\beta^2}{2\alpha_2^2}$$

$$C_{19} = \frac{c\beta^2}{2} \frac{\alpha_A^2}{\alpha_2^2} \gamma_2^2$$

A-4. Coefficients of the Buckling Equations (2.41), (2.42)

(Two-mode case: $k_1 = k_2$)

$$D_1 = \frac{c\beta^2}{16\alpha_1^2}$$

$$D_2 = \frac{c\beta^2}{4} \gamma_1^2$$

$$D_3 = 2c\beta^2\gamma_1^2$$

$$D_4 = \frac{c\beta^2}{2\alpha_1^2}$$

$$D_5 = 2c\beta^2\gamma_1^2$$

APPENDIX B

Coefficients for the Sine Axial Representation

B-1. Coefficients of the Buckling Equations (2.35), (2.36), (2.37)

First introduce the following wave numbers:

$$k_3 = k_1 + k_2$$

$$k_4 = k_1 - k_2$$

$$k_5 = k_1 + i$$

$$k_6 = k_1 - i$$

$$k_7 = k_2 + i$$

$$k_8 = k_2 - i$$

Case C (j odd, $(m_1 \pm m_2)$ even, $k_1 \neq k_2$)

$$C_1 = \frac{-2ik_1k_2}{(k_3^2 - i^2)(k_4^2 - i^2)} \frac{c\beta^2}{\pi\alpha_A^2}$$

$$C_2 = \frac{-2ik_1k_2}{(k_3^2 - i^2)(k_4^2 - i^2)} \frac{c\beta^2}{\pi} \gamma_1^2$$

$$C_3 = \frac{-2ik_1k_2}{(k_3^2 - i^2)(k_4^2 - i^2)} \frac{c\beta^2}{\pi} \gamma_2^2$$

$$C_4 = -\frac{i}{i^2 - 4k_1^2} \frac{c\beta^2}{2\pi\alpha_A^2}$$

$$C_5 = -\frac{i}{i^2 - 4k_1^2} \frac{2c\beta^2}{\pi} \frac{\alpha_1^2}{\alpha_A^2} \gamma_1^2$$

$$C_6 = -\frac{i}{i^2 - 4k_2^2} \frac{c\beta^2}{2\pi\alpha_A^2}$$

$$C_7 = -\frac{i}{i^2-4k_2^2}\,\frac{2c\beta^2}{\pi}\,\frac{\alpha_2^2}{\alpha_A^2}\,\gamma_2^2$$

$$C_8 = \frac{c\beta^2}{\pi}\,\frac{i}{k_1}\left(\frac{\gamma_5^2}{i+2k_1} - \frac{\gamma_6^2}{i-2k_1}\right)$$

$$C_9 = -\frac{4k_1^2}{i(i^2-4k_1^2)}\,\frac{c\beta^2}{\pi\alpha_1^2}$$

$$C_{10} = -\frac{4k_1^2}{i(i^2-4k_1^2)}\,\frac{c\beta^2}{\pi}\,\frac{\alpha_A^2}{\alpha_1^2}\,\gamma_1^2$$

$$C_{11} = \frac{c\beta^2}{\pi}\,\frac{\alpha_A^2}{\alpha_1^2}\,k_1\left(\frac{\gamma_7^2}{k_7^2-k_1^2} - \frac{\gamma_8^2}{k_8^2-k_1^2}\right)$$

$$C_{12} = \frac{-4ik_1k_2}{(k_7^2-k_1^2)(k_8^2-k_1^2)}\,\frac{c\beta^2}{\pi\alpha_1^2}$$

$$C_{13} = \frac{-4ik_1k_2}{(k_7^2-k_1^2)(k_8^2-k_1^2)}\,\frac{c\beta^2}{\pi}\,\frac{\alpha_A^2}{\alpha_1^2}\,\gamma_2^2$$

$$C_{14} = \frac{c\beta^2}{\pi}\,\frac{\alpha_A^2}{\alpha_2^2}\,k_2\left(\frac{\gamma_5^2}{k_5^2-k_2^2} - \frac{\gamma_6^2}{k_6^2-k_2^2}\right)$$

$$C_{15} = \frac{-4ik_1k_2}{(k_5^2-k_2^2)(k_6^2-k_2^2)}\,\frac{c\beta^2}{\pi\alpha_2^2}$$

$$C_{16} = \frac{-4ik_1k_2}{(k_5^2-k_2^2)(k_6^2-k_2^2)}\,\frac{c\beta^2}{\pi}\,\frac{\alpha_A^2}{\alpha_2^2}\,\gamma_1^2$$

$$C_{17} = \frac{c\beta^2}{\pi}\,\frac{i}{k_2}\left(\frac{\gamma_7^2}{i+2k_2} - \frac{\gamma_8^2}{i-2k_2}\right)$$

$$C_{18} = \frac{-4k_2^2}{i(i^2-4k_2^2)}\,\frac{c\beta^2}{\pi\alpha_2^2}$$

$$C_{19} = \frac{-4k_2^2}{i(i^2-4k_2^2)}\,\frac{c\beta^2}{\pi}\,\frac{\alpha_A^2}{\alpha_2^2}\,\gamma_2^2$$

Case A (j even, $(m_1 \pm m_2)$ odd, $k_1 \neq k_2$)

The coefficients of the buckling equations for Case A are identical to those of Case C except the following:

$$C_4 = C_5 = C_6 = C_7 = 0$$

$$C_8 = C_9 = C_{10} = 0$$

$$C_{17} = C_{18} = C_{19} = 0$$

Case B (j odd, $(m_1 \pm m_2)$ odd, $k_1 \neq k_2$)

The coefficients of the buckling equations for Case B are identical to those of Case C except the following:

$$C_1 = C_2 = C_3 = 0$$

$$C_{11} = C_{12} = C_{13} = 0$$

$$C_{14} = C_{15} = C_{16} = 0$$

B-2. Coefficients of the Buckling Equations (2.41), (2.42)

(Two-mode case, $k_1 = k_2 = k$)

$$D_1 = -\frac{i}{i^2-4k^2}\,\frac{c\beta^2}{2\pi\alpha_A^2}$$

$$D_2 = -\frac{k^2}{i(i^2-4k^2)}\,\frac{2c\beta^2}{\pi}\,\gamma_1^2$$

$$D_3 = \frac{c\beta^2}{\pi}\,\frac{i}{k}\left(\frac{\gamma_5^2}{i+2k} - \frac{\gamma_6^2}{i-2k}\right)$$

$$D_4 = -\frac{k^2}{i(i^2-4k^2)}\,\frac{4c\beta^2}{\pi\alpha_1^2}$$

$$D_5 = -\frac{i}{i^2-4k^2}\,\frac{4c\beta^2}{\pi}\,\gamma_1^2$$

APPENDIX C

Coefficients of (5.1) and (5.2) (three-mode solution)

$$S = -(\lambda_1^* + \lambda_2^*)$$

$$T = \lambda_1^*\lambda_2^* - [(C_{11}+C_{13})(\xi_A+\bar{\xi}_A)+C_{12}\xi_A][(C_{14}+C_{16})(\xi_A+\bar{\xi}_A)+C_{15}\xi_A]$$

$$S_1 = \lambda_2^*\bar{\xi}_1 + \xi_A[(C_{11}+C_{12})\bar{\xi}_2+(C_8+C_9)\bar{\xi}_1] - \bar{\xi}_2[(C_{11}+C_{13})(\xi_A+\bar{\xi}_A)+C_{12}\xi_A]$$

$$T_1 = -\lambda_2^*\xi_A[(C_{11}+C_{12})\bar{\xi}_2+(C_8+C_9)\bar{\xi}_1]$$
$$+\xi_A[(C_{14}+C_{15})\bar{\xi}_1+(C_{17}+C_{18})\bar{\xi}_2][(C_{11}+C_{13})(\xi_A+\bar{\xi}_A)+C_{12}\xi_A]$$

$$S_2 = \lambda_1^*\bar{\xi}_2 + \xi_A[(C_{14}+C_{15})\bar{\xi}_1+(C_{17}+C_{18})\bar{\xi}_2] - \bar{\xi}_1[(C_{14}+C_{16})(\xi_A+\bar{\xi}_A)+C_{15}\xi_A]$$

$$T_2 = -\lambda_1^*\xi_A[(C_{14}+C_{15})\bar{\xi}_1+(C_{17}+C_{18})\bar{\xi}_2]$$
$$+\xi_A[(C_{11}+C_{12})\bar{\xi}_2+(C_8+C_9)\bar{\xi}_1][(C_{14}+C_{16})(\xi_A+\bar{\xi}_A)+C_{15}\xi_A]$$

where:

$$\lambda_1^* = \lambda_1+(C_8+C_{10})(\xi_A+\bar{\xi}_A)+C_9\xi_A$$

$$\lambda_2^* = \lambda_2+(C_{17}+C_{19})(\xi_A+\bar{\xi}_A)+C_{18}\xi_A$$

Coefficients of the Fifth Order Polynomial in λ (5.3) (three-mode solution)

$$P_1 = -(\xi_A+\bar{\xi}_A)$$

$$P_2 = \lambda_A\xi_A - 2S(\xi_A+\bar{\xi}_A) - C_1\bar{\xi}_1\bar{\xi}_2 - C_4\frac{\bar{\xi}_1^2}{2} - C_6\frac{\bar{\xi}_2^2}{2}$$

$$P_3 = 2S\lambda_A\xi_A - (S^2+2T)(\xi_A+\bar{\xi}_A) - 2C_1\bar{\xi}_1\bar{\xi}_2S - (\bar{\xi}_1S+S_1)(C_3\bar{\xi}_2+C_5\bar{\xi}_1)$$
$$-(\bar{\xi}_2S+S_2)(C_2\bar{\xi}_1+C_7\bar{\xi}_2) - C_4\bar{\xi}_1^2S - C_6\bar{\xi}_2^2S$$

$$P_4 = (S^2+2T)\lambda_A\xi_A-2ST(\xi_A+\bar{\xi}_A)+C_1[S_1S_2-2\bar{\xi}_1\bar{\xi}_2T+\bar{\xi}_1S_2S+\bar{\xi}_2S_1S]$$
$$+(\bar{\xi}_1S+S_1)(C_3S_2+C_5S_1)+(\bar{\xi}_2S+S_2)(C_2S_1+C_7S_2)$$
$$-(\bar{\xi}_1T+T_1)(C_3\bar{\xi}_2+C_5\bar{\xi}_1)-(\bar{\xi}_2T+T_2)(C_2\bar{\xi}_1+C_7\bar{\xi}_2)$$
$$+C_4\frac{S_1^2}{2}+C_4\bar{\xi}_1(S_1S-\bar{\xi}_1T)+C_6\frac{S_2^2}{2}+C_6\bar{\xi}_2(S_2S-\bar{\xi}_2T)$$

$$P_5 = 2ST\lambda_A\xi_A-(\xi_A+\bar{\xi}_A)T^2+C_1[S_1T_2+S_2T_1]+(S_1T+ST_1)(C_1\bar{\xi}_2+C_4\bar{\xi}_1)$$
$$+(S_2T+ST_2)(C_1\bar{\xi}_1+C_6\bar{\xi}_2)+(\bar{\xi}_1S+S_1)(C_3T_2+C_5T_1)$$
$$+(\bar{\xi}_2S+S_2)(C_2T_1+C_7T_2)+(\bar{\xi}_1T+T_1)(C_3S_2+C_5S_1)$$
$$+(\bar{\xi}_2T+T_2)(C_2S_1+C_7S_2)+C_4S_1T_1+C_6S_2T_2$$

$$P_6 = \lambda_A\xi_AT^2+C_1(T_1T_2+\bar{\xi}_2T_1T+\bar{\xi}_1T_2T)+(\bar{\xi}_1T+T_1)(C_3T_2+C_5T_1)$$
$$+(\bar{\xi}_2T+T_2)(C_2T_1+C_7T_2)+C_4T_1(\frac{T_1}{2}+\bar{\xi}_1T)+C_6T_2(\frac{T_2}{2}+\bar{\xi}_2T)$$

Coefficients of the Third Order Polynomial in λ (5.5) (Two-mode solution)

$$P_1 = -(\xi_A+\bar{\xi}_A)$$

$$P_2 = \xi_A\lambda_A+2\lambda^*(\xi_A+\bar{\xi}_A)-\frac{D_1}{2}\bar{\xi}^2$$

$$P_3 = -2\lambda^*\xi_A\lambda_A-(\xi_A+\bar{\xi}_A)\lambda^{*2}+D_1\bar{\xi}^2\lambda^*-D_2\bar{\xi}^2(Q-\lambda^*)$$

$$P_4 = \xi_A\lambda_A\lambda^{*2}+D_1\bar{\xi}^2Q(\frac{Q}{2}-\lambda^*)+D_2\bar{\xi}^2Q(Q-\lambda^*)$$

where:

$$Q = \xi_A(D_3+D_4)$$

$$\lambda^* = \lambda_1+(D_3+D_5)(\xi_A+\bar{\xi}_A)+D_4\xi_A$$

TABLE I

CHARACTERISTICS OF SHELLS TESTED

Shell	$t.10^3$ inches	L inches	Experimental Buckling Loads
A7	4.494	7.00	0.597
A8	4.640	7.00	0.658
A9	4.540	7.00	0.736
A10	4.740	6.75	0.568
A12	4.740	7.25	0.673
A13	4.440	6.75	0.627
A14	4.370	6.75	0.711

Nominal Radius For All Shells: R = 4 inches

TABLE II

BUCKLING LOADS

Two-Mode Solution. Experimental Modulus Fourier Coefficients for Shell A8

Cosine Axial Representation ($k = \frac{i}{2}$)

i	1	2	3
ℓ	9	13	16
λ_B	0.818	0.748	0.878

Sine Axial Representation (2 i odd)

k \ i	0.5	1.5	2.5
0.5	$\ell = 10$ $\lambda_B = 0.801$	$\ell = 10$ $\lambda_B = 0.775$	$\ell = 10$ $\lambda_B = 0.544$
1	$\ell = 13$ $\lambda_B = 0.968$	$\ell = 13$ $\lambda_B = 0.854$	$\ell = 13$ $\lambda_B = 0.941$
1.5	$\ell = 16$ $\lambda_B = 0.981$	$\ell = 16$ $\lambda_B = 0.943$	$\ell = 16$ $\lambda_B = 0.947$
2	$\ell = 18$ $\lambda_B = 0.991$	$\ell = 18$ $\lambda_B = 0.968$	$\ell = 18$ $\lambda_B = 0.984$
2.5	$\ell = 20$ $\lambda_B = 0.993$	$\ell = 20$ $\lambda_B = 0.976$	$\ell = 20$ $\lambda_B = 0.989$
3	$\ell = 21$ $\lambda_B = 0.999$	$\ell = 21$ $\lambda_B = 0.987$	$\ell = 21$ $\lambda_B = 0.998$

TABLE III

BUCKLING LOADS FOR LOW WAVE NUMBER MODES

Two-Mode Solution. Fitted Imperfection Coefficients

Cosine Axial Representation ($k = \frac{i}{2}$)

i	1	2	3
ℓ	16	13	16
λ	0.819	0.936	0.956

Sine Axial Representation ($j = 2i$ odd)

k \ i	ℓ	0.5	1.5	2.5
0.5	10	0.780	0.835	0.935
1	13	0.947	0.899	0.903
1.5	16	0.971	0.963	0.921
2	18	0.983	0.978	0.971
2.5	20	0.988	0.986	0.982
3	21	0.993	0.991	0.989

TABLE IV

BUCKLING LOADS FOR HIGH WAVE NUMBER MODES

Two-Mode Solution. Fitted Imperfection Coefficients

Cosine Axial Representation ($k = \frac{i}{2}$)

i	5	8	11	15
ℓ	20	24	26	27
λ_B	0.969	0.969	0.949	0.923

Sine Axial Representation (j = 2i odd)

k \ i	ℓ	14.5
0.5	10	0.965
2.5	20	0.959
4	24	0.949
7	27	0.827
11.5	23	0.870

k \ i	ℓ	11.5
1.5	16	0.978
5.5	26	0.851
7	27	0.955

TABLE V

BUCKLING LOADS

Three-Mode Solution. Cosine Axial Representation. Experimental Imperfection Coefficients for Shell A8. Fourier Series A.

k_1 / i	0.5	1.0	1.5	2.0	2.5	3.0
0.5		two-mode case (D)	k_2 = 1 (A) ℓ = 13 λ_B = 0.943	k_2 = 1.5(A) ℓ = 10 λ_B = 0.958	k_2 = 2 (A) ℓ = 10 λ_B = 0.961	k_2 = 2.5(A) ℓ = 10 λ_B = 0.991
1.0	k_2 = 0.5(B_1) ℓ = 13 λ_B = 0.936		k_2 = 0.5(A) ℓ = 13 λ_B = 0.943	two-mode case (D)	k_2 = 1.5 ℓ = 15 λ_B = 0.851	k_2 = 2(A) ℓ = 13 λ_B = 0.947
1.5	k_2 = 1(B_1) ℓ = 13 λ_B = 0.964	k_2 = 0.5(C_1) ℓ = 10 λ_B = 0.891		k_2 = 0.5(A) ℓ = 10 λ_B = 0.958	k_2 = 1(A) ℓ = 15 λ_B = 0.851	two-mode case (D)

TABLE V (cont'd)

BUCKLING LOADS

Three-Mode Solution. Cosine Axial Representation. Experimental Imperfection Coefficients for Shell A8. Fourier Series A.

k_1^i	0.5	1.0	1.5	2.0	2.5	3.0
2.0	$k_2 = 1.5(B_1)$ $\ell = 17$ $\lambda_B = 0.987$	$k_2 = 1(B_1)$ $\ell = 13$ $\lambda_B = 0.992$	$k_2 = 0.5(B_1)$ $\ell = 17$ $\lambda_B = 0.999$		$k_2 = 0.5$ $\ell = 10$ $\lambda_B = 0.961$	$k_2 = 1$ $\ell = 13$ $\lambda_B = 0.941$
2.5	$k_2 = 2(B_1)$ $\ell = 19$ $\lambda_B = 0.978$	$k_2 = 1.5(B_1)$ $\ell = 20$ $\lambda_B = 0.996$	$k_2 = 1(B_1)$ $\ell = 13$ $\lambda_B = 0.993$	$k_2 = 0.5(B_1)$ $\ell = 20$ $\lambda_B = 0.987$		$k_2 = 0.5$ $\ell = 10$ $\lambda_B = 0.991$
3.0	$k_2 = 2.5(B_1)$ $\ell = 21$ $\lambda_B = 0.979$	$k_2 = 2(B_1)$ $\ell = 21$ $\lambda_B = 0.995$	$k_2 = 1.5(B_1)$ $\ell = 21$ $\lambda_B = 996$	$k_2 = 1(C_1)$ $\ell = 13$ $\lambda_B = 0.750$	$k_2 = 0.3(B_1)$ $\ell = 10$ $\lambda_B = 0.984$	

TABLE VI

BUCKLING LOADS

Three-Mode Solution. Cosine Axial Representation. Experimental Imperfection Coefficients for Shell A8. Fourier Series B.

k_1 \ i	0.5	1.0	1.5	2.0	2.5	3.0
0.5		two-mode case (D)	k_2 = 1(A) ℓ = 13 λ_B = 0.944	k_2 = 1.5(A) ℓ = 10 λ_B = 0.944	k_2 = 2(A) ℓ = 10 λ_B = 0.954	k_2 = 2.5(A) ℓ = 10 λ_B = 0.984
1.0	k_2 = 0.5(B_1) ℓ = 13 λ_B = 0.966		k_2 = 0.5(A) ℓ = 13 λ_B = 0.944	two-mode case (D)	k_2 = 1.5(A) ℓ = 14 λ_B = 0.850	k_2 = 2(A) ℓ = 14 λ_B = 0.939
1.5	k_2 = 1(B_1) ℓ = 13 λ_B = 0.978	k_2 = 0.5(C_1) ℓ = 9 λ_B = 0.820		k_2 = 0.5(A) ℓ = 10 λ_B = 0.944	k_2 = 1(A) ℓ = 14 λ_B = 0.850	two mode case (D)

TABLE VI (cont'd)

BUCKLING LOADS

Three-Mode Solution. Cosine Axial Representation. Experimental Imperfection Coefficients for Shell A8. Fourier Series A.

k_1	i	0.5	1.0	1.5	2.0	2.5	3.0
2.0		$k_2 = 1.5(B_1)$ $\ell = 17$ $\lambda_B = 0.974$	$k_2 = 1.5(B_1)$ $\ell = 13$ $\lambda_B = 0.995$	$k_2 = 0.5(B_1)$ $\ell = 17$ $\lambda_B = 0.997$		$k_2 = 0.5(A)$ $\ell = 10$ $\lambda_B = 954$	$k_2 = 1(A)$ $\ell = 14$ $\lambda_B = 0.939$
2.5		$k_2 = 2(B_1)$ $\ell = 18$ $\lambda_B = 0.983$	$k_2 = 1.5(B_1)$ $\ell = 20$ $\lambda_B = 0.996$	$k_2 = 1(B_1)$ $\ell = 13$ $\lambda_B = 0.996$	$k_2 = 0.5(B_1)$ $\ell = 10$ $\lambda_B = 0.983$		$k_2 = 0.5$ $\ell = 10$ $\lambda_B = 0.984$
3.0		$k_2 = 2.5(A)$ $\ell = 21$ $\lambda_B = 0.972$	$k_2 = 2(B_1)$ $\ell = 18$ $\lambda_B = 0.997$	$k_2 = 1.5(B_1)$ $\ell = 16$ $\lambda_B = 0.996$	$k_2 = 1.0(C_1)$ $\ell = 13$ $\lambda_B = 0.770$	$k_2 = 0.5(B_1)$ $\ell = 10$ $\lambda_B = 0.982$	

TABLE VII

BUCKLING LOADS

Three-Mode Solution. Cosine Axial Representation. Fitted Imperfection Coefficients

k_1 ^{i}	0.5	1.0	1.5	2.0	2.5	3.0
0.5		two-mode case (D)	k_2 = 1(A) ℓ = 10 λ_B = 0.981	k_2 = 1.5(A) ℓ = 10 λ_B = 0.990	k_2 = 2(A) ℓ = 10 λ_B = 0.994	k_2 = 2.5(A) ℓ = 10 λ_B = 0.999
1.0	k_2 =0.5(B_1) ℓ = 10 λ_B = 0.976		k_2 = 0.5(A) ℓ = 10 λ_B = 0.981	two-mode case (D)	k_2 = 1.5(A) ℓ = 13 λ_B = 0.992	k_2 = 2(A) ℓ = 13 λ_B = 0.997
1.5	k_2 = 1(B_1) ℓ = 13 λ_B = 0.992	k_2 = 0.5(C_1) ℓ = 10 λ_B = 0.813		k_2 = 0.5(A) ℓ = 10 λ_B = 990	k_2 = 1(A) ℓ = 13 λ_B = 992	two mode case (D)

TABLE VII (cont'd)

BUCKLING LOADS

Three-Mode Solution. Cosine Axial Representation. Fitted Imperfection Coefficients.

k_1 i	0.5	1.0	1.5	2.0	2.5	3.0
2.0	$k_2 = 1.5(B_1)$ $\ell = 16$ $\lambda_B = 0.996$	$k_2 = 1(B_1)$ $\ell = 13$ $\lambda_B = 0.998$	$k_2 = 0.5(B_1)$ $\ell = 10$ $\lambda_B = 0.999$		$k_2 = 0.5(A)$ $\ell = 10$ $\lambda_B = 0.996$	$k_2 = 1(A)$ $\ell = 13$ $\lambda_B = 0.997$
2.5	$k_2 = 2(B_1)$ $\ell = 18$ $\lambda_B = 0.997$	$k_2 = 1.5(B_1)$ $\ell = 16$ $\lambda_B = 0.998$	$k_2 = 1(B_1)$ $\ell = 13$ $\lambda_B = 0.999$	$k_2 = 0.5(B_1)$ $\ell = 10$ $\lambda_B = 1.000$		$k_2 = 0.5(A)$ $\ell = 10$ $\lambda_B = 0.999$
3.0	$k_2 = 2.5(B_1)$ $\ell = 20$ $\lambda_B = 0.997$	$k_2 = 2(B_1)$ $\ell = 18$ $\lambda_B = 0.998$	$k_2 = 1.5(B_1)$ $\ell = 16$ $\lambda_B = 998$	$k_2 = 1.0(C_1)$ $\ell = 13$ $\lambda_B = 0.934$	$k_2 = 0.5(B_1)$ $\ell = 10$ $\lambda_B = 1.000$	

TABLE VIII

BUCKLING LOADS

Three-Mode Solution - Sine Axial Representation. Experimental Fourier Coefficients C for Shell A8

k_1 i		0.5		1		1.5		2		2.5	
	k_2	ℓ	λ_B	ℓ	λ_B	ℓ	λ_B	ℓ	λ_B	ℓ	λ_B
0.5	1	10	0.933(B)	10	0.851(A)	10	0.864(B)	10	0.955(A)	14	0.998(B)
	1.5	10	0.934(C)			10	0.852(C)			10	0.983(C)
	2	10	0.934(B)	18	0.996(A)	10	0.864(B)	10	0.936(A)	10	0.984(B)
	2.5	10	0.933(C)			10	0.861(C)			10	0.984(C)
1	1.5	14	0.976(B)	14	0.909(A)	14	0.862(B)	14	0.861	14	0.948(B)
	2	18	0.948(C)			19	1.002(C)			18	0.875(C)
	2.5	14	0.976(B)	20	0.998(A)	14	0.863(B)	14	0.971(A)	14	0.948(B)
1.5	2	16	0.981(B)	17	0.941(A)	16	0.953(B)	17	0.954(A)	16	0.966(B)
	2.5	19	0.969(C)			16	1.017(C)			19	0.927(C)
2	2.5	18	0.993(B)	19	0.954(A)	18	0.970(B)	19	0.969(A)	18	0.986(B)

TABLE 1X

BUCKLING LOADS

Three-Mode Solution - Sine Axial Representation. Experimental Fourier Coefficients D for Shell A8

k_1	i	0.5		1		1.5		2		2.5	
	k_2	ℓ	λ_B	ℓ	λ_B	ℓ	λ_B	ℓ	λ_B	ℓ	λ_B
0.5	1	10	0.803(B)	10	0.776(A)	10	0.777(B)	10	0.923(A)	13	0.941(B)
	1.5	10	0.809(C)			10	0.773(C)			10	0.960(C)
	2	10	0.803(B)	18	0.996(A)	10	0.777(B)	10	0.898(A)	10	0.945(B)
	2.5	10	0.804(C)			10	0.771(C)			10	0.944(C)
1	1.5	13	0.969(B)	14	0.906(A)	14	0.874(B)	14	0.858	13	0.941(B)
	2	13	0.966(C)			19	1.004(C)			13	0.947(C)
	2.5	13	0.968(B)	20	0.994(A)	13	0.850(B)	20	0.970(A)	13	0.941(B)
1.5	2	16	0.989(B)	17	0.924(A)	16	0.944(B)	17	0.943(A)	16	0.949(B)
	2.5	20	0.947(C)			16	1.014(C)			20	0.900(C)
2	2.5	18	0.993(B)	19	0.943(A)	18	0.971(B)	19	0.962(A)	18	0.987(B)

TABLE X

BUCKLING LOADS

Three-Mode Solution. Sine Axial Representation. Fitted Imperfection Coefficients

k_1	i	0.5		1		1.5		2		2.5	
	k_2	ℓ	λ_B	ℓ	λ_B	ℓ	λ_B	ℓ	λ_B	ℓ	λ_B
0.5	1	10	0.780(B)	10	0.894(A)	10	0.835(B)	10	0.970(A)	13	0.903(B)
	1.5	10	0.786(C)			10	0.851(C)			10	0.950(C)
	2	10	0.780(B)	10	0.994(A)	10	0.835(B)	10	0.980(A)	10	0.935(B)
	2.5	10	0.780(C)			10	0.831(C)			10	0.933(C)
1	1.5	13	0.947(B)	14	0.949(A)	13	0.898(B)	14	0.962(A)	13	0.904(B)
	2	14	0.937(C)			14	0.907(C)			13	0.945(C)
	2.5	13	0.947(B)	13	0.994(A)	13	0.899(B)	13	0.992(A)	13	0.903(B)
1.5	2	16	0.971(B)	17	0.957(A)	16	0.963(B)	17	0.982(A)	16	0.921(B)
	2.5	16	0.947(C)			17	0.938(C)			17	0.889(C)
2	2.5	18	0.983(B)	19	0.963(A)	18	0.979(B)	19	0.984(A)	18	0.971(B)

TABLE XI

BUCKLING LOADS

Three-Mode Solution. Fitted Imperfection Coefficients

Case of Two Classical Asymmetric Modes

a. Cosine Axial Representation

i	k_1	k_2	ℓ	λ_B
15	0.5	14.5	10	0.901
15	1.5	13.5	16	0.918
15	2.5	12.5	20	0.920
15	5.5	9.5	26	0.923

i	k_1	k_2	ℓ	λ_B
14	14.5	0.5	10	0.904
12	13.5	1.5	16	0.948
10	12.5	2.5	20	0.976
4	9.5	5.5	26	0.995

i	k_1	k_2	ℓ	λ_B
7	10.5	3.5	23	0.984

TABLE XII

BUCKLING LOADS

Three-Mode Solution. Fitted Imperfection Coefficients

Case of Two Classical Asymmetric Modes

b. Sine Axial Representation

i	k_1	k_2	ℓ	λ_B
1.5	0.5	14.5	10	0.613
1.5	1.5	13.5	16	0.829
3.5	1.5	13.5	16	0.768
3.5	3.5	11.5	24	0.936
7.5	3.5	11.5	24	0.829
11.5	5.5	9.5	26	0.807
14.5	0.5	14.5	10	0.734
15	3	11.5	22	0.825
15	5.5	9	26	0.827

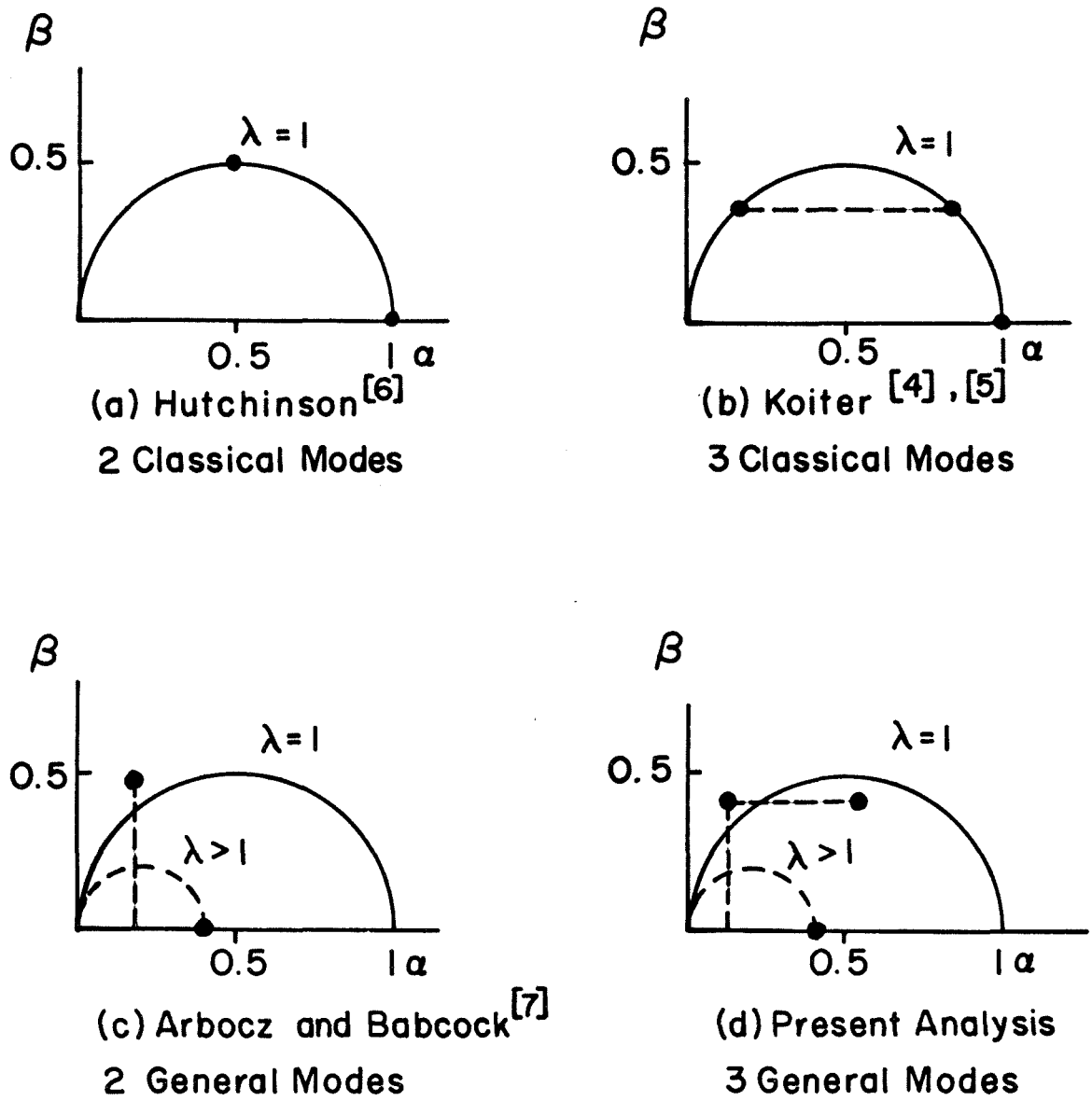

FIG. 1 COMPARISON OF MODE SELECTION IN PREVIOUS INVESTIGATIONS AND IN THE PRESENT ANALYSIS

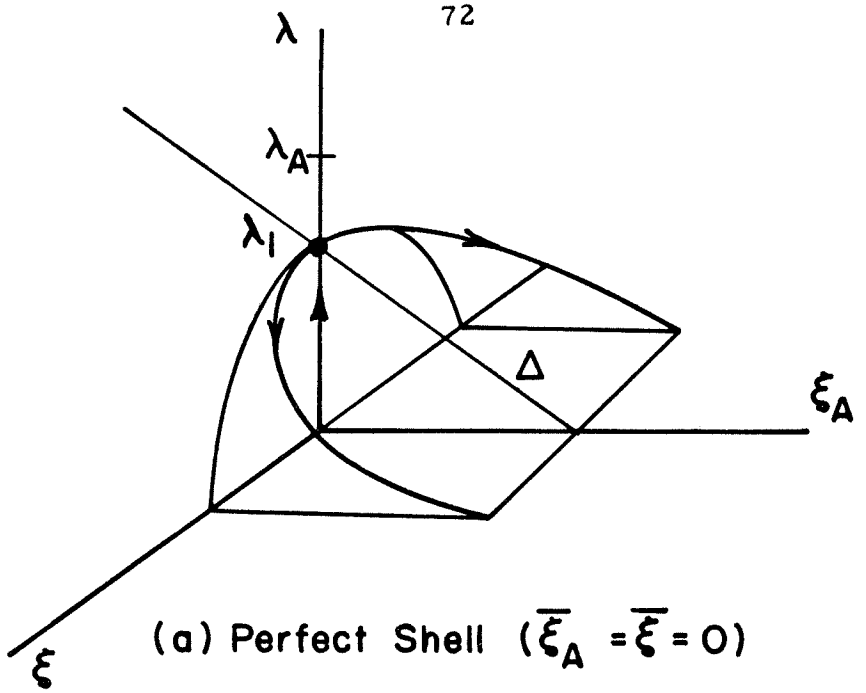

(a) Perfect Shell ($\bar{\xi}_A = \bar{\xi} = 0$)

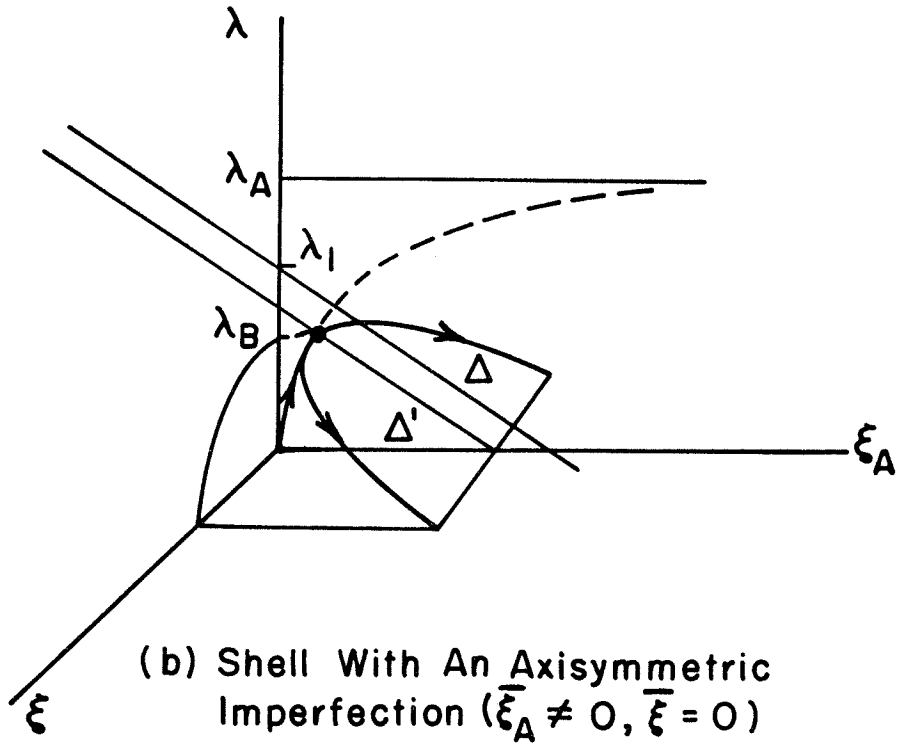

(b) Shell With An Axisymmetric Imperfection ($\bar{\xi}_A \neq 0, \bar{\xi} = 0$)

FIG. 2 BUCKLING OF A PERFECT SHELL AND OF A SHELL WITH AN AXISYMMETRIC IMPERFECTION FOR THE TWO-MODE SOLUTION

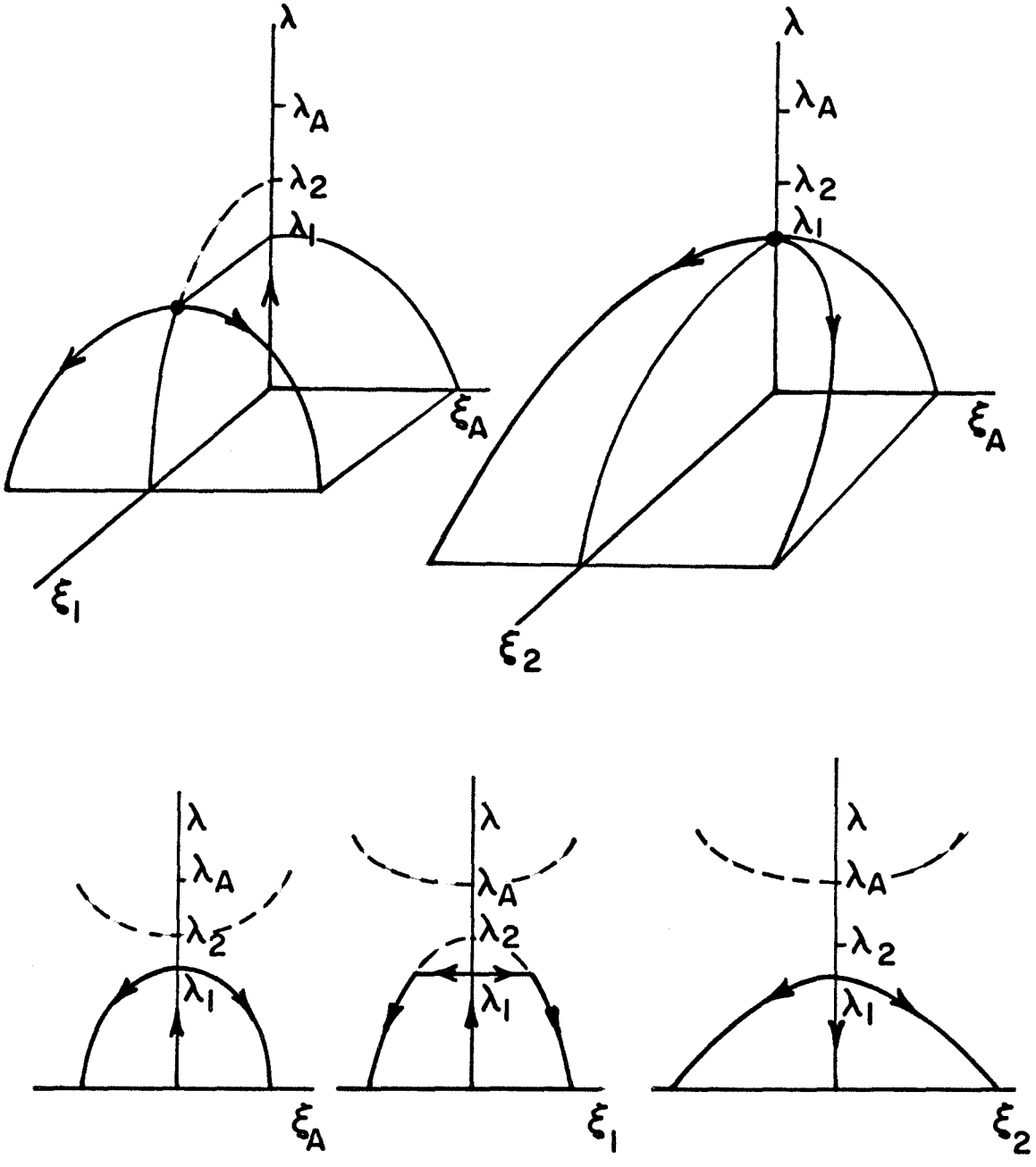

FIG. 3 BUCKLING OF A PERFECT SHELL FOR THE THREE-MODE SOLUTION

CASES A AND B
(COSINE AXIAL REPRESENTATION)

CASE A
(SINE AXIAL REPRESENTATION)

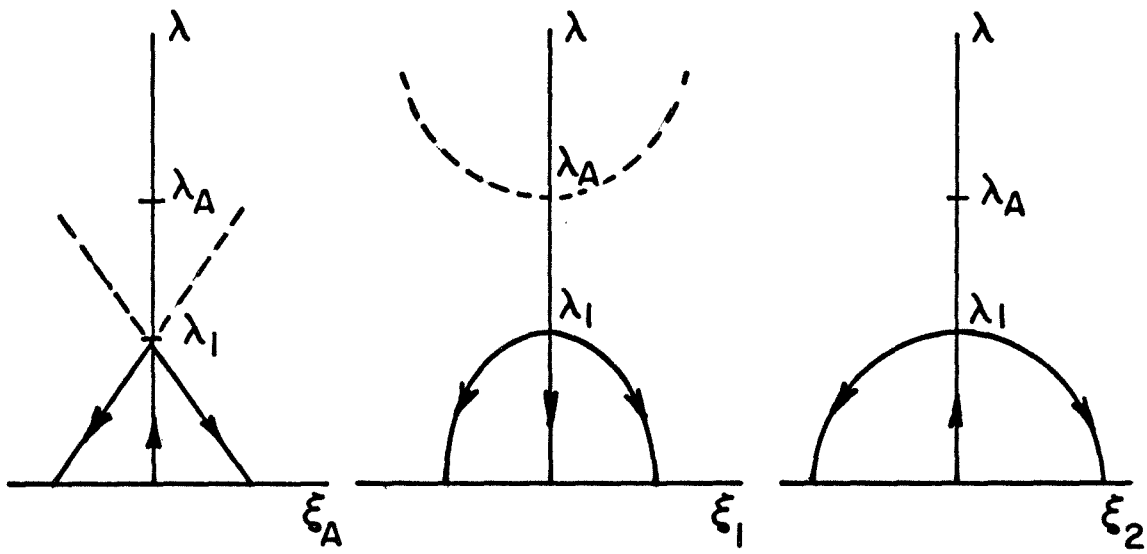

FIG. 4 BUCKLING OF A PERFECT SHELL FOR THE THREE-MODE SOLUTION IF $\lambda_1 = \lambda_2$

CASES A AND B
(COSINE AXIAL REPRESENTATION)
CASE A
(SINE AXIAL REPRESENTATION)

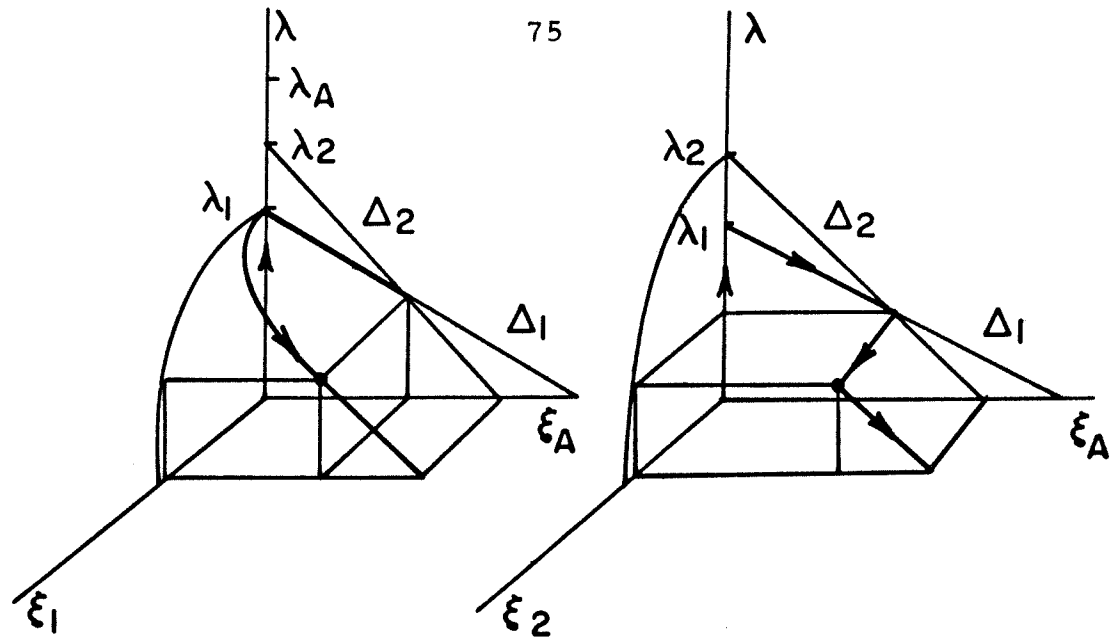

(a) $\lambda_1 < \lambda_2$

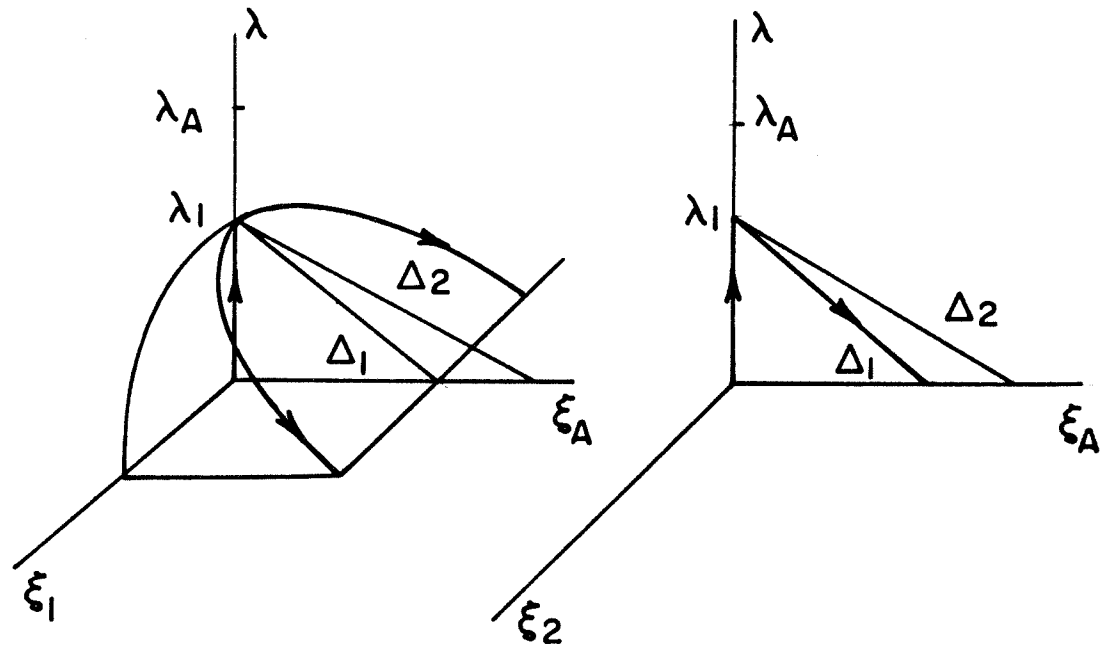

(b) $\lambda_1 = \lambda_2$

FIG. 5 BUCKLING OF A PERFECT SHELL FOR THE THREE-MODE SOLUTION

CASE B (SINE AXIAL REPRESENTATION)

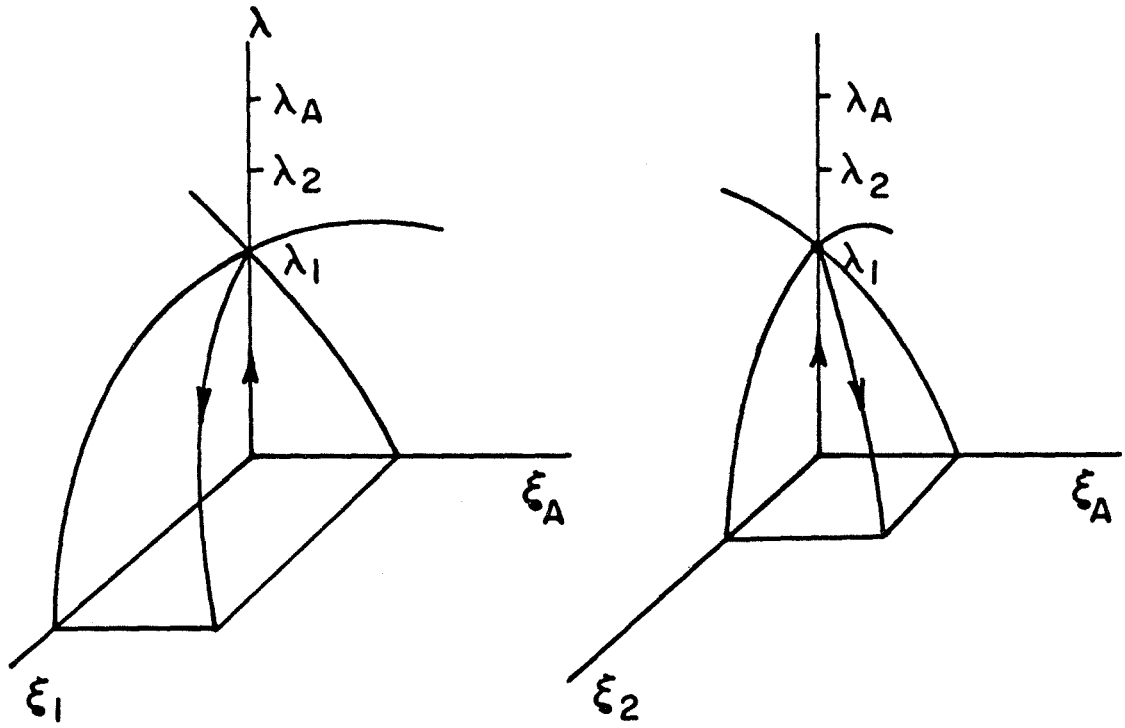

FIG. 6 BUCKLING OF A PERFECT SHELL FOR THE THREE-MODE SOLUTION (CASE C)

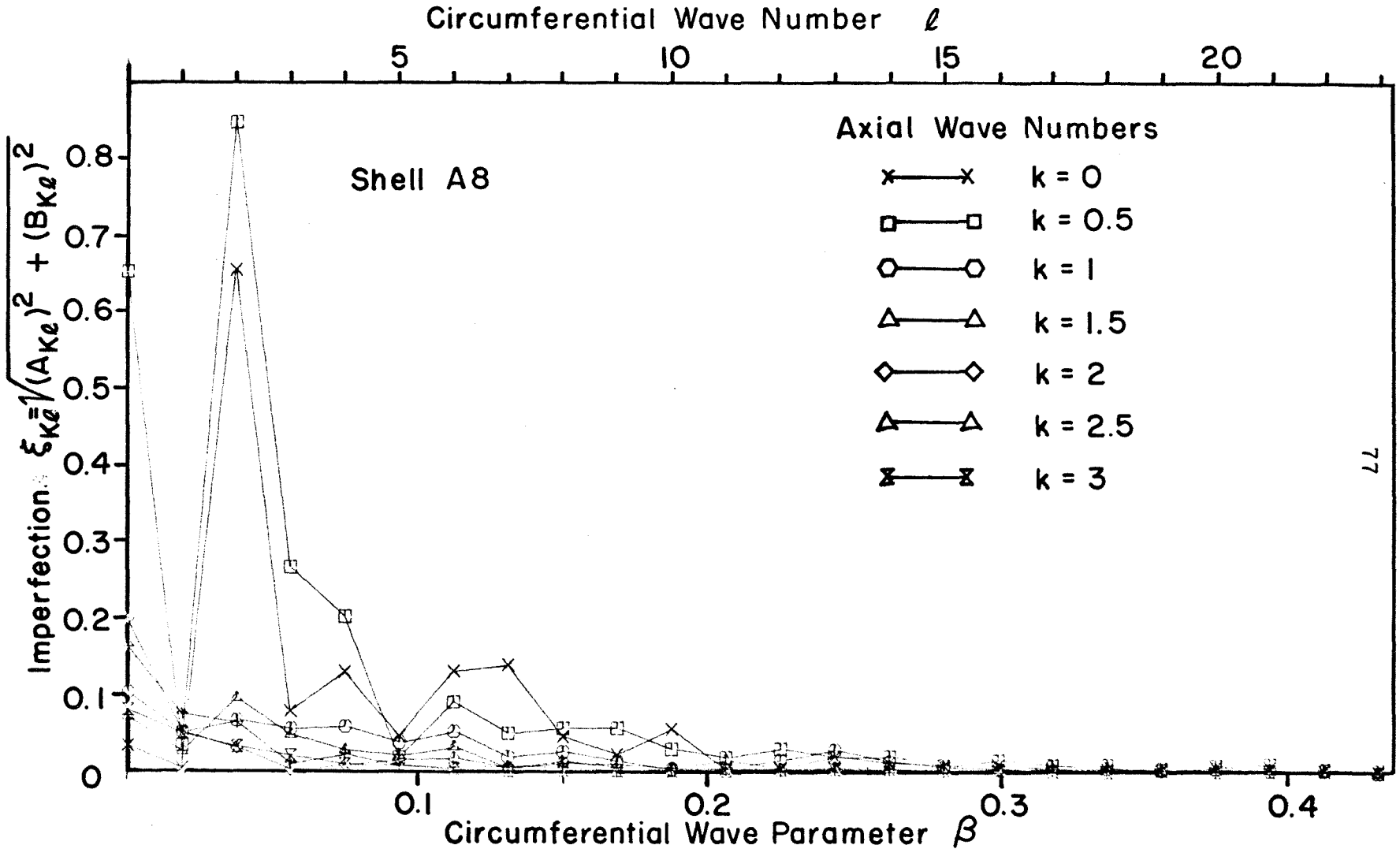

FIG. 7 EXPERIMENTAL FOURIER COEFFICIENTS–COSINE AXIAL REPRESENTATION

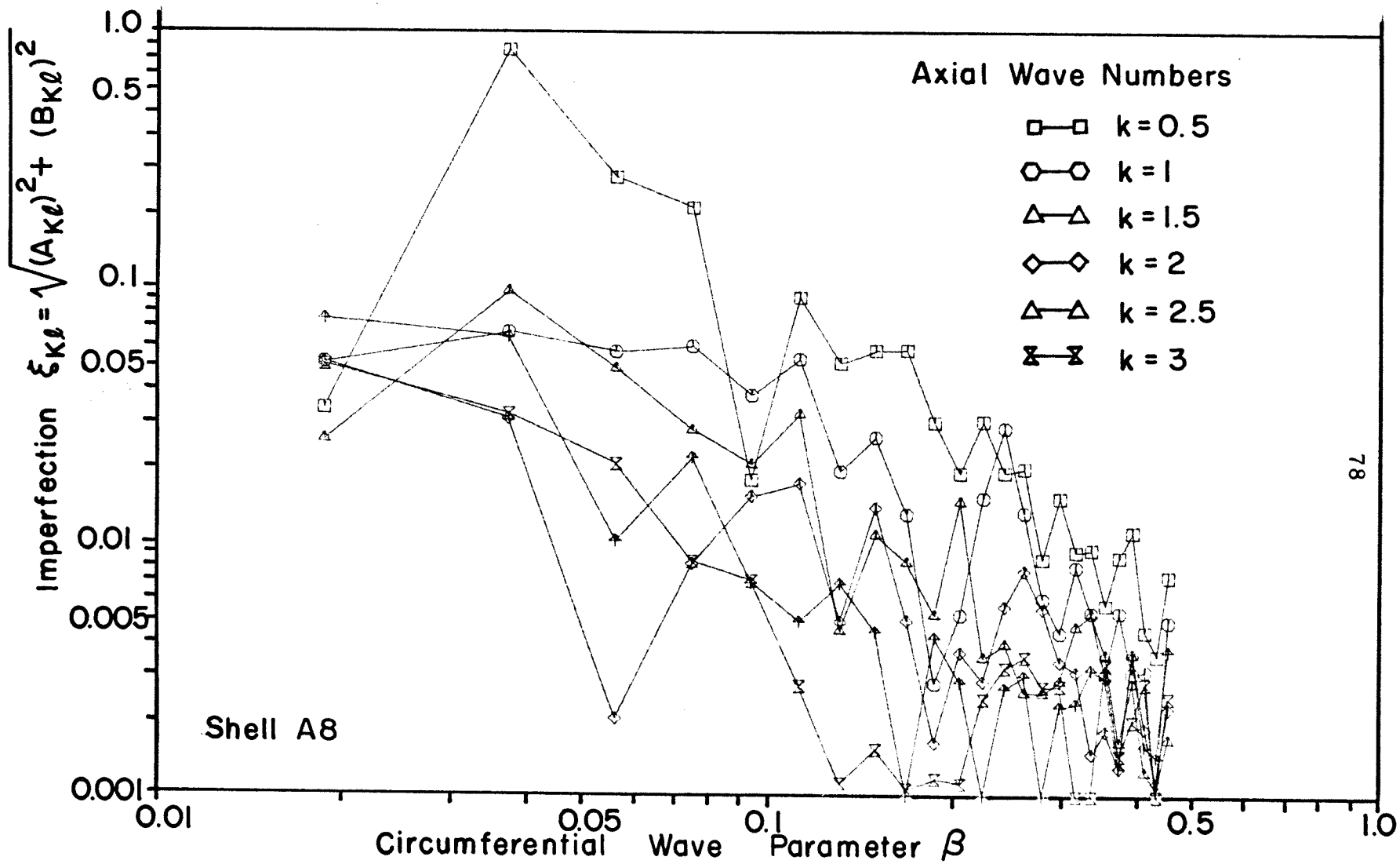

FIG. 8 EXPERIMENTAL FOURIER COEFFICIENTS-COSINE AXIAL REPRESENTATION

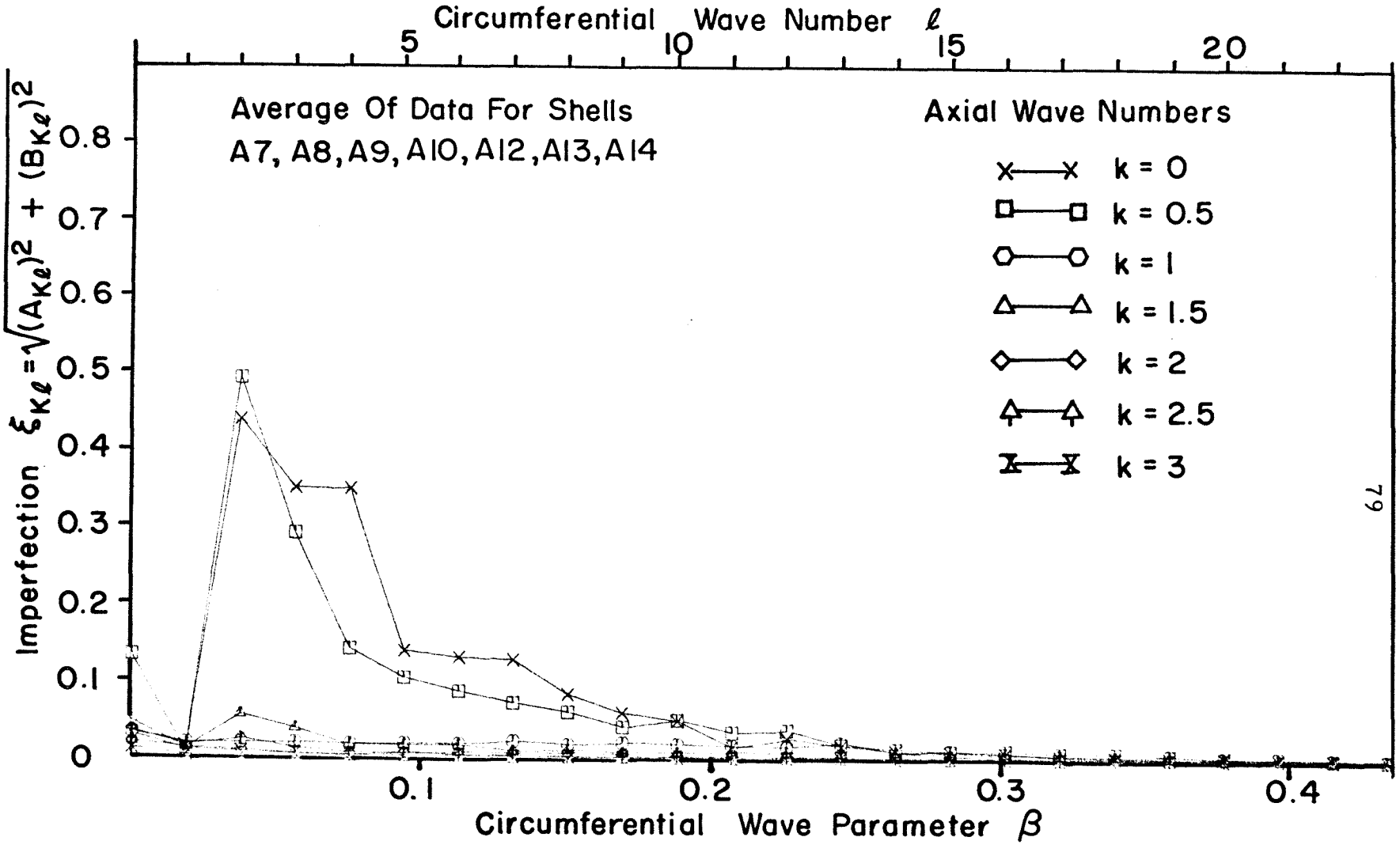

FIG. 9 EXPERIMENTAL FOURIER COEFFICIENTS - COSINE AXIAL REPRESENTATION

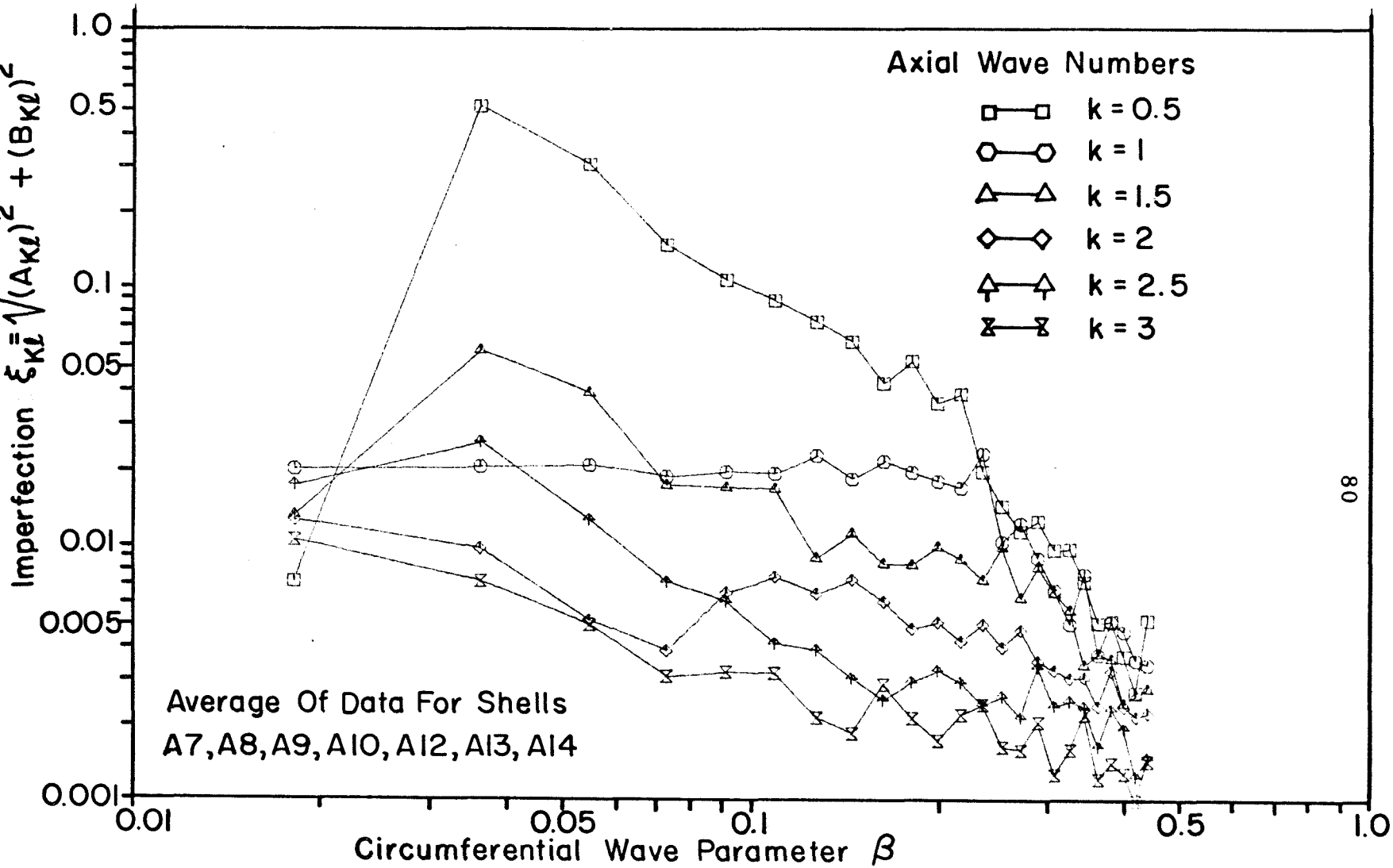

FIG. 10 EXPERIMENTAL FOURIER COEFFICIENTS - COSINE AXIAL REPRESENTATION

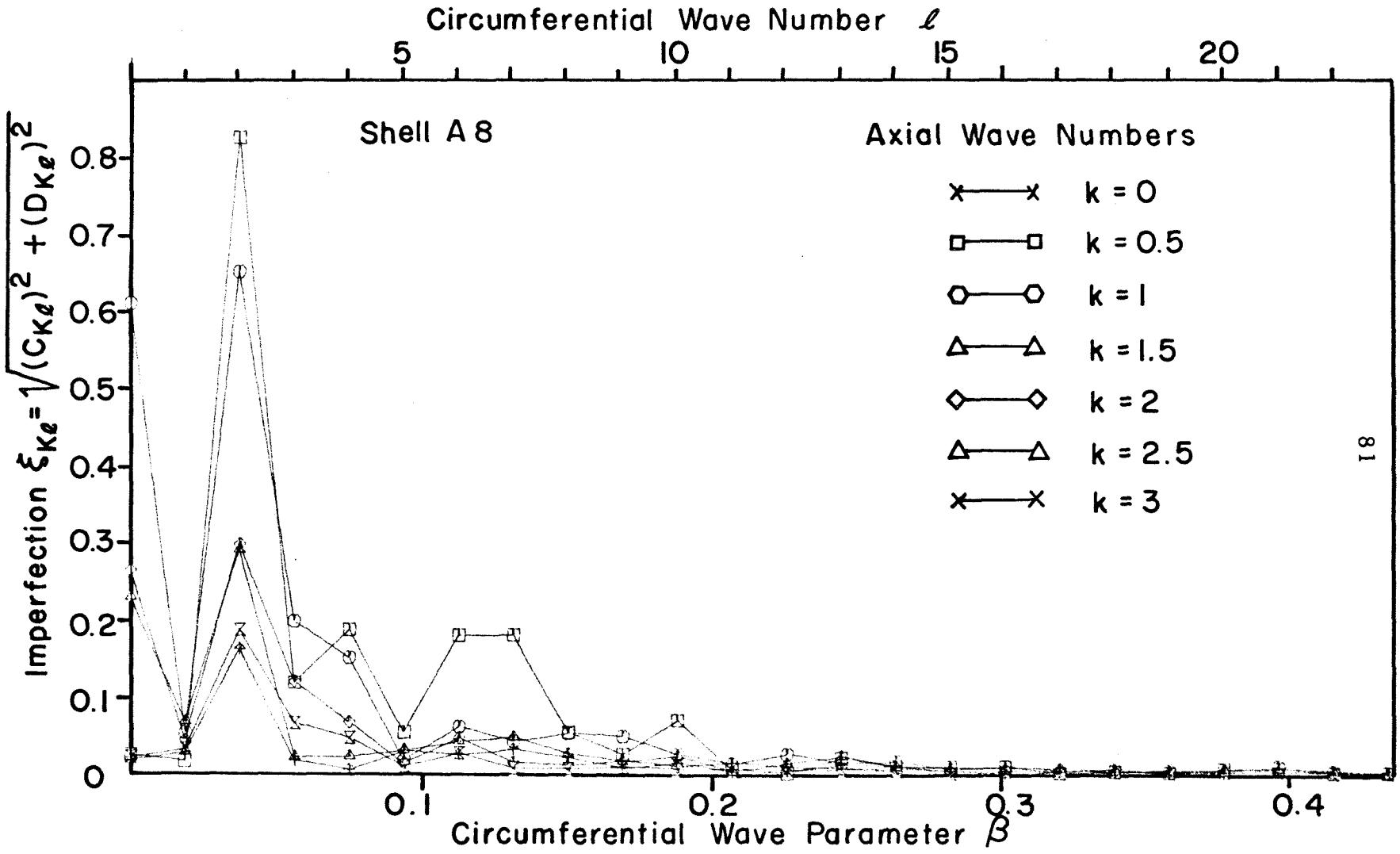

FIG. 11 EXPERIMENTAL FOURIER COEFFICIENTS-SINE AXIAL REPRESENTATION

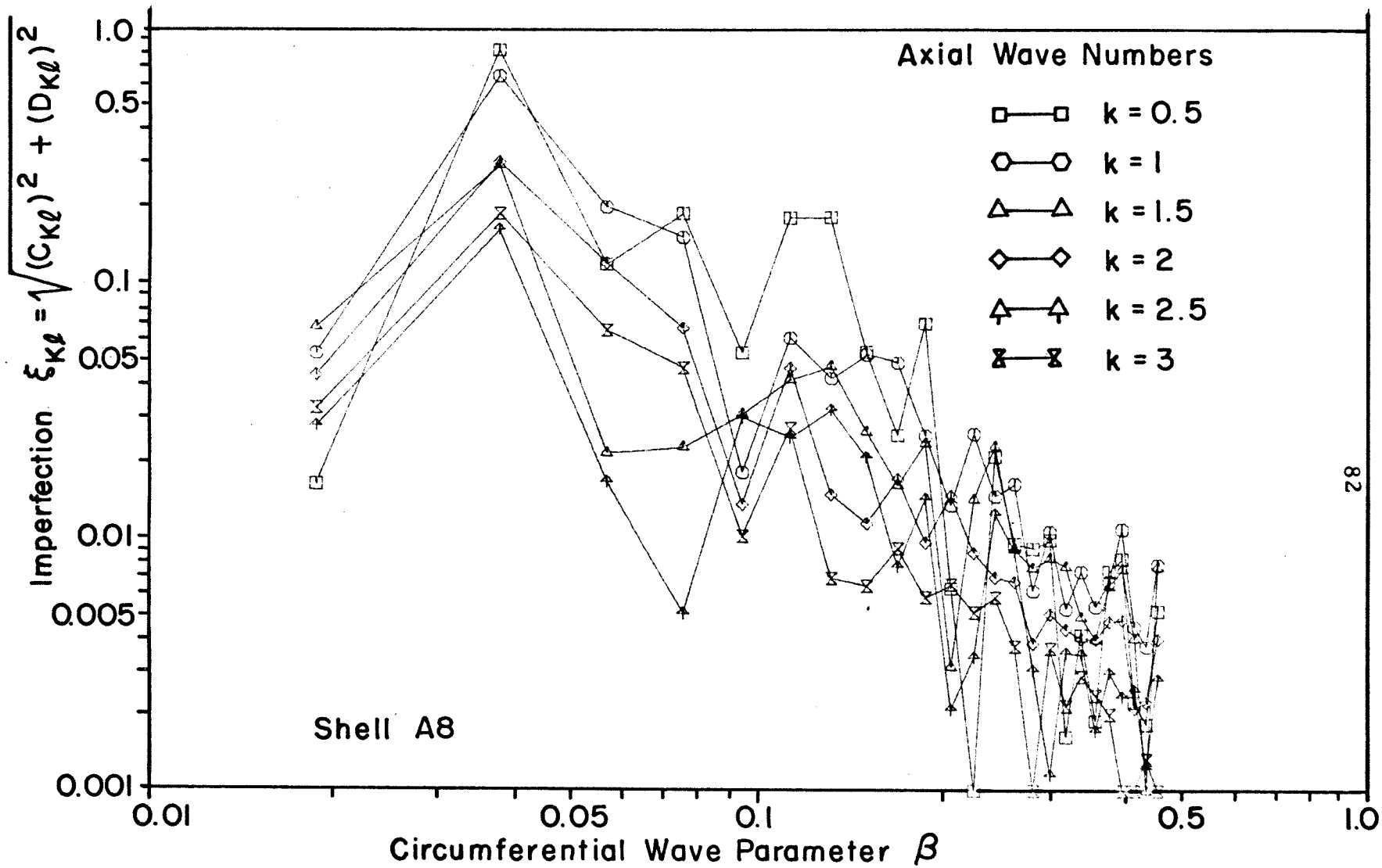

FIG. 12 EXPERIMENTAL FOURIER COEFFICIENTS - SINE AXIAL REPRESENTATION

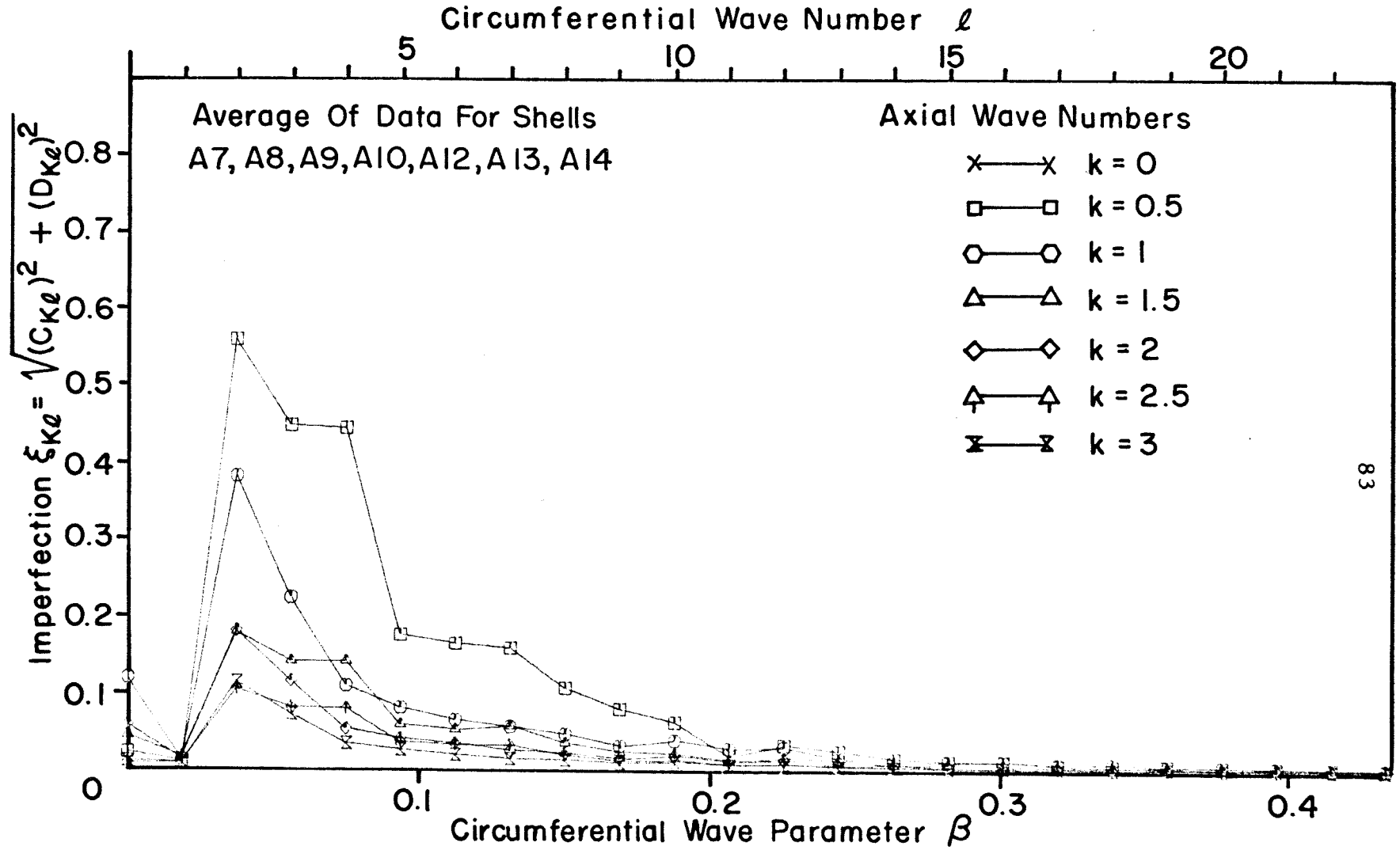

FIG. 13 EXPERIMENTAL FOURIER COEFFICIENTS - SINE AXIAL REPRESENTATION

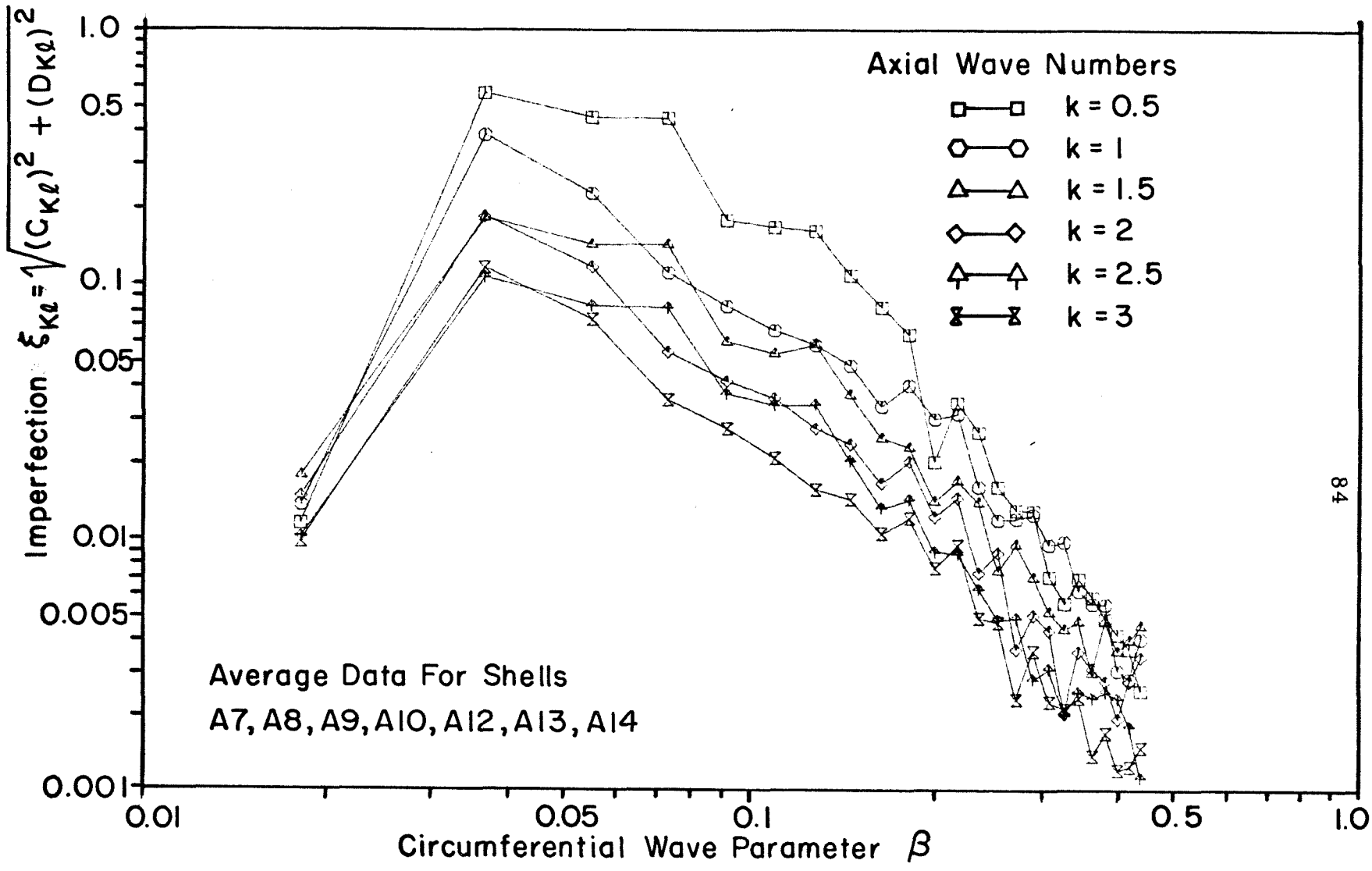

FIG.14 EXPERIMENTAL FOURIER COEFFICIENTS-SINE AXIAL REPRESENTATION

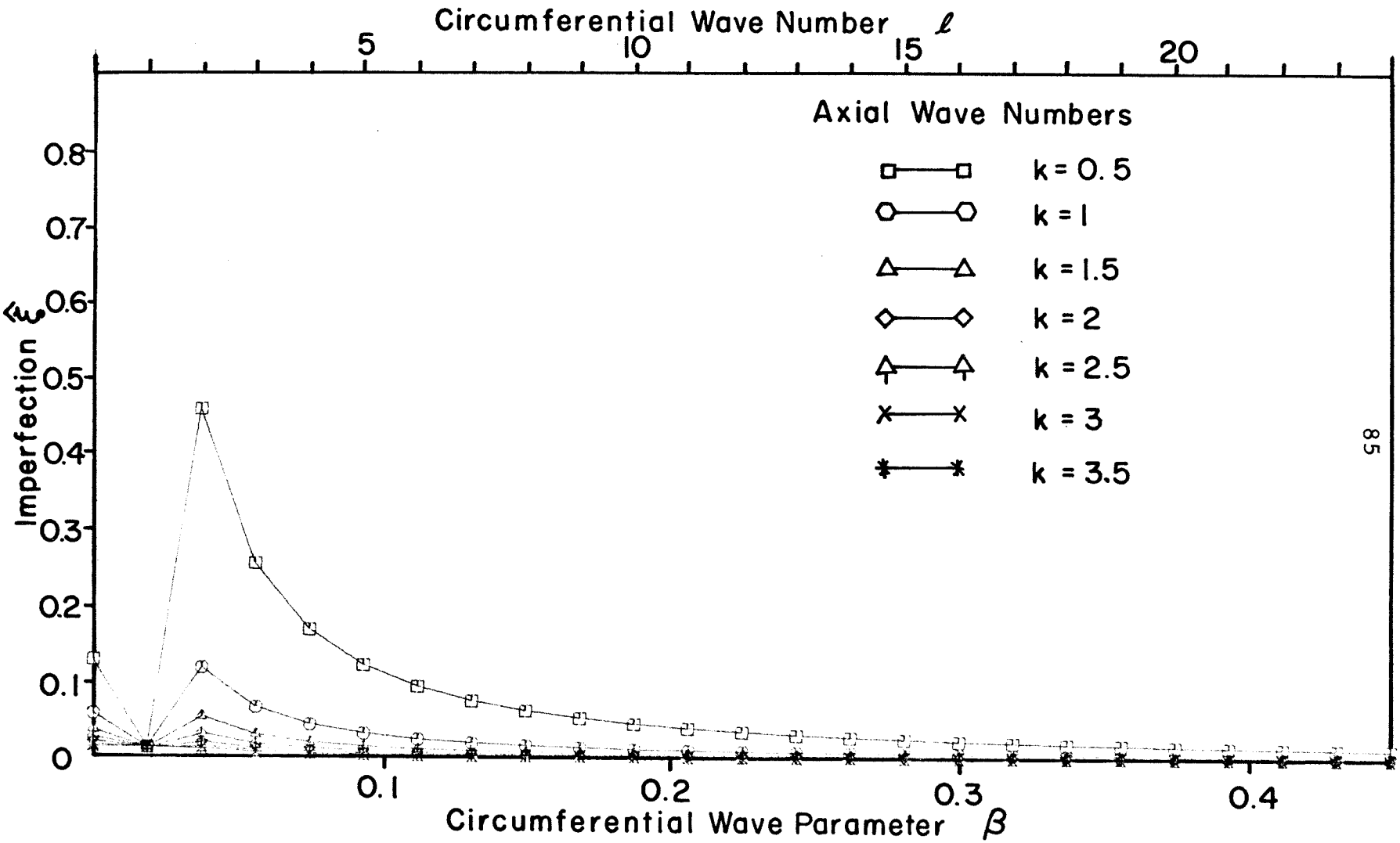

FIG. 15 FITTED IMPERFECTION COEFFICIENTS — COSINE AXIAL REPRESENTATION

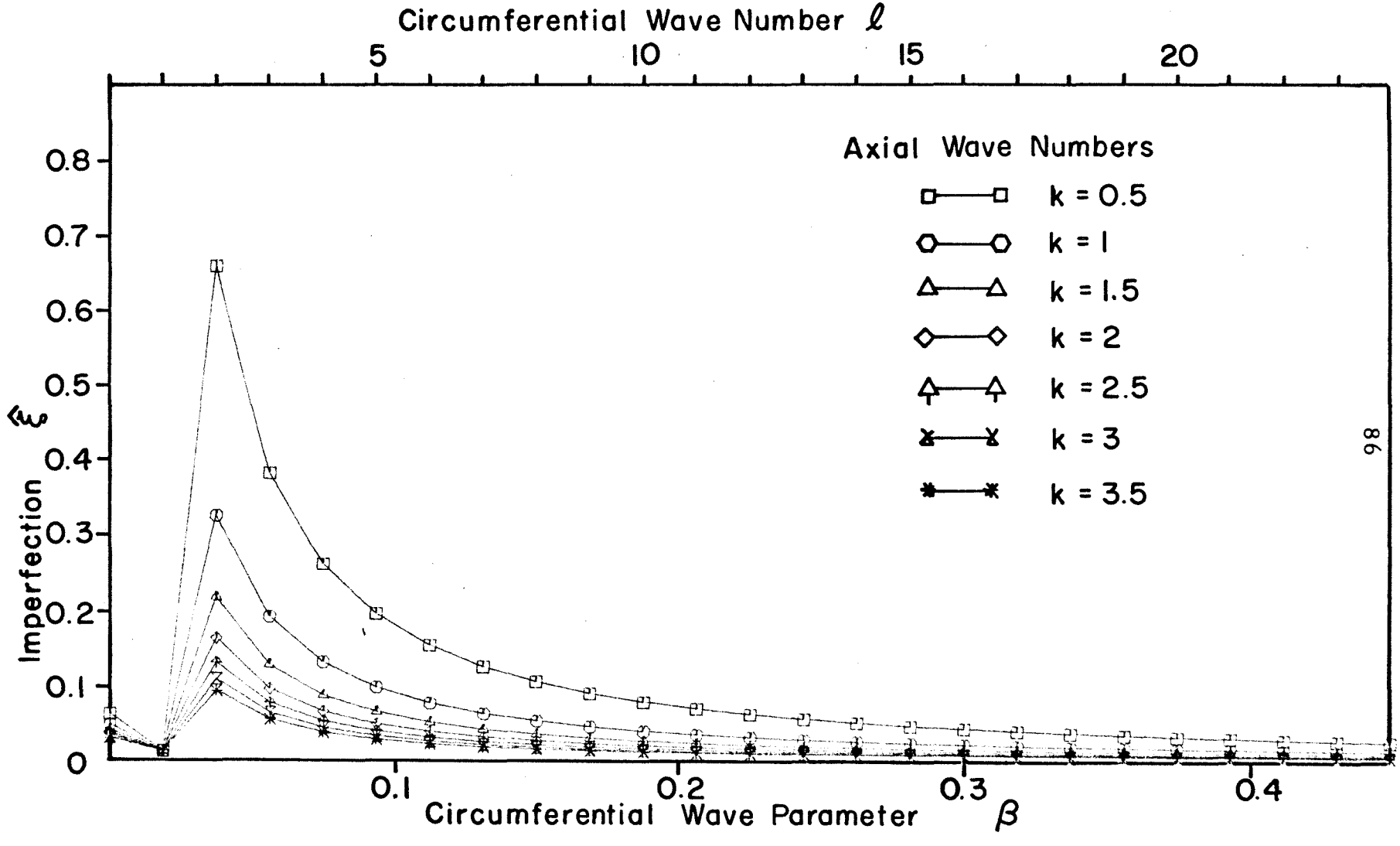

FIG. 16 FITTED IMPERFECTION COEFFICIENTS — SINE AXIAL REPRESENTATION

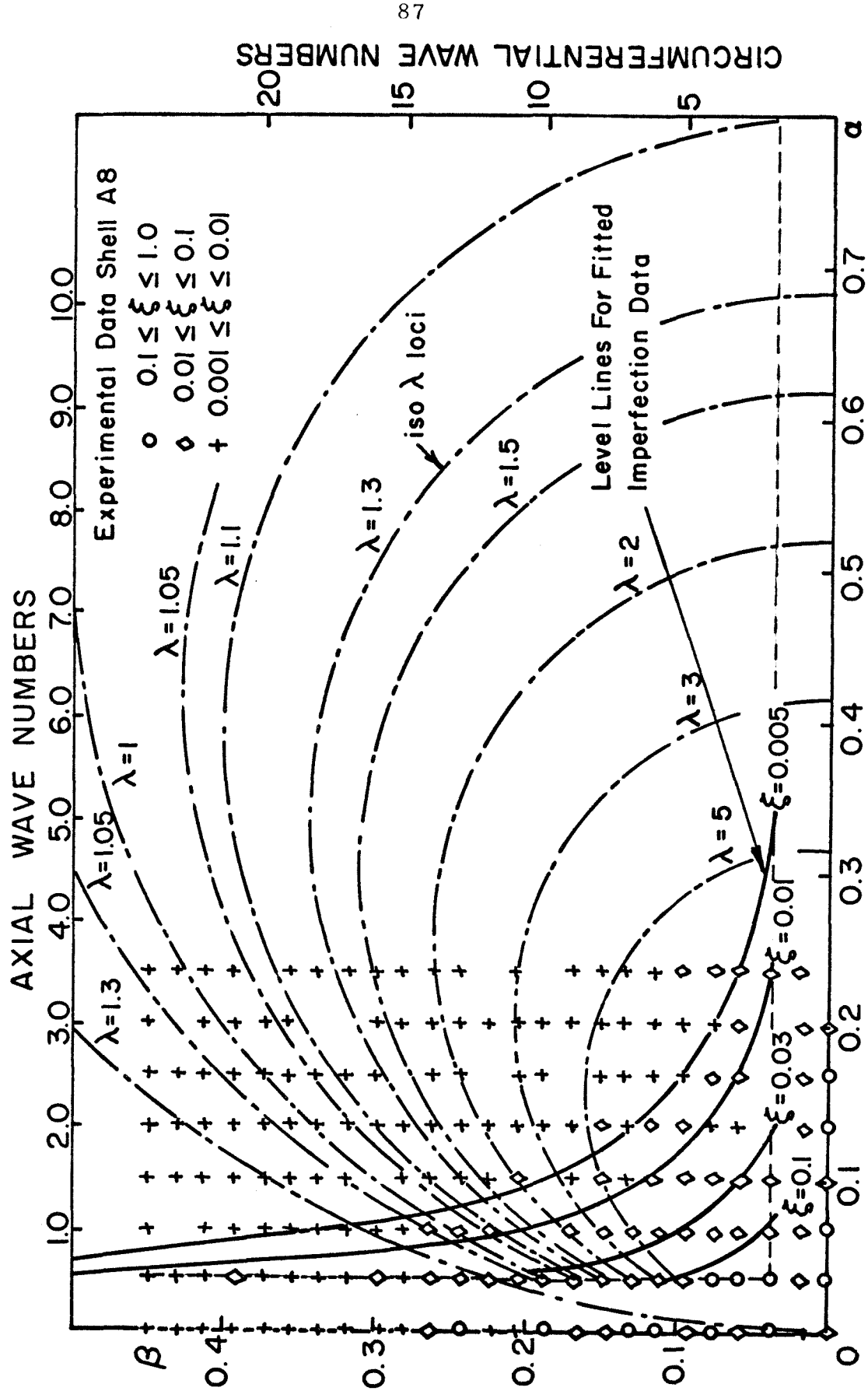

FIG. 17 IMPERFECTIONS FOR THE COSINE AXIAL REPRESENTATION

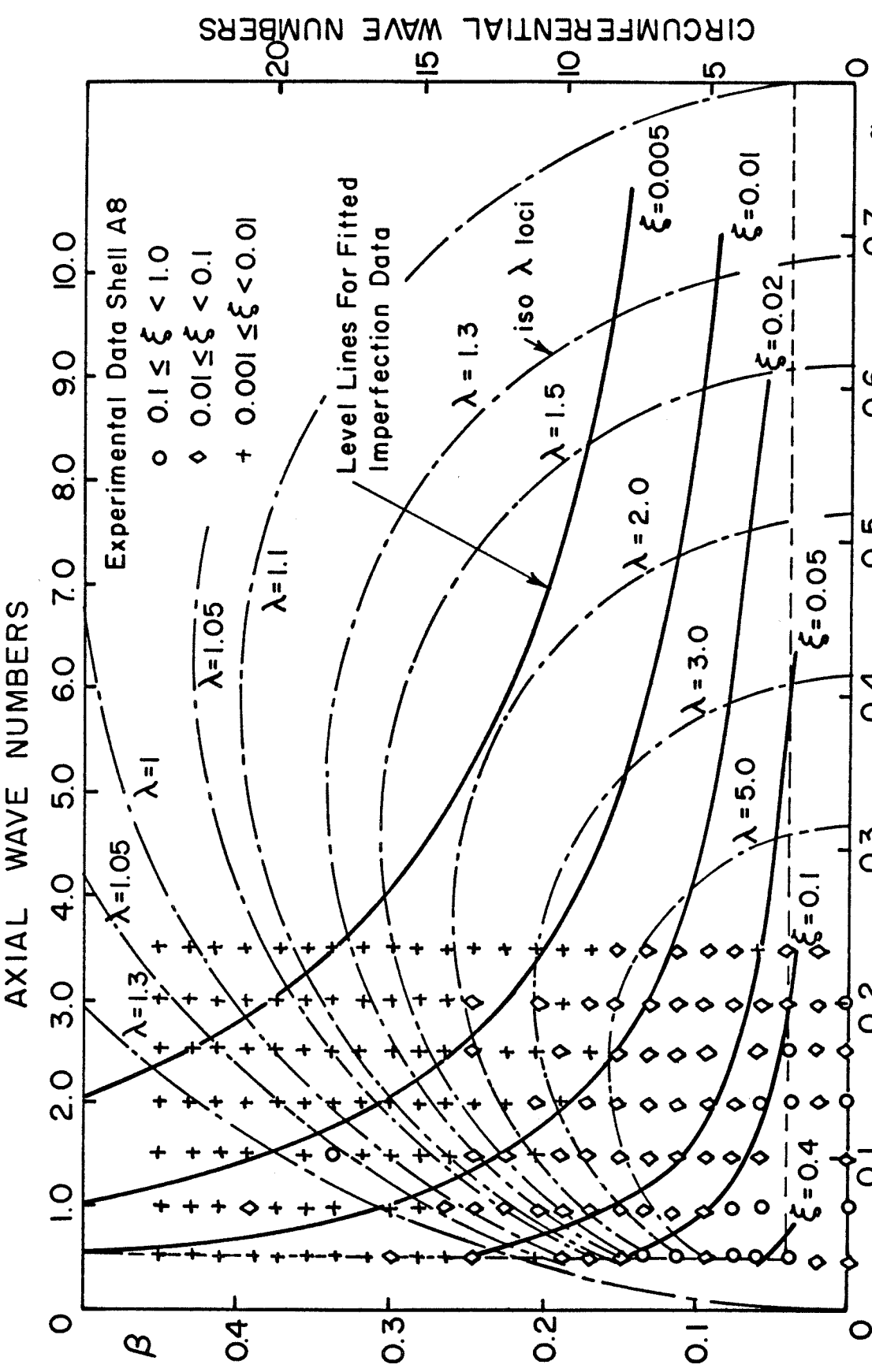

FIG. 18 IMPERFECTIONS FOR THE SINE AXIAL REPRESENTATION

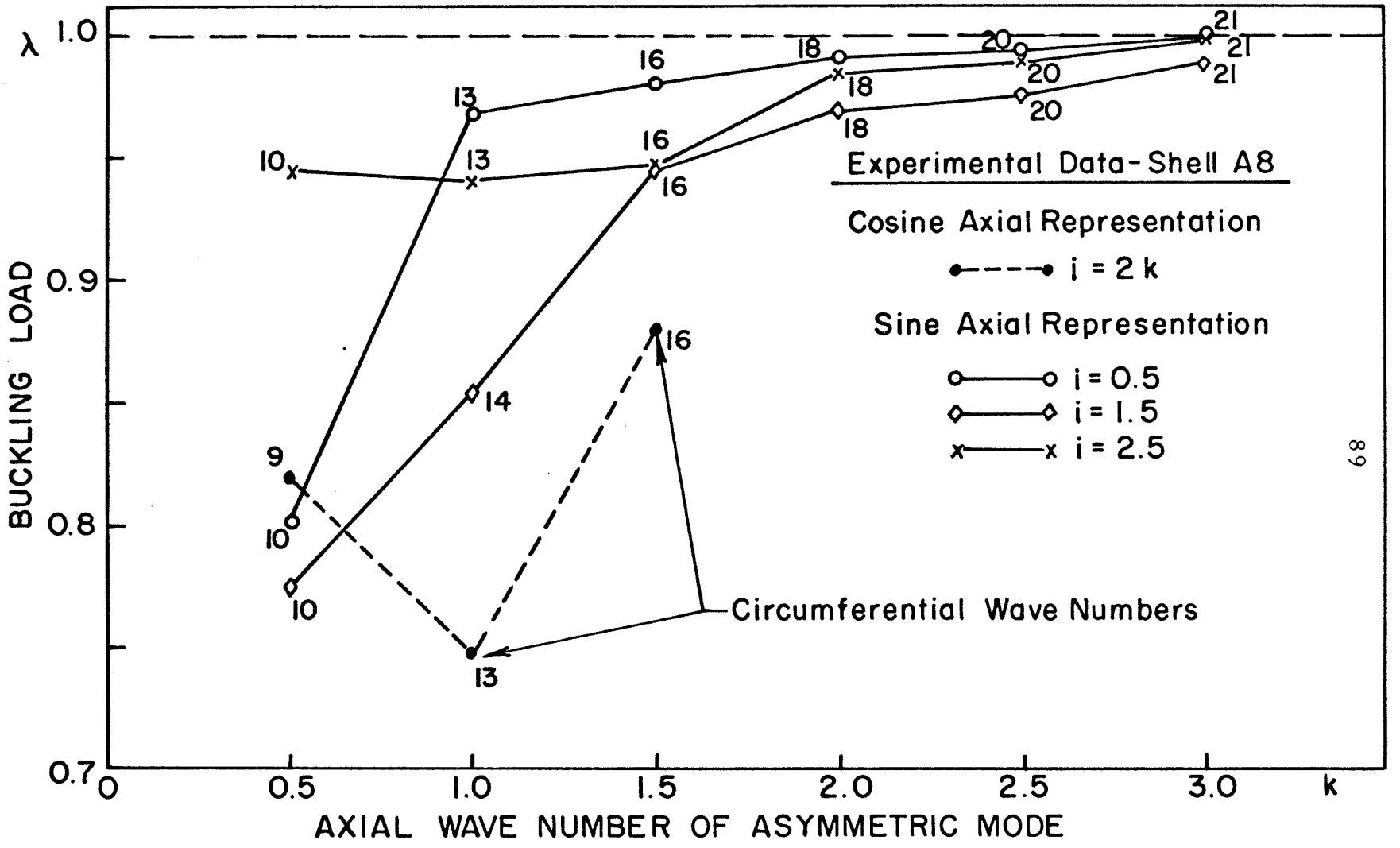

FIG.19 RESULTS FOR THE TWO-MODE SOLUTION

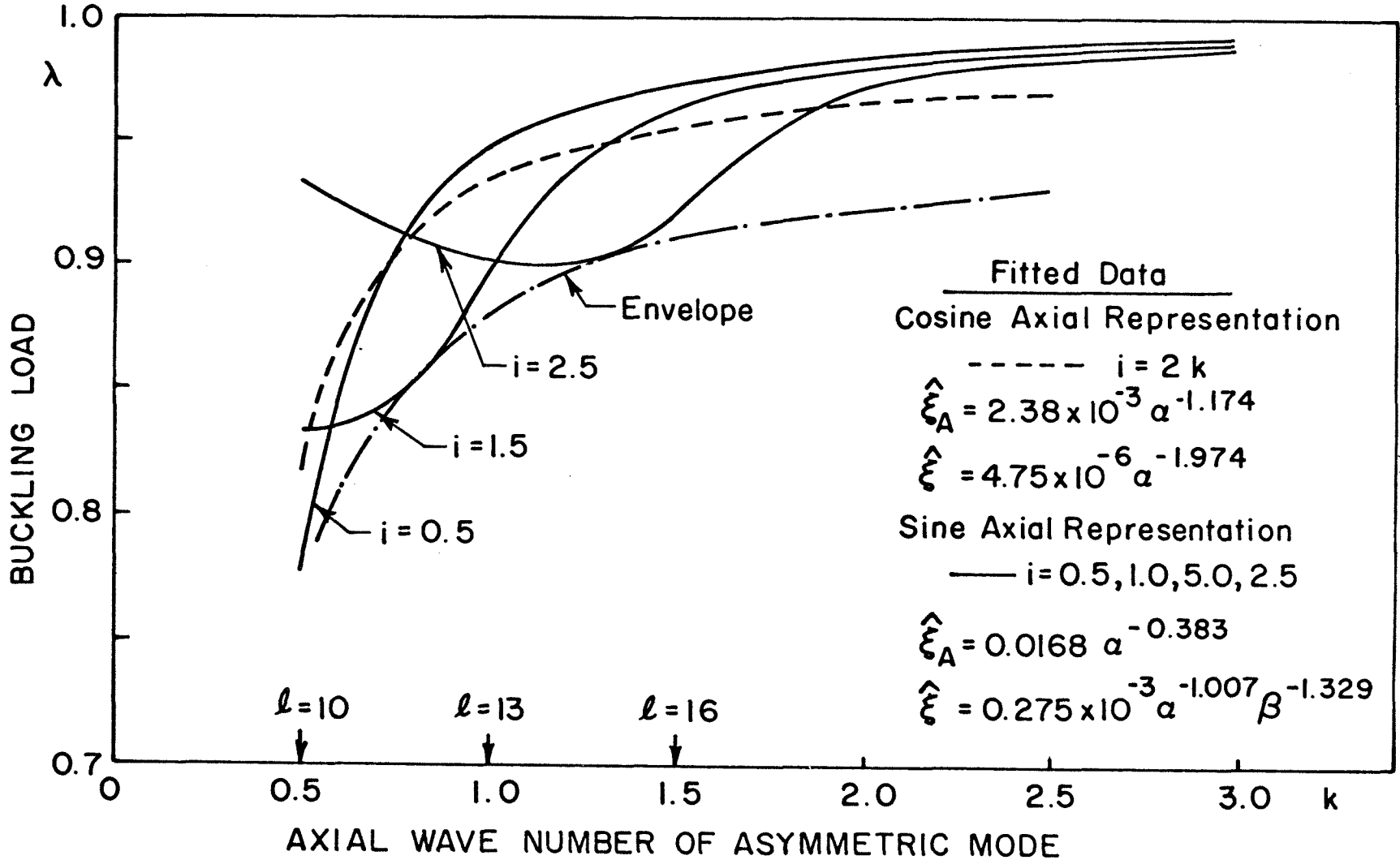

FIG. 20 RESULTS FOR THE TWO-MODE SOLUTION

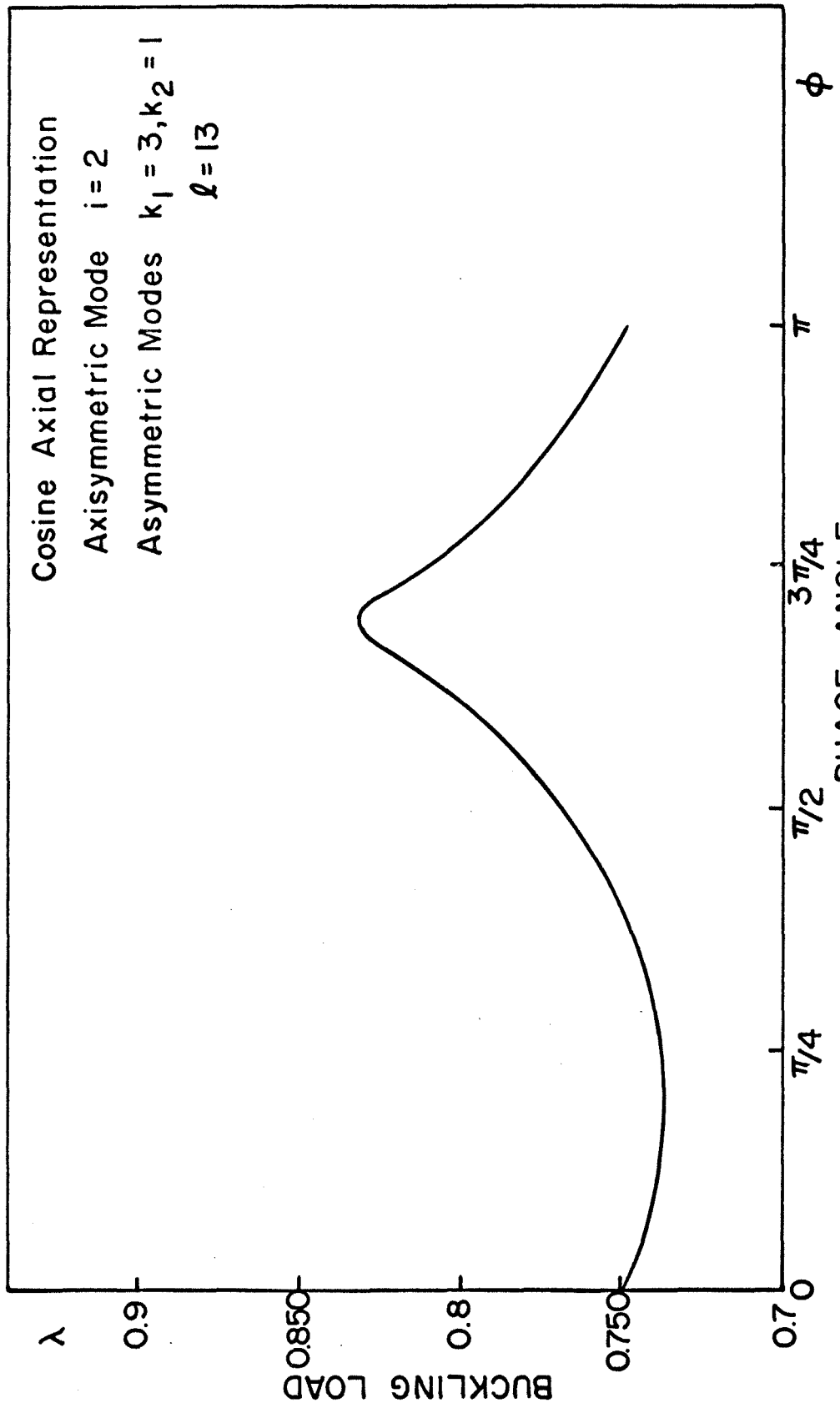

FIG. 21 EFFECT OF PHASE SHIFTING (THREE-MODE SOLUTION)

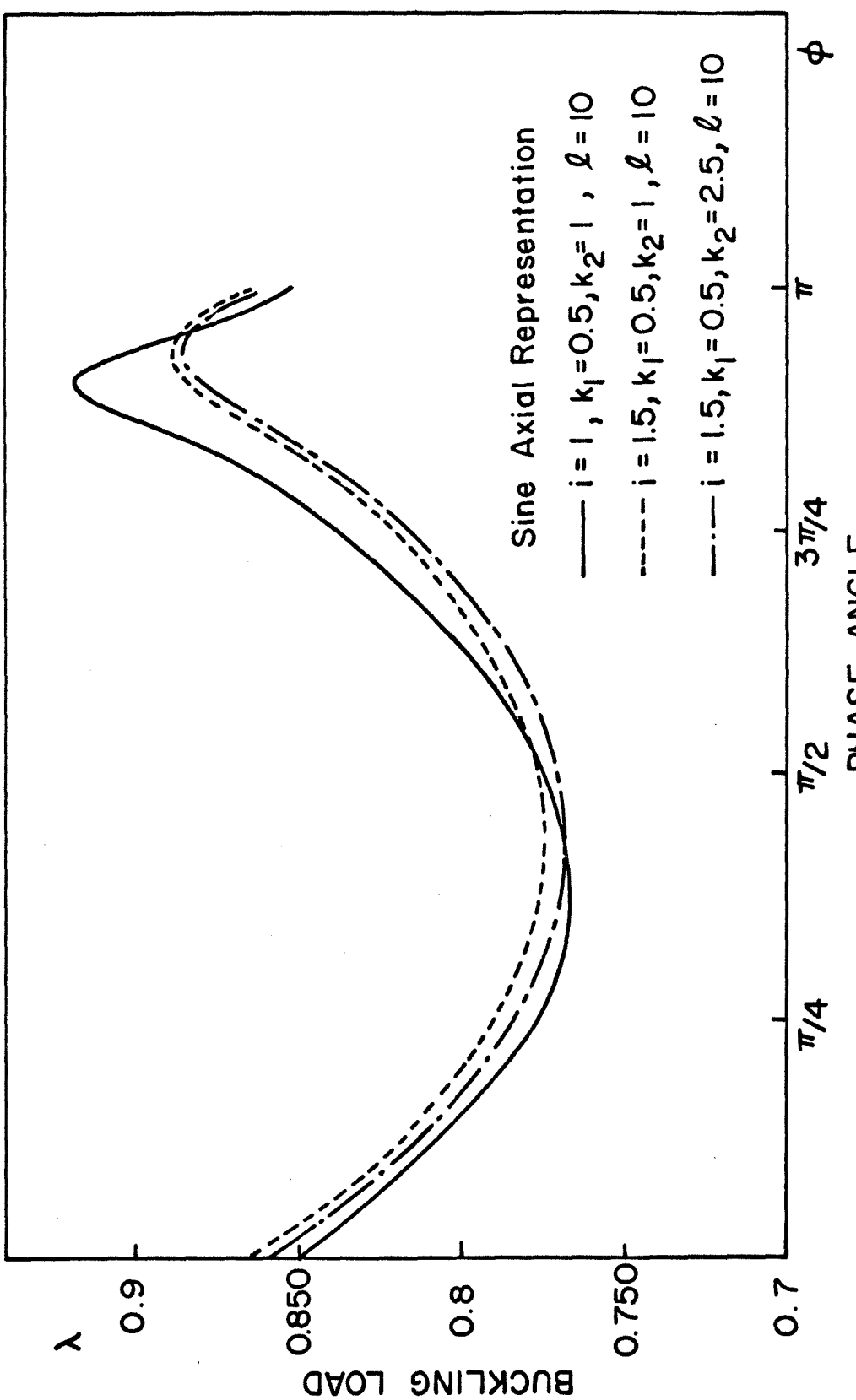

FIG. 22 EFFECT OF PHASE SHIFTING (THREE-MODE SOLUTION)

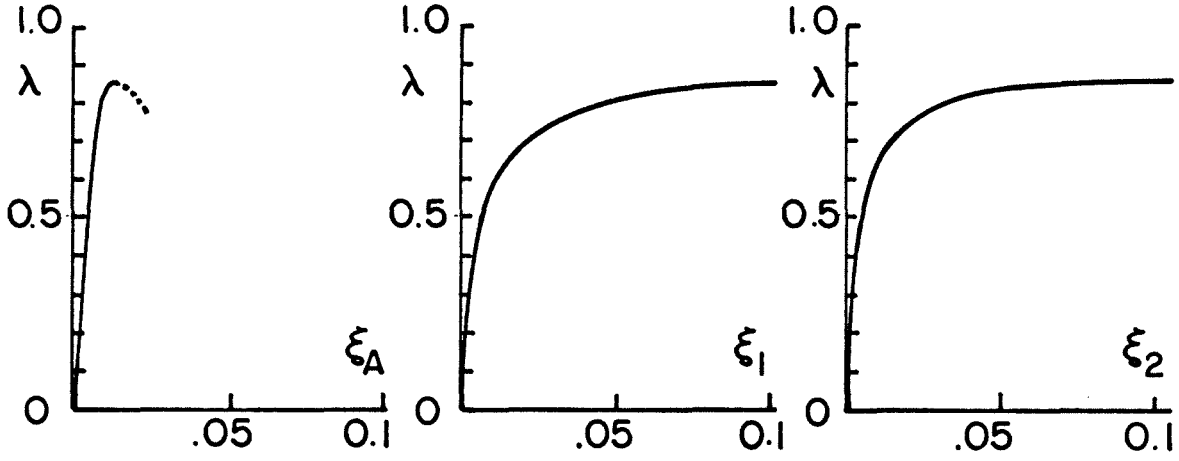

(a) Cosine Axial Representation $i = 2.5, k_1 = 1, k_2 = 1.5, \ell = 15$ (A)

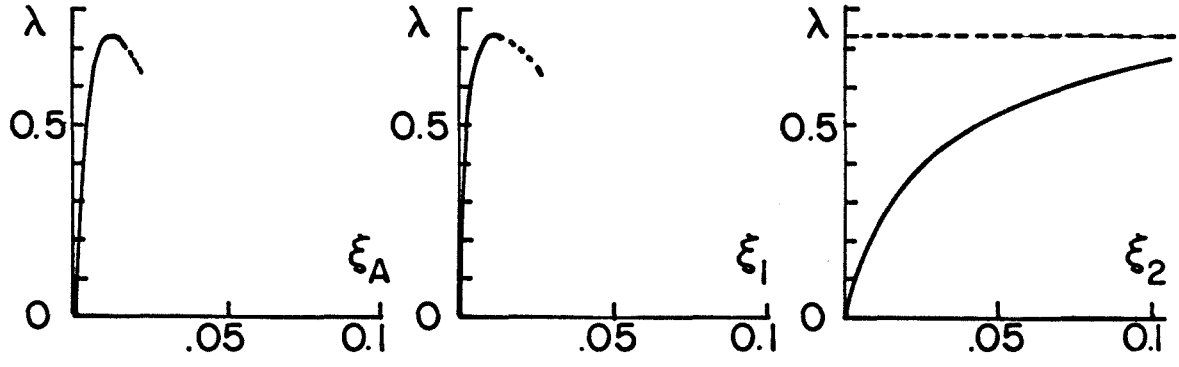

(b) Cosine Axial Representation $i = 2, k_1 = 3, k_2 = 1, \ell = 13$ (B_1)

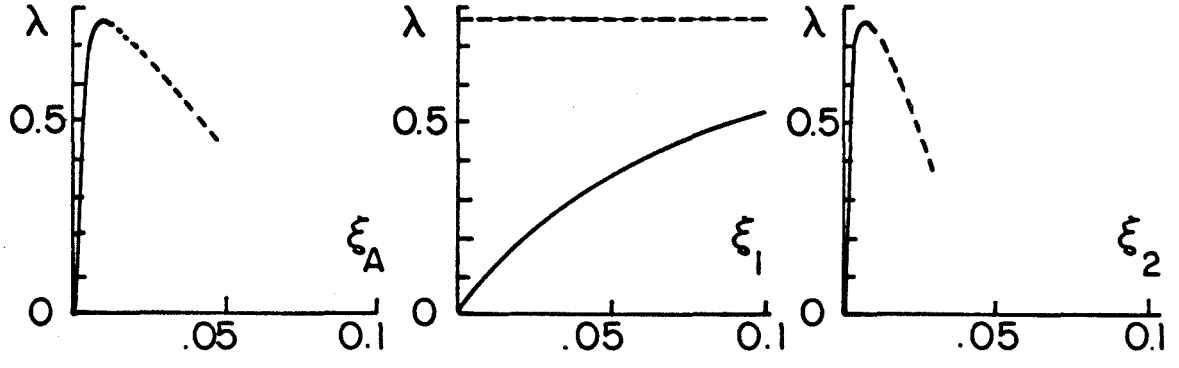

(c) Sine Axial Representation $i = 1.5, k_1 = 0.5, k_2 = 2.5, \ell = 10$(C)

FIG. 23 COMPARISON OF SOME MODE COMBINATIONS FOR THE THREE-MODE SOLUTION (EXPERIMENTAL IMPERFECTION COEFFICIENTS)

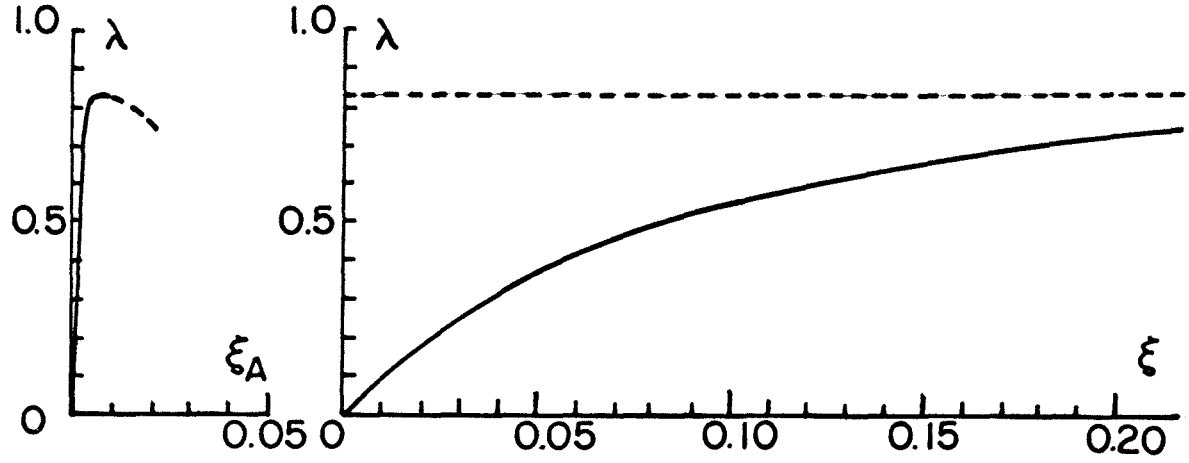

(a) Two-Mode Solution (Sine Axial Representation)

$i = 1.5$, $k = 0.5$, $\ell = 10$

$\bar{\xi}_A = 0.040$, $\bar{\xi} = 0.077$

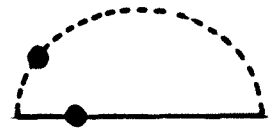

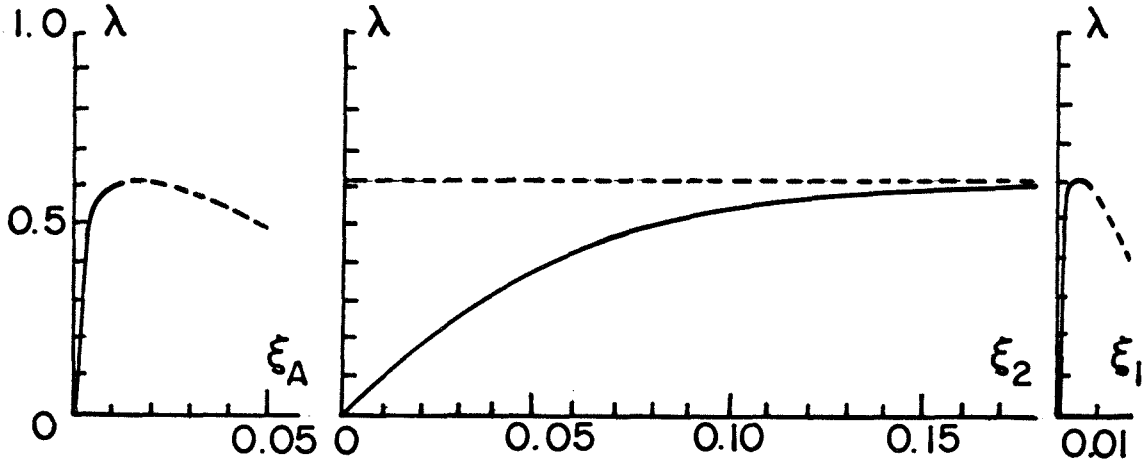

(b) Three-Mode Solution (Sine Axial Representation)

$i = 1.5$, $k_2 = 0.5$, $k_1 = 14.5$, $\ell = 10$ (Case C)

$\bar{\xi}_A = 0.040$, $\bar{\xi}_2 = 0.077$ $\bar{\xi}_1 = 0.003$

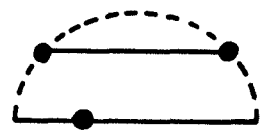

FIG. 24 COMPARISON BETWEEN THE TWO-MODE AND THE THREE-MODE SOLUTION WITH ALL CLASSICAL ASYMMETRIC MODES (FITTED IMPERFECTION COEFFICIENTS)

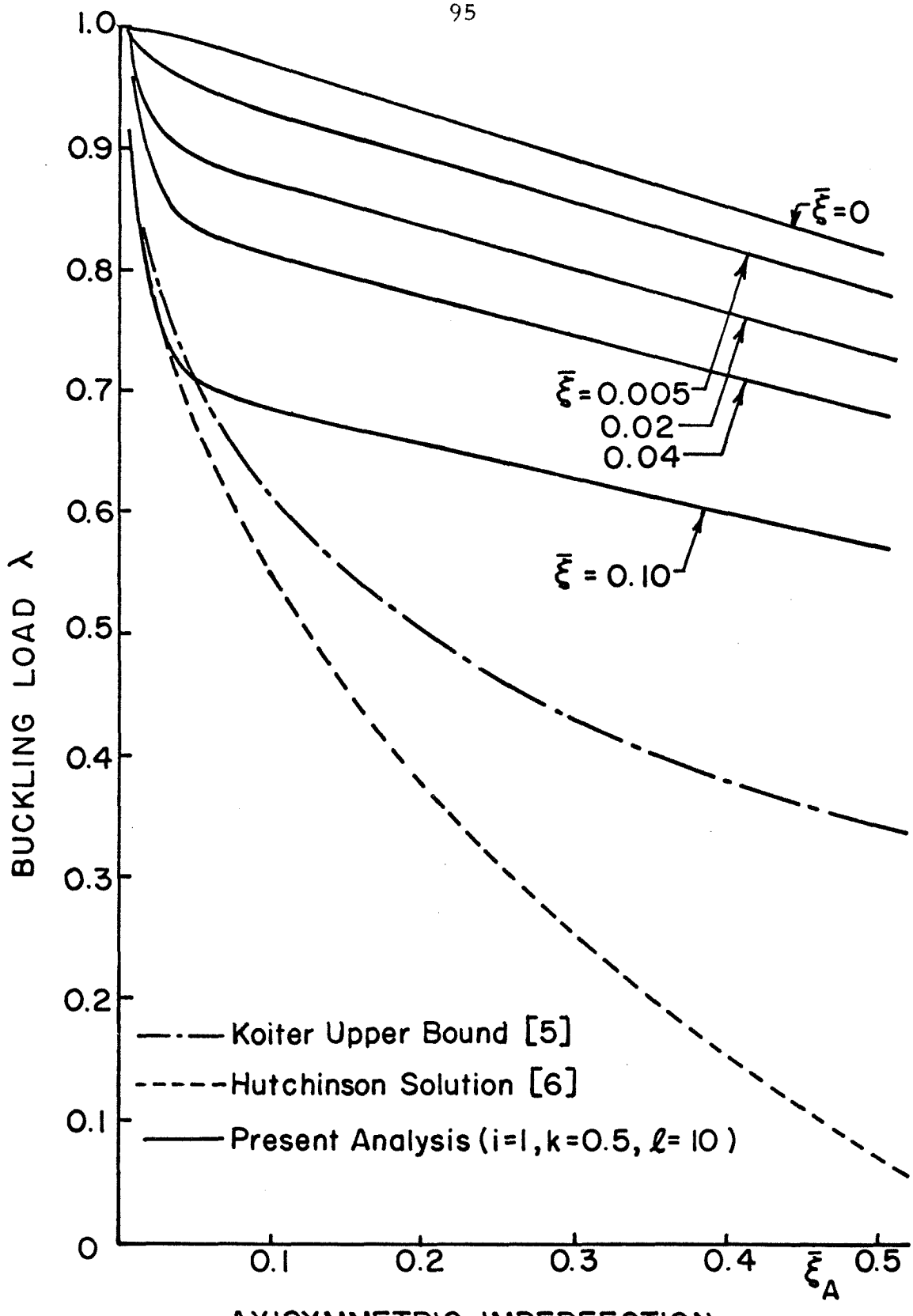

FIG. 25 IMPERFECTION SENSITIVITY (COSINE AXIAL REPRESENTATION)

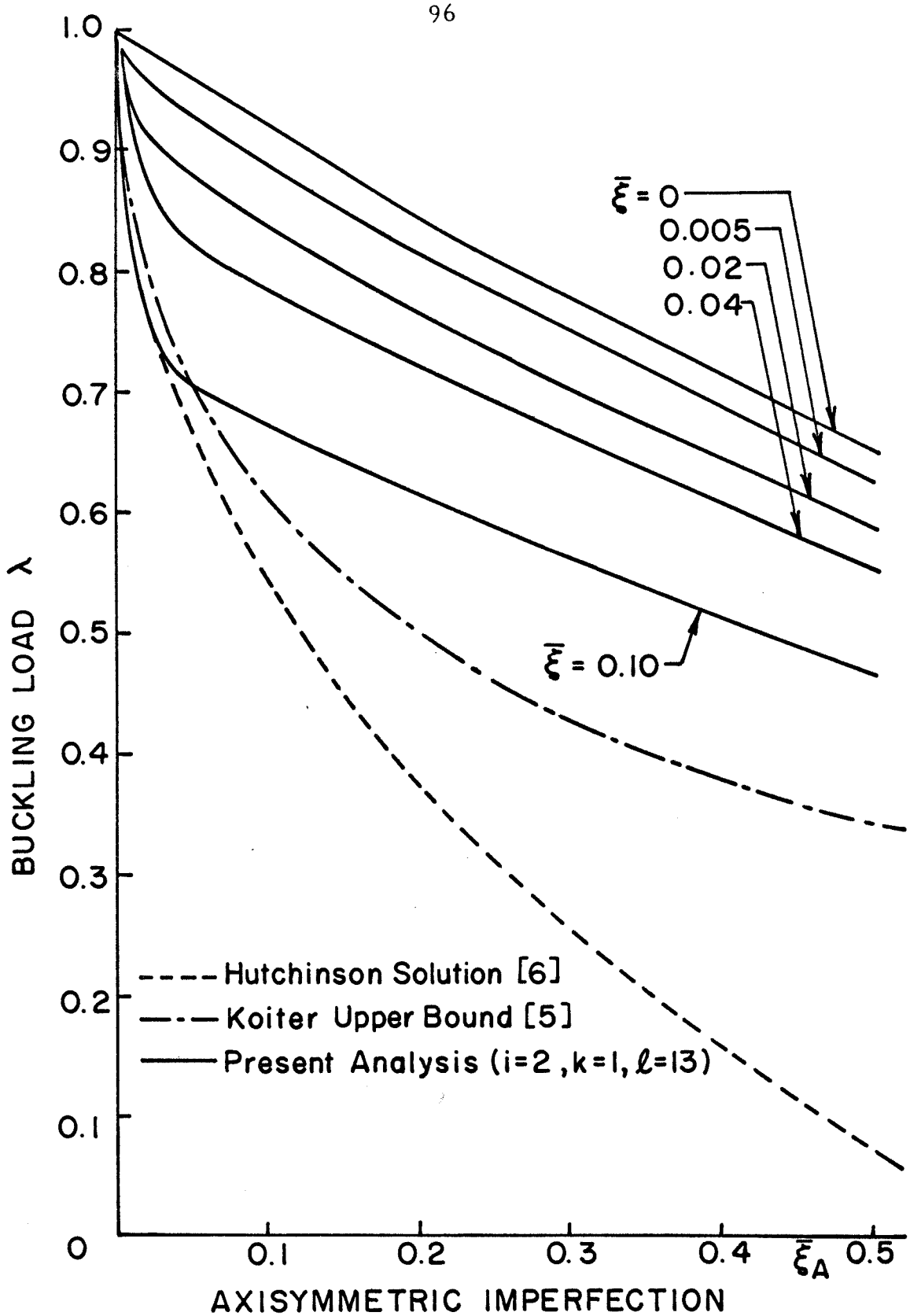

FIG. 26 IMPERFECTION SENSITIVITY (COSINE AXIAL REPRESENTATION)

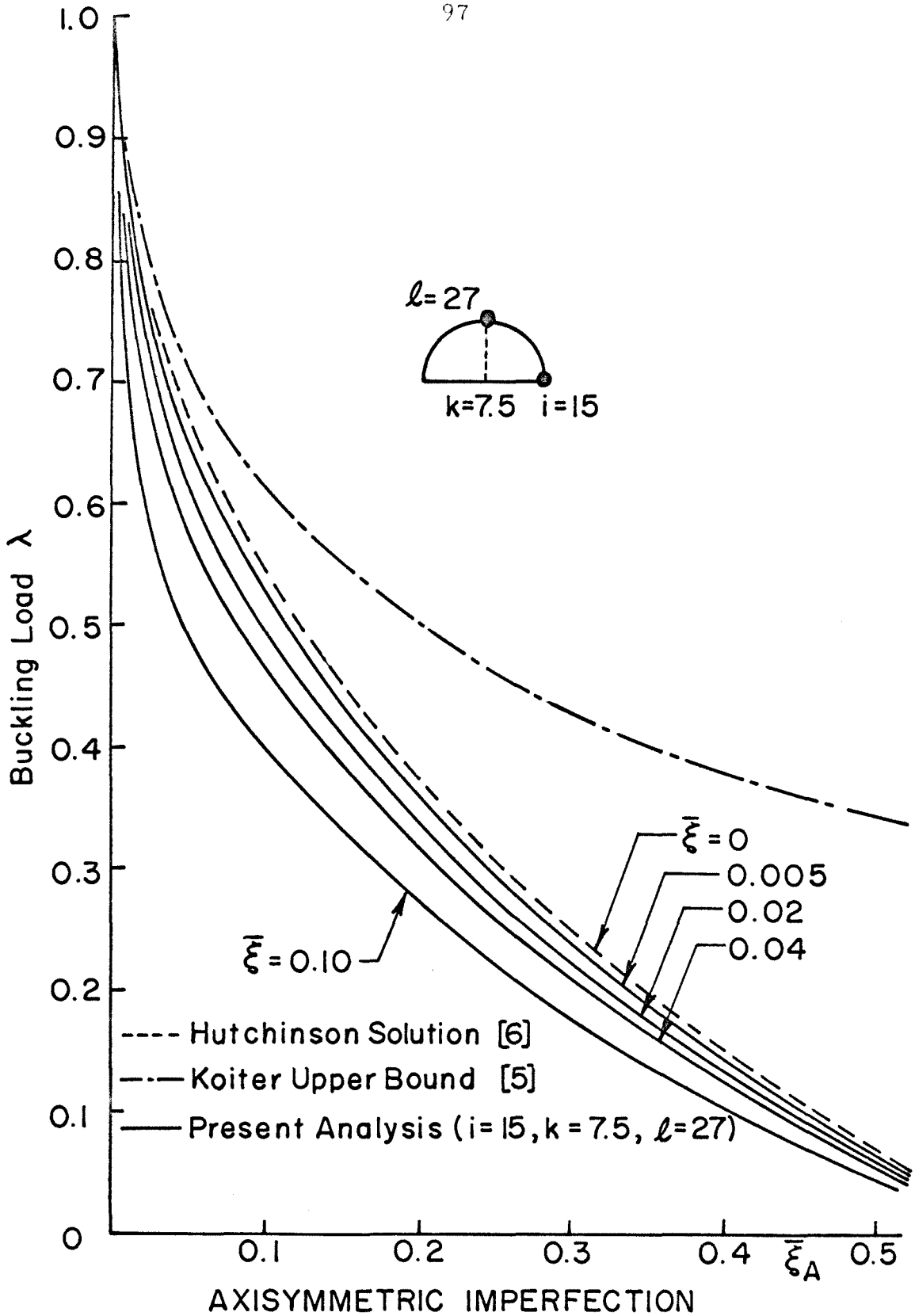

FIG. 27 IMPERFECTION SENSITIVITY (COSINE AXIAL REPRESENTATION)

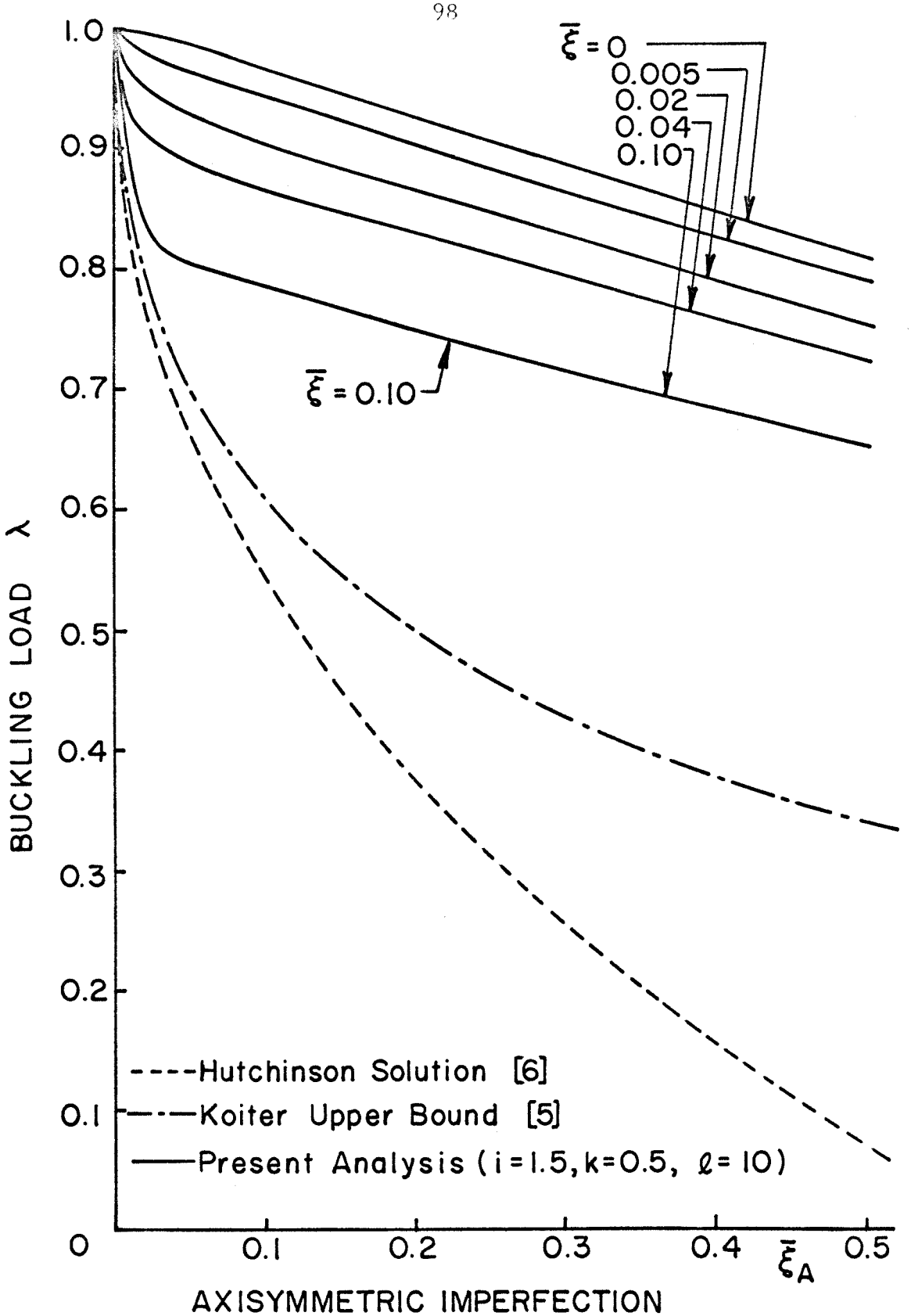

FIG. 28 IMPERFECTION SENSITIVITY (SINE AXIAL REPRESENTATION)

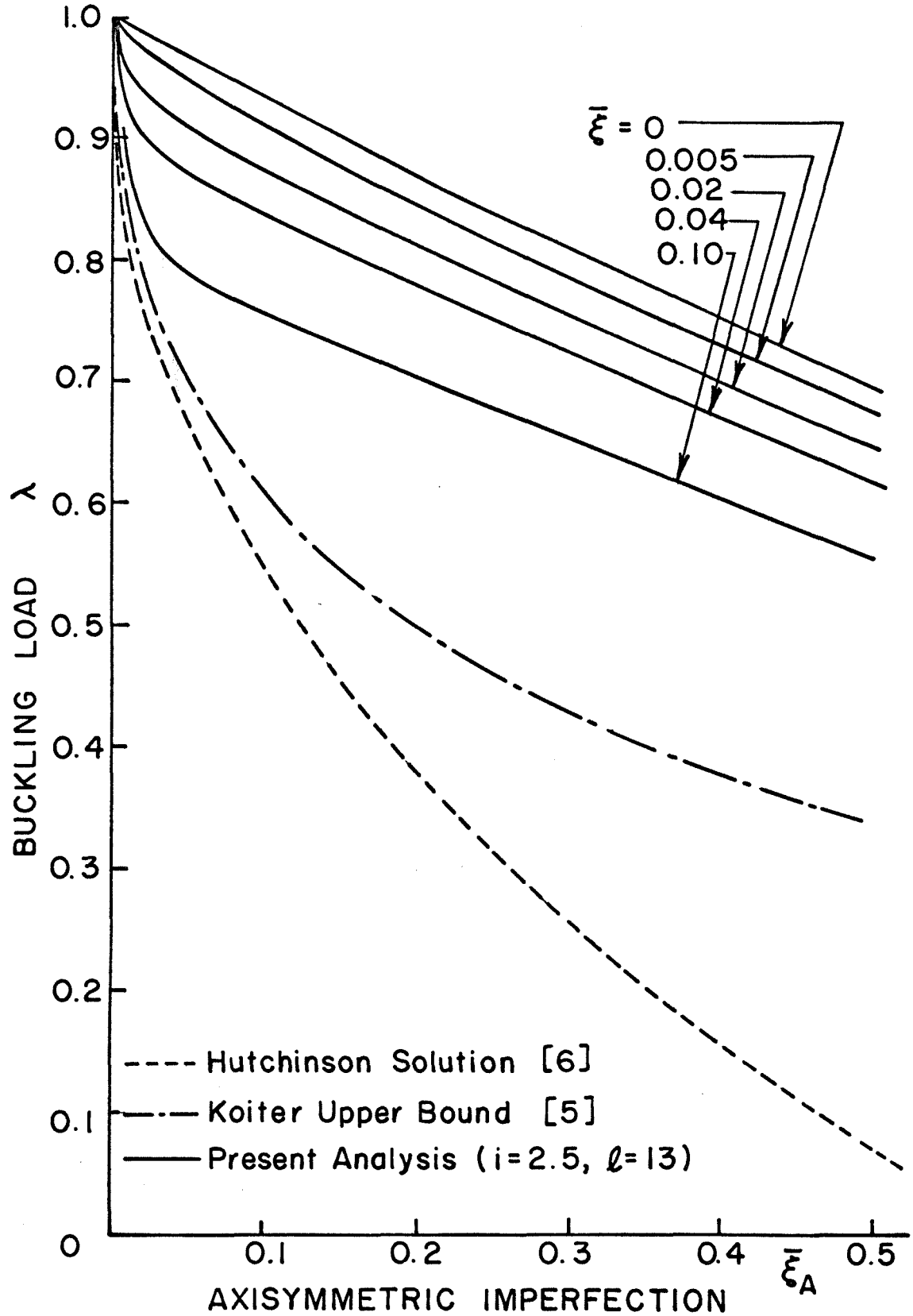

FIG. 29 IMPERFECTION SENSITIVITY (SINE AXIAL REPRESENTATION)

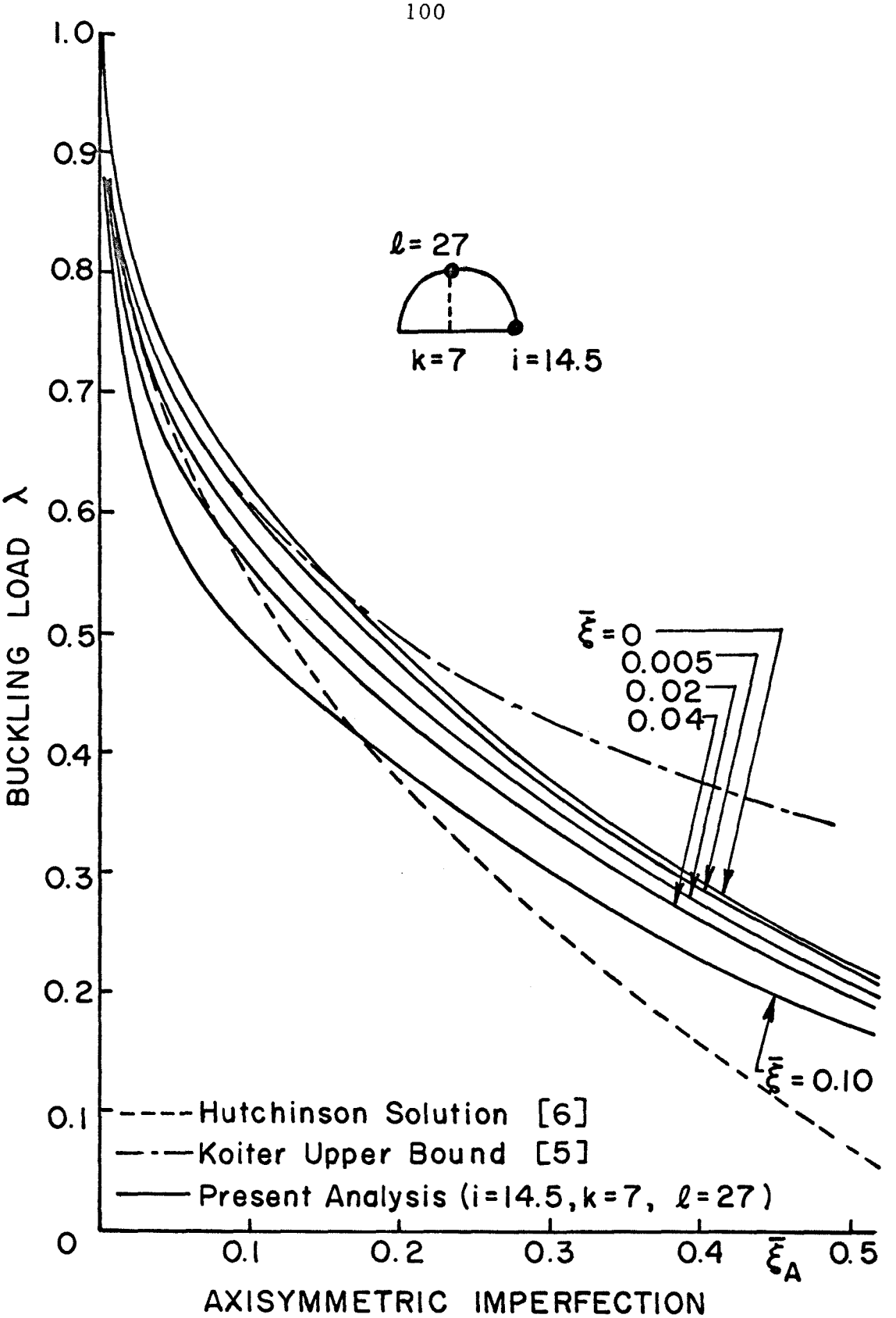

FIG. 30 IMPERFECTION SENSITIVITY (SINE AXIAL REPRESENTATION)